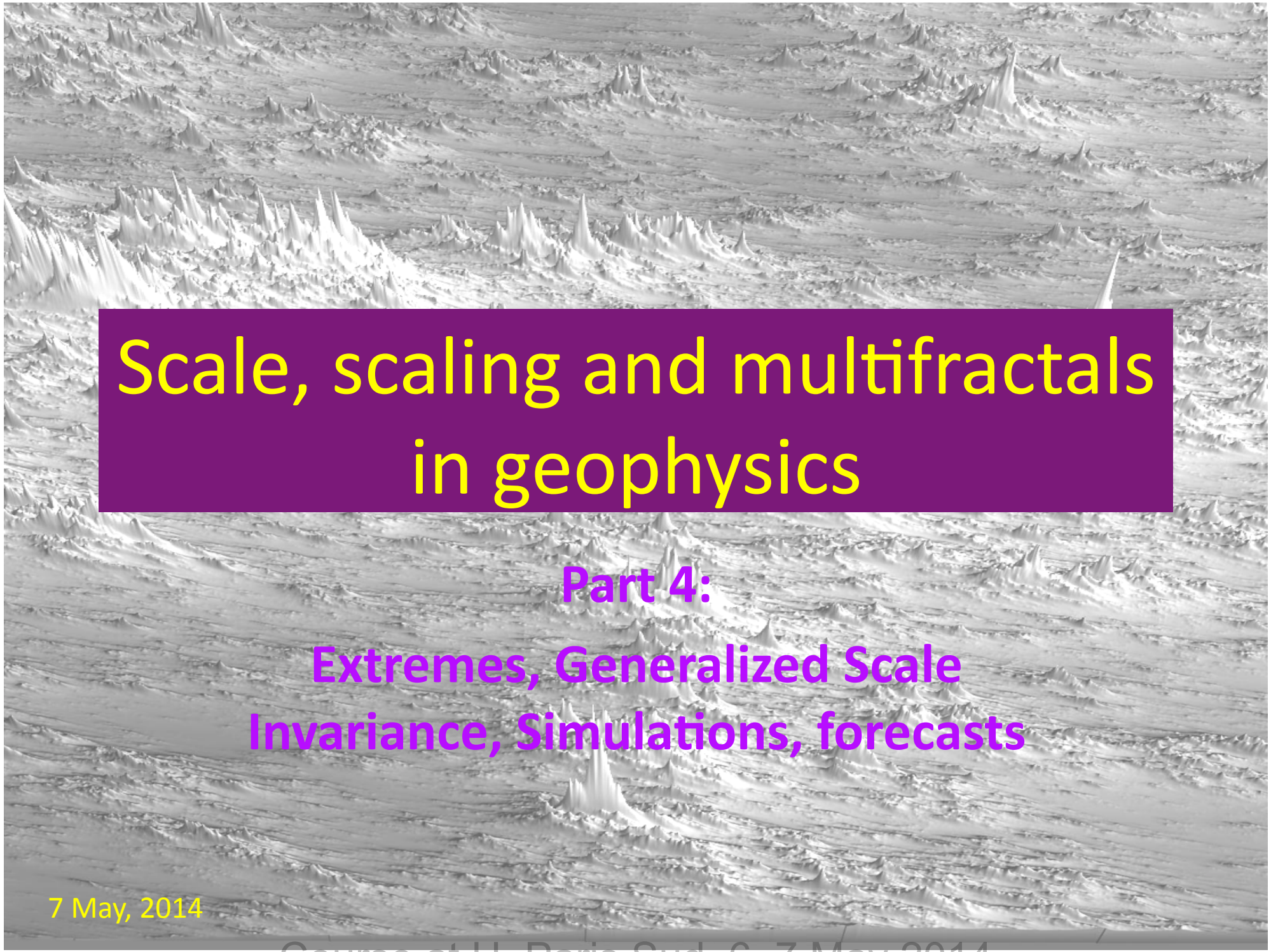

Scale, scaling and multifractals in geophysics

Part 4:

Extremes, Generalized Scale Invariance, Simulations, forecasts

7 May, 2014

Extremes,
Divergence of moments,
Self-organized criticality

Course at U. Paris Sud, 6, 7 May 2014

Bare and dressed Cascades

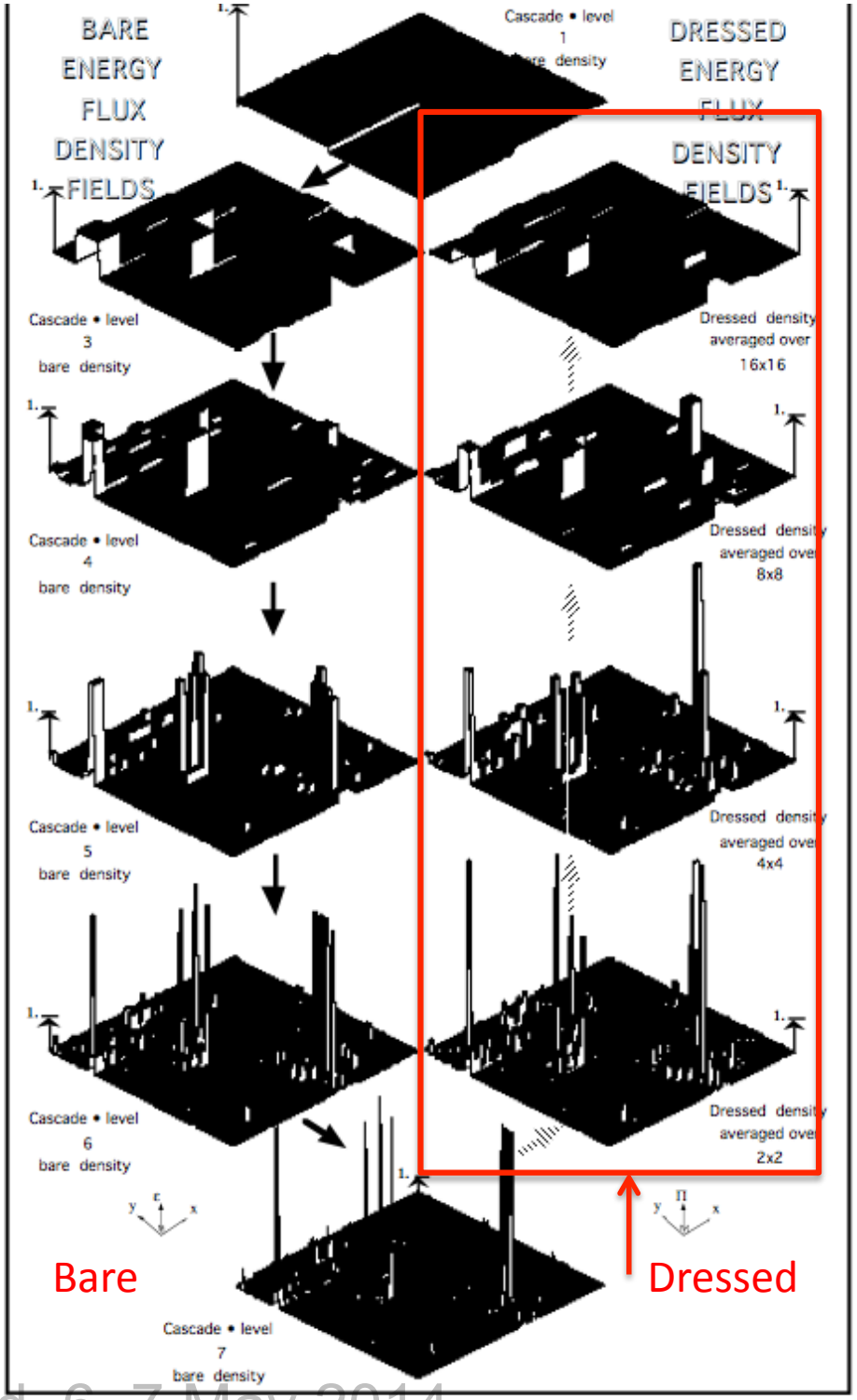

Factorization property of the cascade

$$\varepsilon_\Lambda = \varepsilon_\lambda T_\lambda\left(\varepsilon_{\Lambda/\lambda}\right)$$

ε_λ

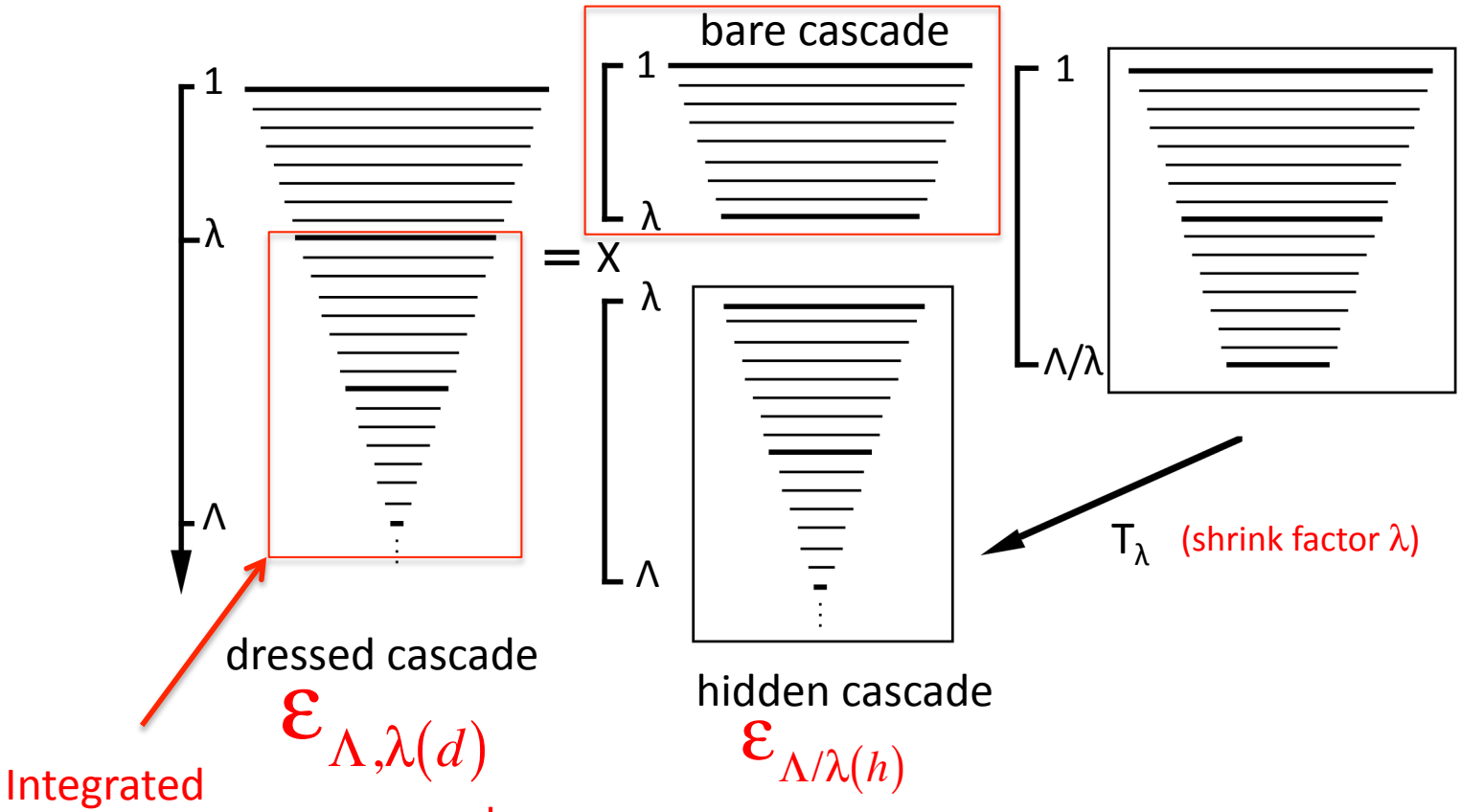

$\varepsilon_{\Lambda,\lambda(d)}$ $\varepsilon_{\Lambda/\lambda(h)}$

bare

$$\varepsilon_{\Lambda,\lambda(d)} = \varepsilon_\lambda \varepsilon_{\Lambda/\lambda(h)} \xrightarrow{\Lambda \to \infty} \varepsilon_{\lambda(d)} = \varepsilon_\lambda \varepsilon_{\infty(h)}$$

partially dressed — Partially hidden — Fully dressed — hidden

Multifractal Butterfly effect

$$\varepsilon_{\lambda(d)} = \varepsilon_{\lambda}\varepsilon_{\infty(h)}$$

Full cascade averaged at scale λ^{-1}

large scales (scale range λ)

small scales: integrated fully developped cascade

The hidden moments diverge:

$$\left\langle \varepsilon^{q}_{\infty,(h)} \right\rangle \approx \begin{cases} O(1); & q < q_D \\ \infty; & q \geq q_D \end{cases}$$

Divergence due to small scales: the multifractal butterfly effect

q_D is the solution to the implicit equation $K(q_D) = D(q_D - 1)$

Discontinuity in first derivative = first order multifractal phase transition

Divergence of dressed moments:

$$\left\langle \varepsilon^{q}_{\lambda(d)} \right\rangle = \lambda^{K_d(q)} \quad \text{where:} \quad K_d(q) = \begin{cases} K(q); & q < q_D \\ \infty; & q \geq q_D \end{cases}$$

Long range dependencies place this outside the framework of Extreme Value Theory

Probability distributions

$$\left\langle \varepsilon^{q}_{\lambda(d)} \right\rangle = \infty,\ q \geq q_D \quad \Leftrightarrow \quad \Pr(\varepsilon_{\lambda(d)} > s) \sim s^{-q_D},\ s >> 1$$

Mandelbrot 1974, S+L 1987

Self-Organized criticality (SOC)

Operational definition of SOC:
Spatial scaling and Power law probabilities

Sandpile "mean shape"
= result of extreme
avalanches

The mean field results from catastrophes!

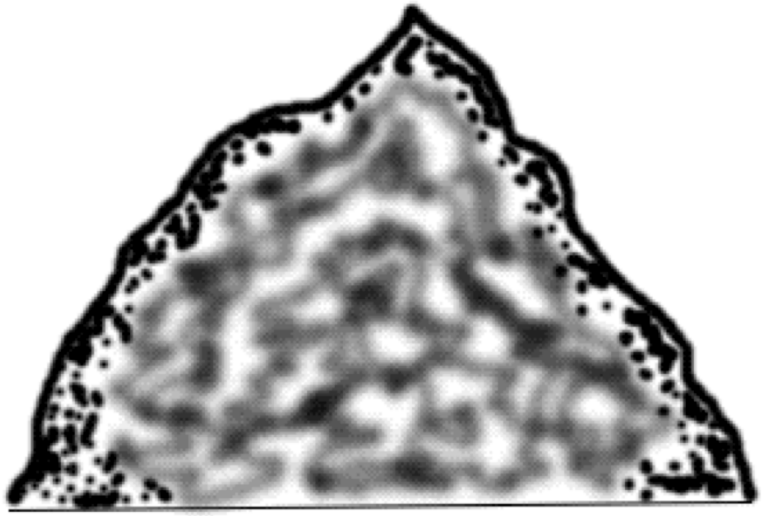

Classical SOC: zero flux limit
Nonclassical multifractal SOC: quasi constant flux

Divergence of moments in Laboratory turbulence

$$\Pr(\varepsilon > s) \approx s^{-q_{D,\varepsilon}}$$

Dissipation Range:

$$\varepsilon \approx \nu \underline{v} \cdot \nabla^2 \underline{v} \approx \nu \frac{\Delta v^2}{\Delta x^2} \qquad \Pr(\varepsilon > s) = \Pr\left(\frac{\nu \Delta v^2}{\Delta x^2} > s \right) \qquad q_{D,\varepsilon} = q_{D,v(diss)} / 2$$

Inertial Range:

$$\varepsilon \approx \frac{\Delta v^3}{\Delta x} \qquad \Pr(\varepsilon > s) = \Pr\left(\frac{\Delta v^3}{\Delta x} > s \right) \qquad q_{D,\varepsilon} = q_{D,v(inertial)} / 3$$

Laboratory Data:

Dissipation range estimate: $q_{D,v(diss)} \approx 5.4;$ $q_{D,\varepsilon} \approx 2.7$

Inertial range estimate: $q_{D,v(inertial)} \approx 7.7;$ $q_{D,\varepsilon} \approx 2.6$

Radelescu, L+S+M 2002

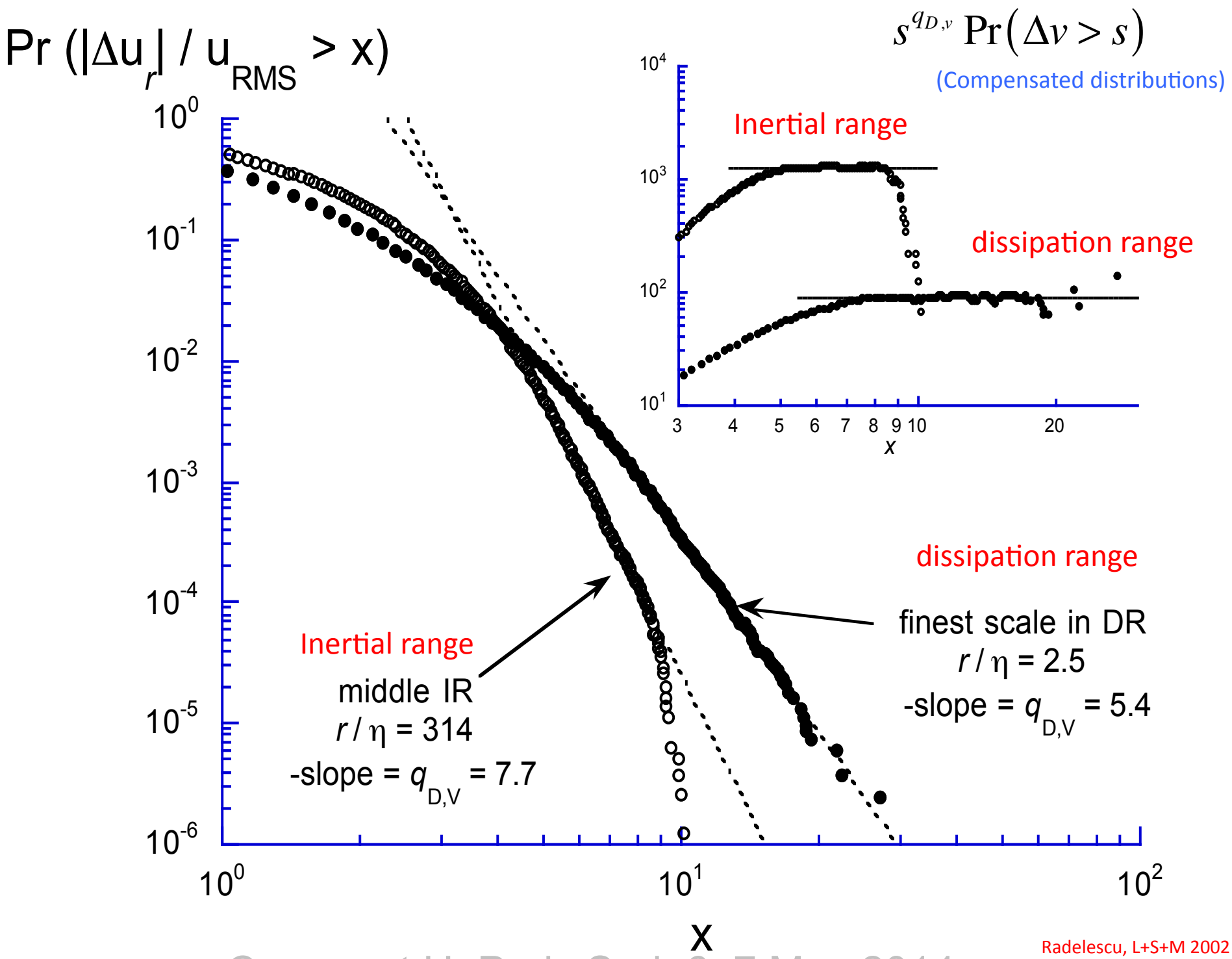

Radelescu, L+S+M 2002

Divergence of moments in the horizontal wind field

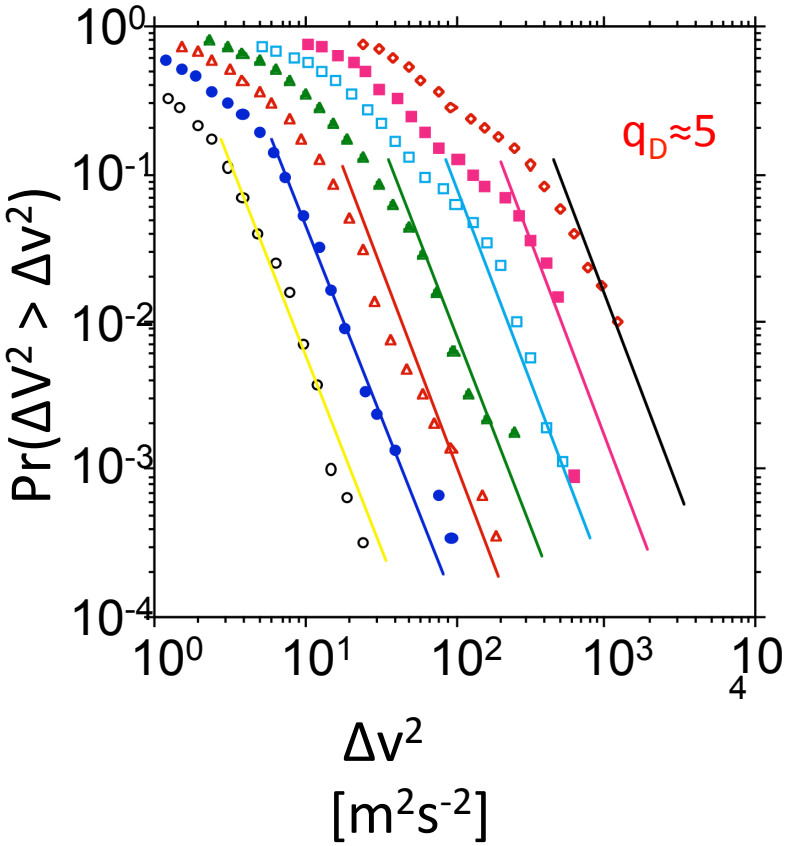

Across vertical layers

radiosondes

Layers 50,100, 200, 400,…3200m

(S+L1985)

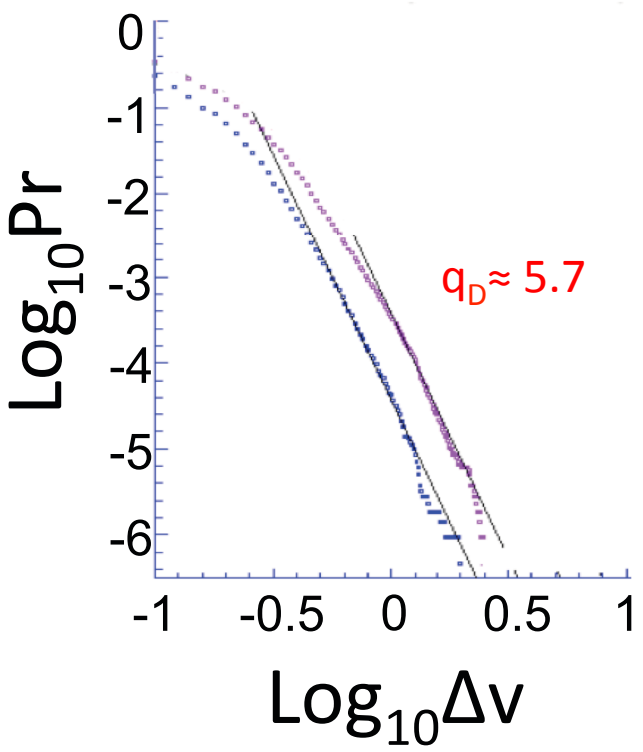

In the horizontal

aircraft: 40, 80 m

(L+S 2007)

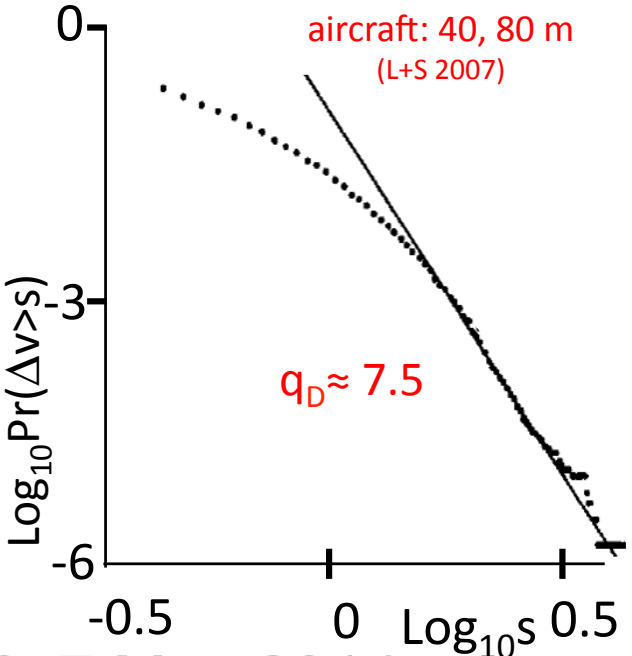

In time

sonic probe, 10 Hz

(Schmitt, S+L 1994)

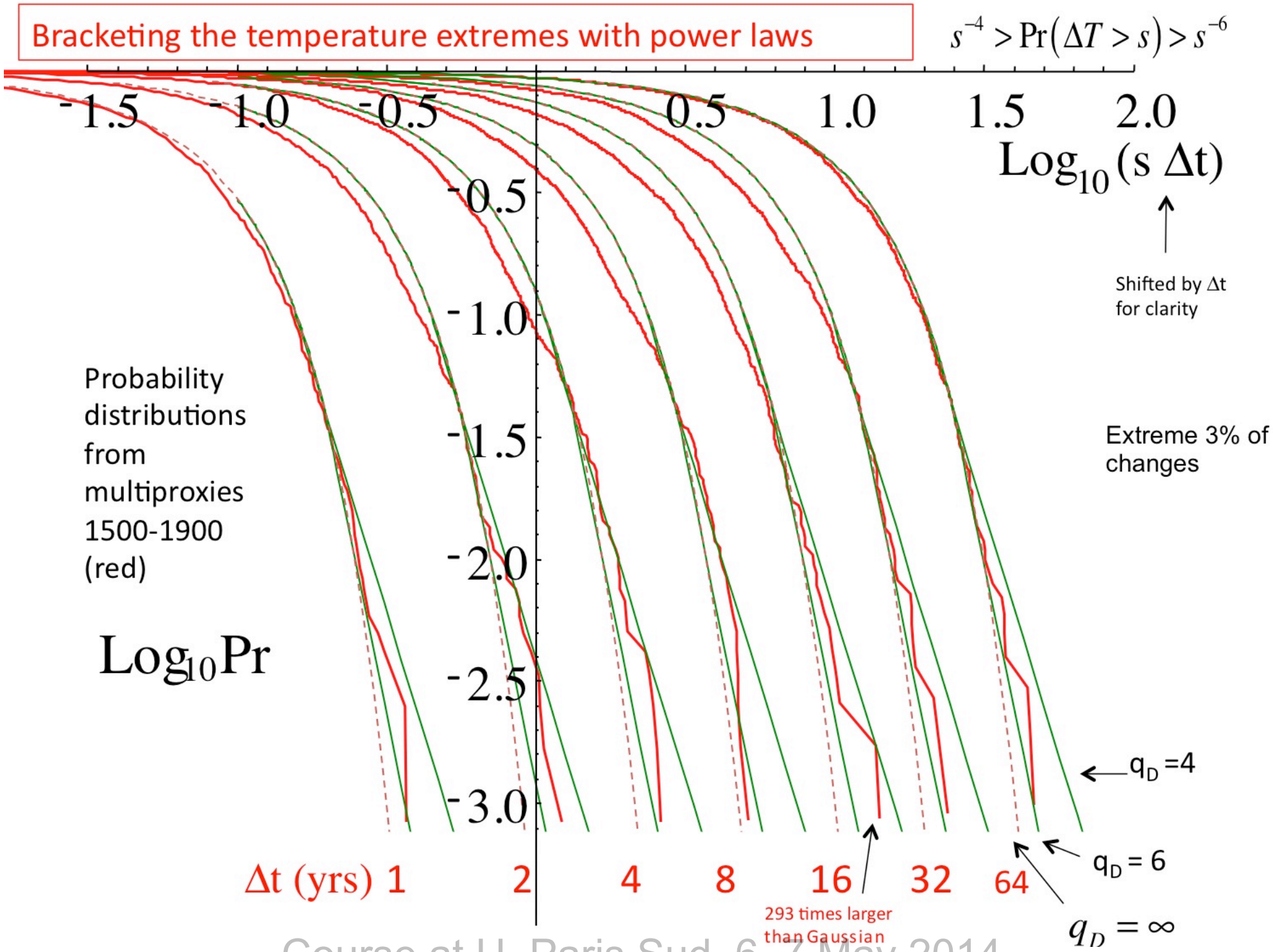
Bracketing the temperature extremes with power laws
$s^{-4} > \Pr(\Delta T > s) > s^{-6}$
-1.5
-1.0
-0.5
0.5
1.0
1.5
2.0
$\mathrm{Log}_{10}(s\,\Delta t)$
Shifted by Δt for clarity
Probability distributions from multiproxies 1500-1900 (red)
$\mathrm{Log}_{10}\mathrm{Pr}$
-0.5
-1.0
-1.5
-2.0
-2.5
-3.0
Extreme 3% of changes
q_D =4
q_D = 6
$q_D = \infty$
Δt (yrs) 1
2
4
8
16
32
64
293 times larger than Gaussian

q_D estimates for various geophysical fields

Table 5.1a A summary of various estimates of the critical order of divergence of moments (q_D) for various atmospheric fields.

Field	Data source	Type	q_D	Reference
Horizontal wind	Sonic	10Hz, time	7.5	Schmitt *et al.*, 1994
	Sonic	10 Hz	7.3	Finn *et al.*, 2001
	Hot wire probe	Inertial range	7.7	Fig. 5.22, Radulescu *et al.*, 2002
	Hot wire probe	Dissipation range	5.4	Fig. 5.22, Radulescu *et al.*, 2002
	Anemometer	15 minutes	7	Tchiguirinskaia *et al.*, 2006
	Anemometer	Daily	7	Tchiguirinskaia *et al.*, 2006
	Aircraft, stratosphere	Horizontal, 40 m	5.7	Lovejoy and Schertzer, 2007
	Aircraft, troposphere	Horizontal, 280 m – 36 km	≈ 5	Fig. 5.10
	Aircraft, troposphere	Horizontal, 40 m – 20 km	≈ 7 ± 1	Chigirinskaya *et al.*, 1994
	Aircraft, troposphere	Horizontal, 100 m	≈ 5	Schertzer and Lovejoy, 1985
	Radiosonde	Vertical, 50 m	5	Schertzer and Lovejoy, 1985, Lazarev *et al.*, 1994
	Scaling gyroscopes cascade (SGC) model (Box 3.4)	Time	6.9 ± 0.2	Chigirinskaya and Schertzer, 1996
Potential temperature	Radiosonde	Vertical, 50 m	3.3	Schertzer and Lovejoy, 1985
Humidity	Aircraft, troposphere	Horizontal, 280 m – 36 km	≈ 5	Fig. 5.10
Temperature	Aircraft, troposphere	Horizontal, 280 m – 36 km	≈ 5	Fig. 5.10
	Hemispheric, global	Annual, monthly	≈ 5, 5	Lovejoy and Schertzer, 1986, and unpublished analysis respectively
	Daily, stations	Average over 53 stations in France, daily single station (Macon)	4.5, 4.5	Ladoy *et al.*, 1991
Paleotemperatures	Ice cores	350 years (time), 0.55 m, 1 m (depth)	5, 5	Lovejoy and Schertzer, 1986, Fig. 5.21 respectively
Geopotential anomalies	Reanalyses	500 mb, daily	2.7	Sardeshmukh and Sura, 2009
Vorticity anomalies	Reanalyses	300 mb, daily	1.7	Sardeshmukh and Sura, 2009
Visible radiances (ocean surface)	Remote sensing	7 m resolution MIES data	3.6	Lovejoy *et al.*, 2001
Passive scalar (SF_6)	Fast response SF_6 analyzer	1 Hz	4.7	Finn *et al.*, 2001
Vertical CO_2 flux (above a field)	Aircraft new ground	Horizontal ≈ 1 km resolution	5.3	Austin *et al.*, 1991
Seveso pollution	Ground concentrations	In-situ measurements	2.2	Salvadori *et al.*, 1993
Chernobyl fallout	Ground concentrations	In-situ measurements	1.7	Chigirinskaya *et al.*, 1998; Salvadori *et al.*, 1993
Density of meteorological stations	WMO surface network	Geographic location of stations	3.7 ± 0.1	Tessier *et al.*, 1994

Most exponents: range 3-5

L+S 2013

q_D estimates for various hydrological fields

Table 5.1b A summary of various estimates of the critical order of divergence of moments (q_D) for various hydrological fields.

Field	Data source	Type	q_D	Reference
Radar reflectivity of rain	Radar reflectivity factor	1 km^3 resolution	1.1	Schertzer and Lovejoy, 1987
Rain rate	Gauges	Daily, Nimes	2.6	Ladoy *et al.*, 1991
	Gauges	Daily, time, France	≈ 3	Ladoy *et al.*, 1993
	Gauges	Daily, USA	1.7–3	Georgakakos *et al.*, 1994
	High-resolution gauges	8 minutes	≈ 2	Olsson, 1995
	High-resolution gauges	15 s	2.8–8.5	Harris *et al.*, 1996
	Gauges	Daily, time	3.6 ± 0.07	Tessier *et al.*, 1996
	Gauges	1–8 days	3.5	De Lima, 1998
	Gauges	Hourly, time	4.0	Kiely and Ivanova, 1999
	Gauges	Daily, four series from 18th century	3.78 ± 0.46	Hubert *et al.*, 2001
	Gauges	Hourly, time	≈ 3	Fig. 5.10c; Schertzer *et al.*, 2010
	Gauges	Hourly, time	≈ 3	Fig. 5.20b; Lovejoy *et al.*, 2012
	High-resolution gauges	15 s, averaged to 30 minutes	2.23	Verrier, 2011
Raindrop volumes	Stereophotography	10 m^3 sampling volume	5	Lovejoy and Schertzer, 2008
Liquid water at turbulent scales	Stereophotography	Total water in 40 cm cubes	3	Lovejoy and Schertzer, 2006b
Stream flow	River gauges (France)	Daily	3.2 ± 0.07	Tessier *et al.*, 1996
	River gauges (USA)	Daily	3.2 ± 0.07	Pandey *et al.*, 1998; Tessier *et al.*, 1996
	River gauges (France)	Daily	2.5–10	Schertzer *et al.*, 2006

Most exponents: ≈ 3

L+S 2013

Abrupt events, extreme changes

Course at U. Paris Sud, 6, 7 May 2014

Abrupt events, extreme changes

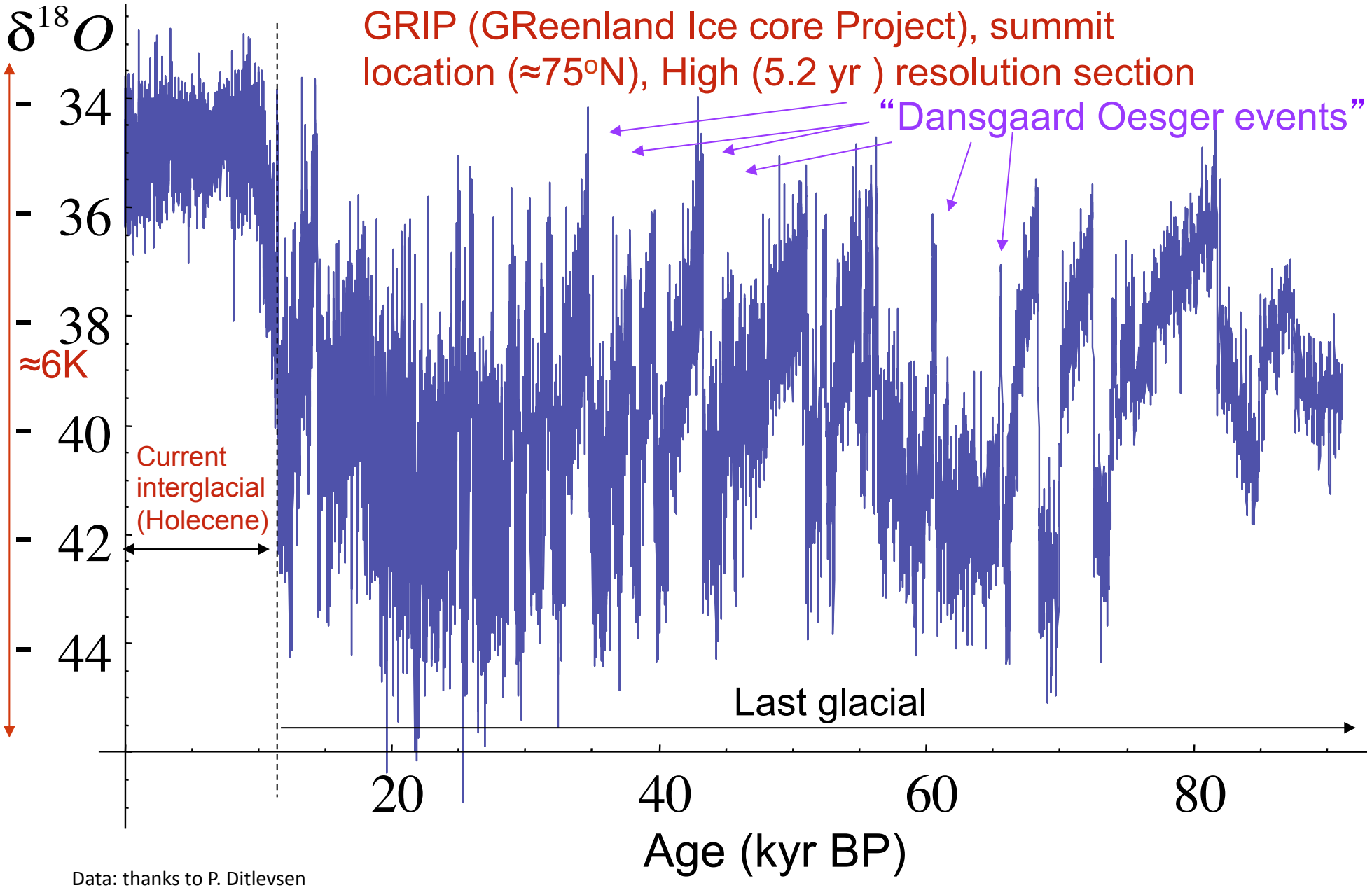

Data: thanks to P. Ditlevsen

GRIP Probabilities of extreme changes

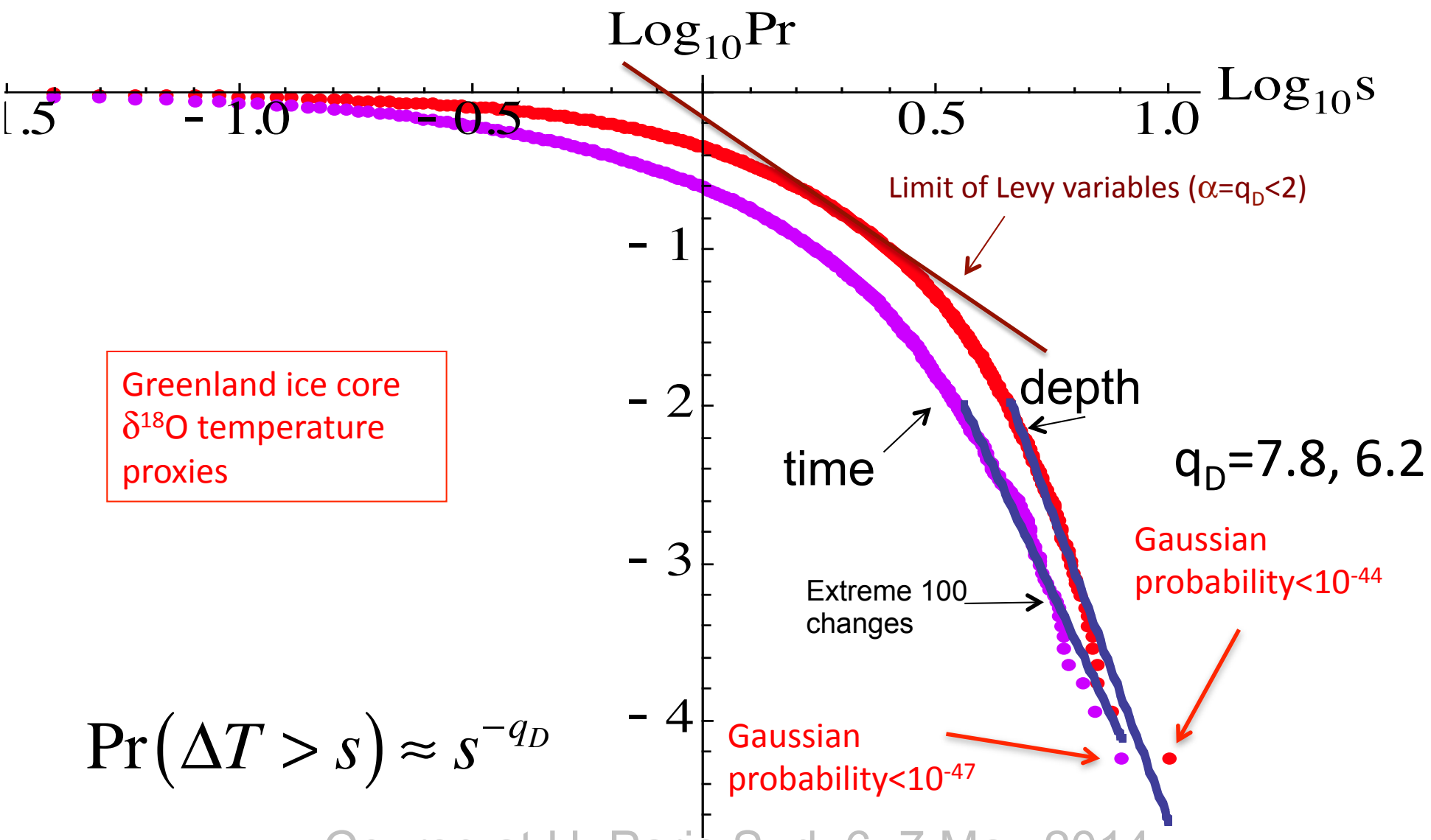

$$\Pr(\Delta T > s) \approx s^{-q_D}$$

Observables:
additive and multiplicative processes

$$\Delta T = \varphi \Delta t^{H}$$

Linear scaling part, additive

Observable: multiplicative and additive

Multiplicative cascade

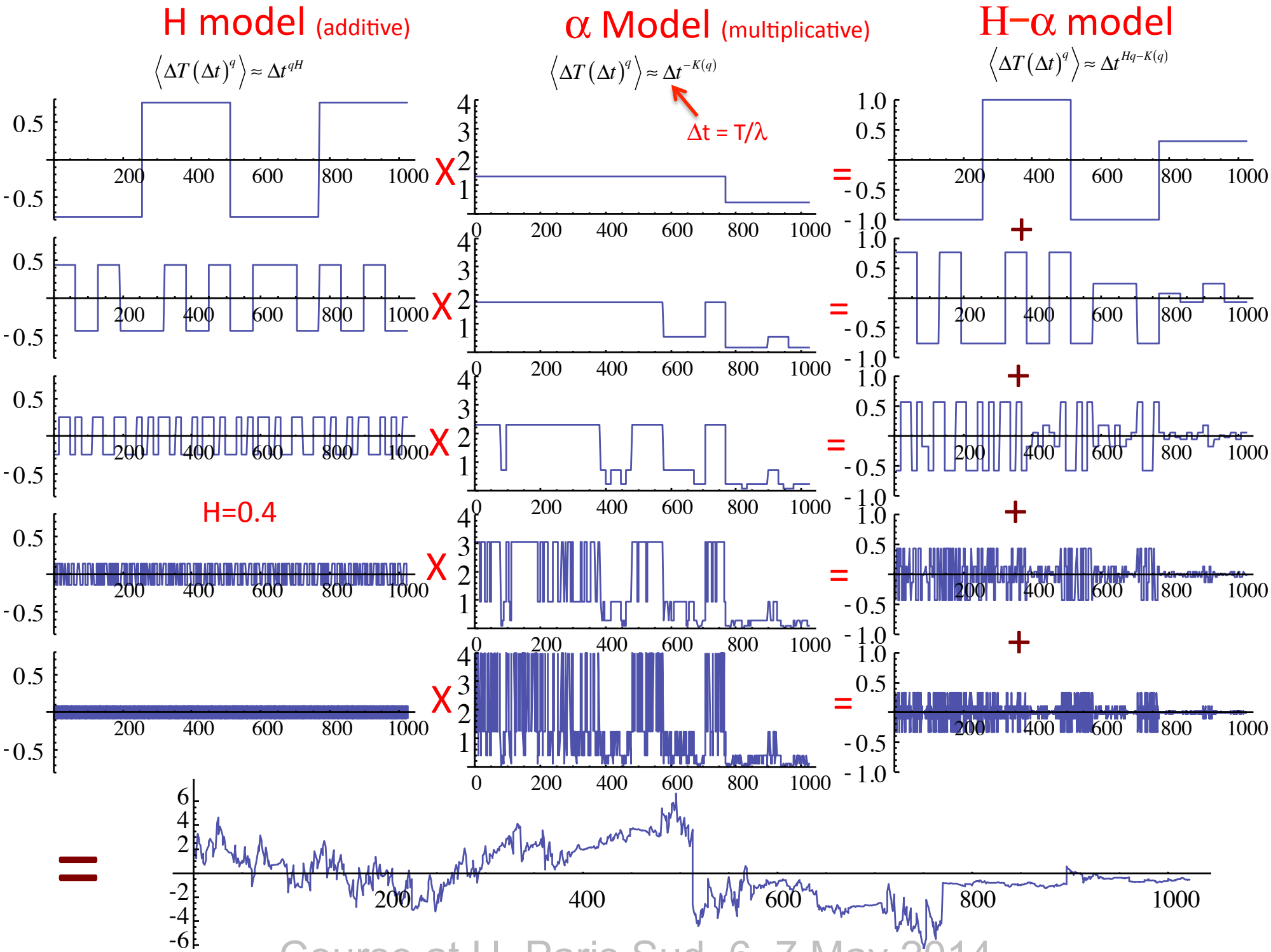
H model (additive)
$\langle \Delta T (\Delta t)^q \rangle \approx \Delta t^{qH}$
α Model (multiplicative)
$\langle \Delta T (\Delta t)^q \rangle \approx \Delta t^{-K(q)}$
Δt = T/λ
H−α model
$\langle \Delta T (\Delta t)^q \rangle \approx \Delta t^{Hq-K(q)}$
H=0.4
X
=
+
=

Simulating isotropic continuous in scale multifractals

Continuous in scale multifractal modeling

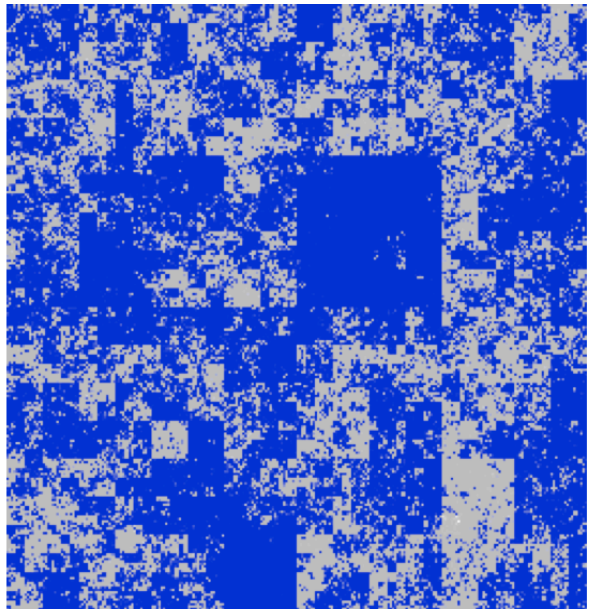

A discrete in scale simulation of a universal multifractal with basic scale ratio $\lambda_0 = 2$, $\lambda = 2^9$, $\alpha = 1.8$, C_1=0.1.

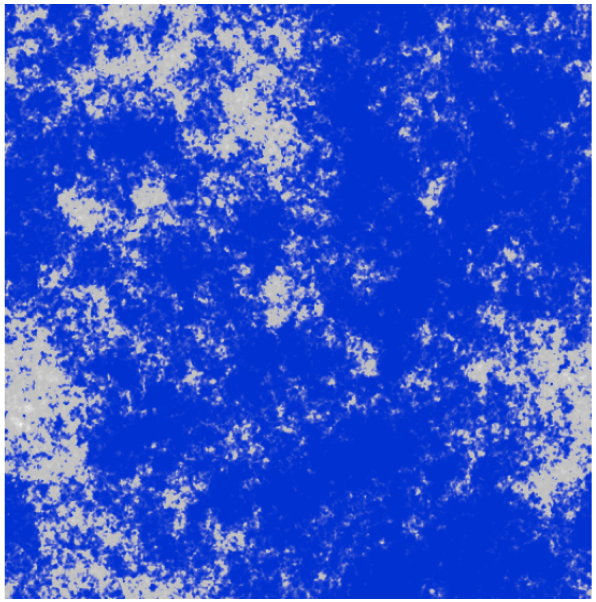

The corresponding continuous in scale simulation.

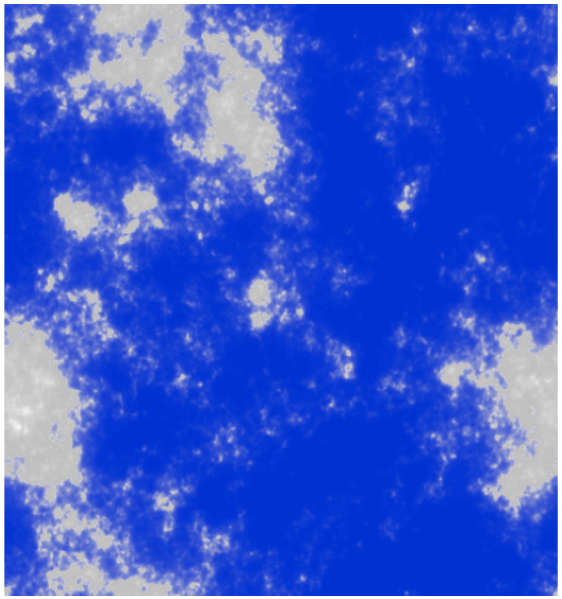

Same as at left but with an additional fractional integration of order $H = 1/3$ (a scale invariant smoothing); to simulate a turbulent passive scalar density; notice that the structures are smoothed.

Multiplicative Cascade processes

The process

$$\varepsilon_\lambda = e^{\Gamma_\lambda}$$

Multifractal process over scale range λ= Multiplicative cascade

The generator= Additive process

$$\Gamma(\underline{r}) \propto C_1^{1/\alpha} \gamma_\alpha(\underline{r}) * |\underline{r}|_{[1,\lambda^{-1}]}^{-D/\alpha'}$$

Dimension of space

Auxiliary variable α'

$$\frac{1}{\alpha'} + \frac{1}{\alpha} = 1$$

$$\tilde{\Gamma}(\underline{k}) = \tilde{\gamma}_\lambda(\underline{k}) |\underline{k}|^{-D/\alpha}$$

The codimension of the mean= Amplitude of the generator, sparseness of ε

i.i.d. Levy noise index α= subgenerator

Convolution with singularity over range 1 to λ^{-1}

Fourier space= power law filter

The statistics

$$\langle \varepsilon_\lambda^q \rangle = \lambda^{K(q)}$$

General multifractal statistics, convex K(q)

$$K(q) = \frac{C_1}{\alpha - 1}(q^\alpha - q)$$
$$q < q_D$$

Universal multifractals ("multiplicative central limit theorem")

$$\Pr(\varepsilon_\lambda > s) \approx s^{-q_D}$$
$$s >> 1$$

Extremes: "Fat tails"

Levy sub generators $\gamma_\alpha(\underline{r})$

Gaussian (α =2)

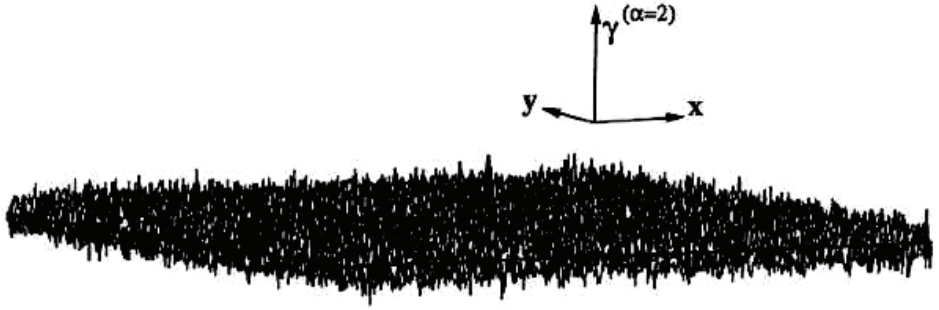

Levy (α =1.6)

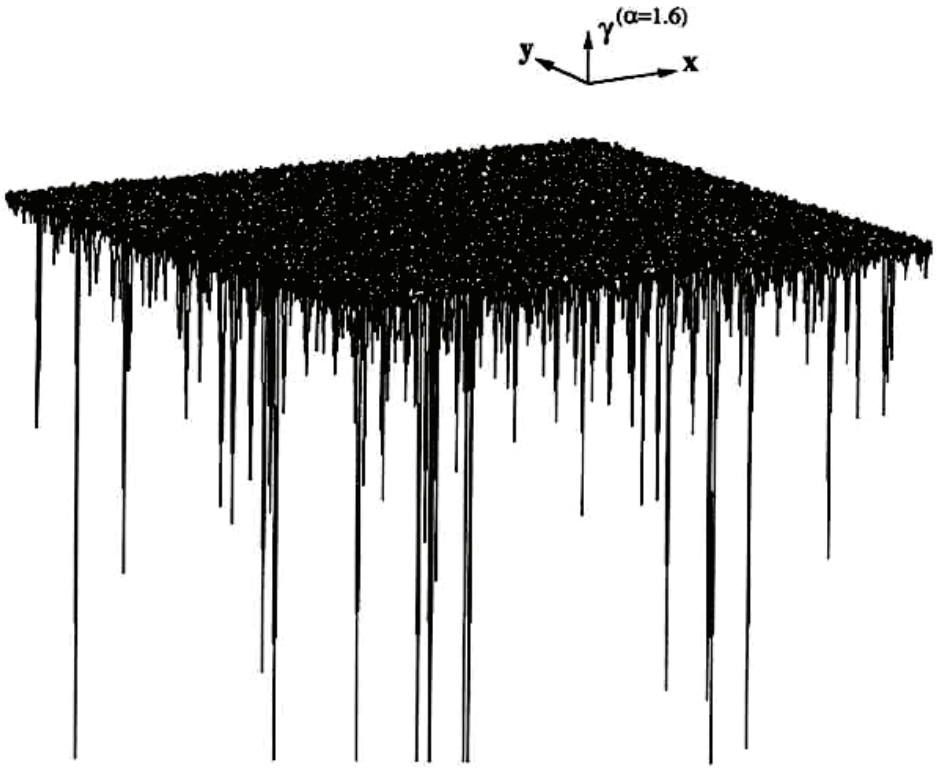

A comparison of the Gaussian (α =2, top) and Levy (α =1.6, bottom) subgenerators γ_α showing that whereas the former is both positive – negative symmetric with low amplitude excursions, the latter is asymmetric with huge (algebraic) excursions for negative values.

Fractionally Integrated Flux (FIF) model (both additive and multiplicative)

Object: to yield: $\Delta I(\underline{\Delta r}) = \varepsilon_{\underline{\Delta r}} |\underline{\Delta r}|^H$ S+L 1987

The process

$$I(\underline{r}) = \varepsilon_\lambda(\underline{r}) * |\underline{r}|^{-(D-H)} \quad \longleftrightarrow \quad \tilde{I}(\underline{k}) = \tilde{\varepsilon}_\lambda(\underline{k}) |\underline{k}|^{-H}$$

Convolution= fractional integration order H

Fourier space= power law filter

The statistics

$$S_q(\underline{\Delta r}) = \left\langle \Delta I(\underline{\Delta r})^q \right\rangle = \left\langle \varepsilon_\lambda^q \right\rangle |\underline{\Delta r}|^{qH} = |\underline{\Delta r}|^{\xi(q)} \qquad \xi(q) = qH - K(q)$$

q^{th} order structure function

fluctuation

Note: $\lambda = L/|\underline{\Delta r}|$, $\left\langle \varepsilon_\lambda^q \right\rangle = \lambda^{K(q)}$

structure function exponent

FIF simulations 1-D

FIF simulations with α = 0.3, 0.5, …1.9, (bottom to top), C_1 = 0.1, each offset for clarity, each with the same random seed.

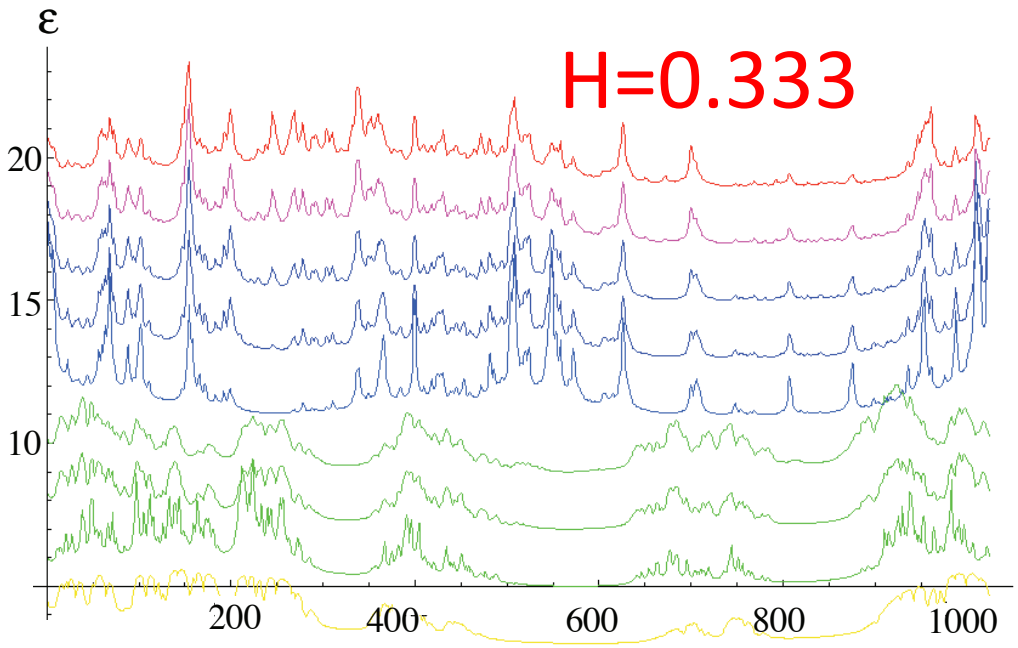

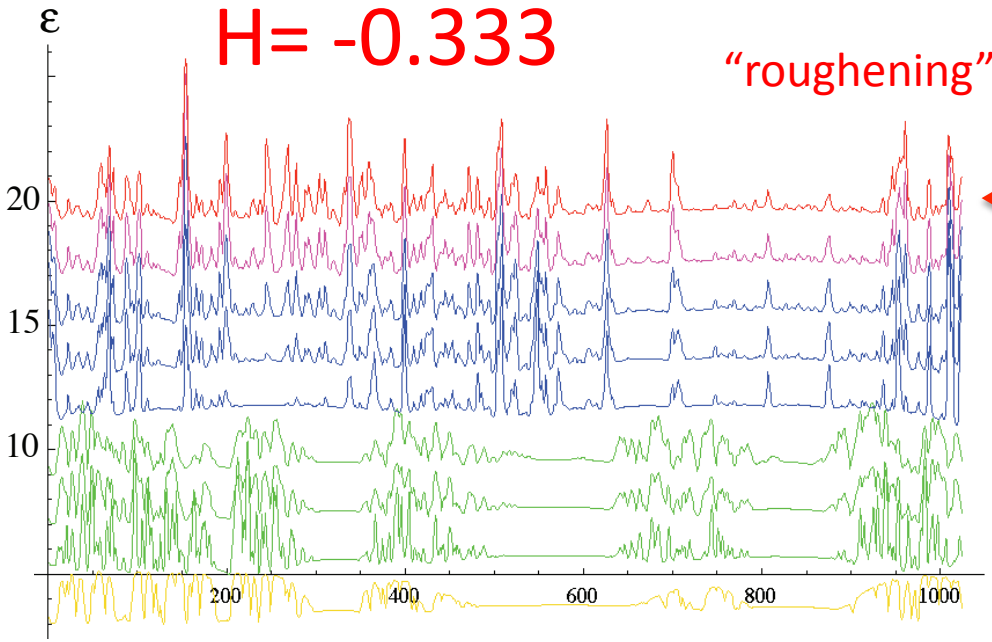

"roughening"

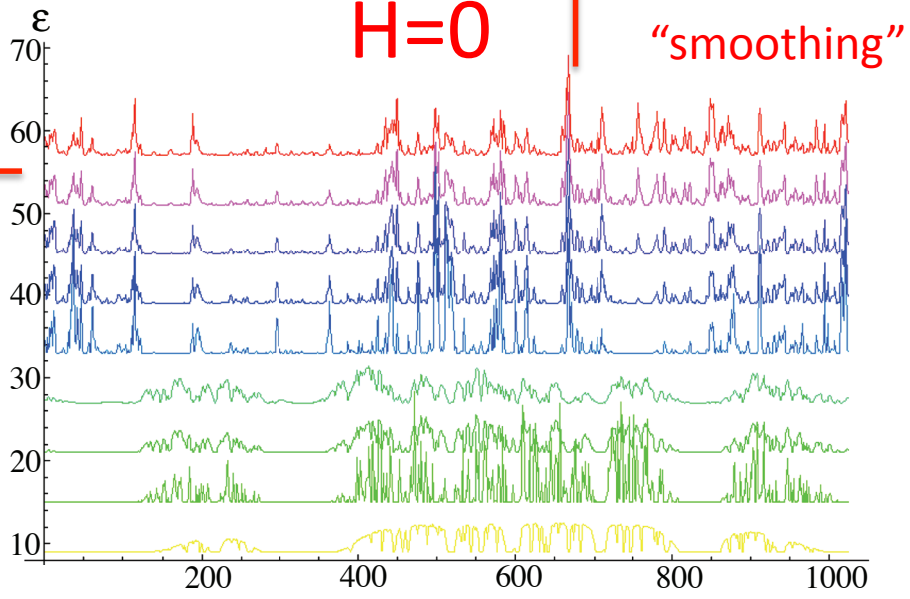

"smoothing"

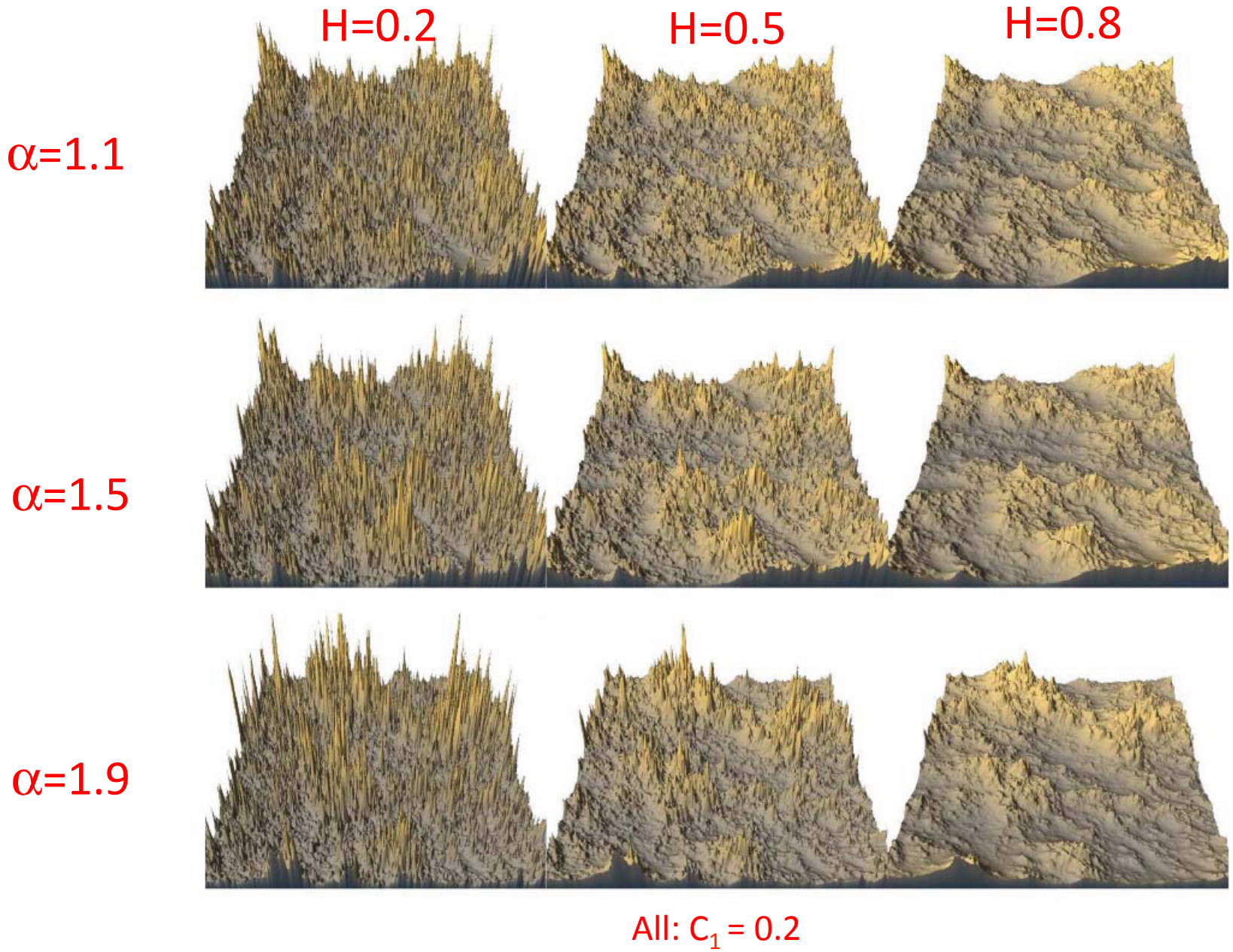

Isotropic (i.e. self-similar) multifractal simulations showing the effect of varying the parameters α and H (C_1=0.1 in all cases). From left to right, H = 0.2, 0.5 and 0.8. From top to bottom, α =1.1, 1.5 and 1.8. As H increases, the fields become smoother and as α decreases, one notices more and more prominent "holes" (i.e. low smooth regions). The realistic values for topography (α=1.79, C_1=0.12, H=0.7) correspond to the two lower right hand simulations. All the simulations have the same random seed.

FIF on a sphere

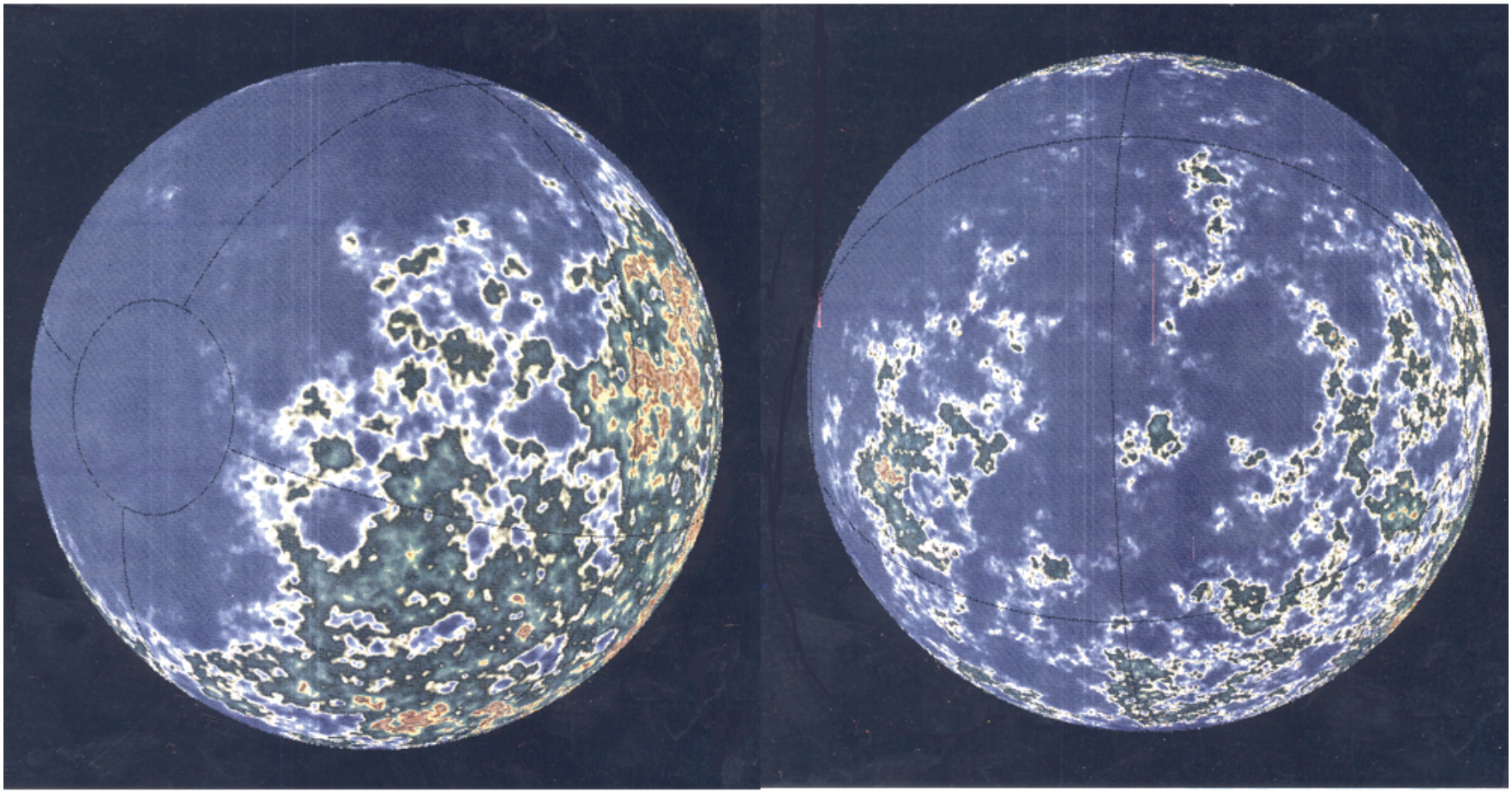

A simulation of an (isotropic) multifractal topography on a sphere using the spherical harmonic method discussed in the appendix (both sides of a single simulation are shown, using false colours). The simulation parameters are close to the measured values: α =1.8, C_1= 0.1, H = 0.7. The absence of mountain "chains" and other typical geomorphological features are presumably due to the absence of anisotropy.

Generalized Scale Invariance

CASCADES

(isotropic)

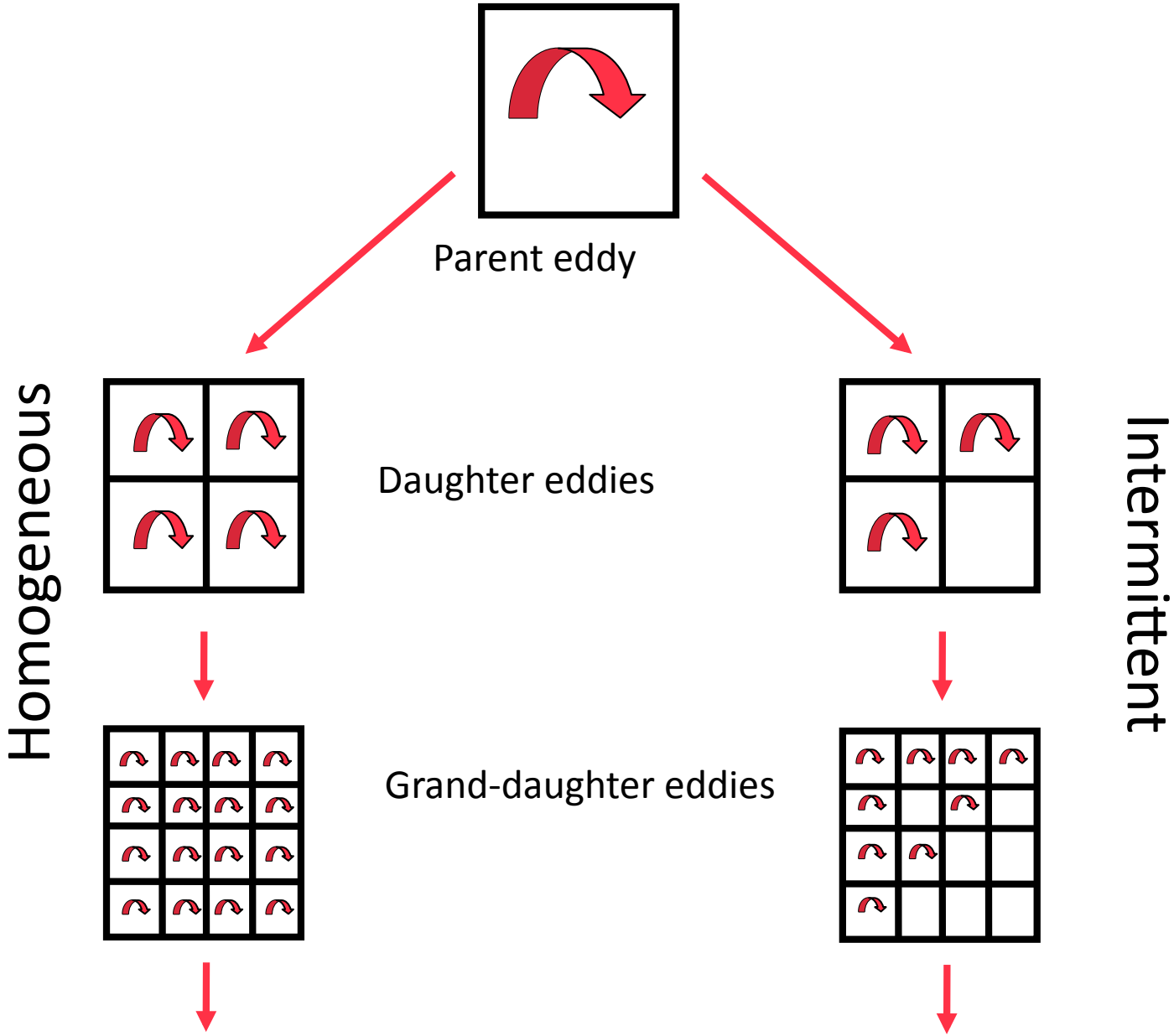

Stratified CASCADES

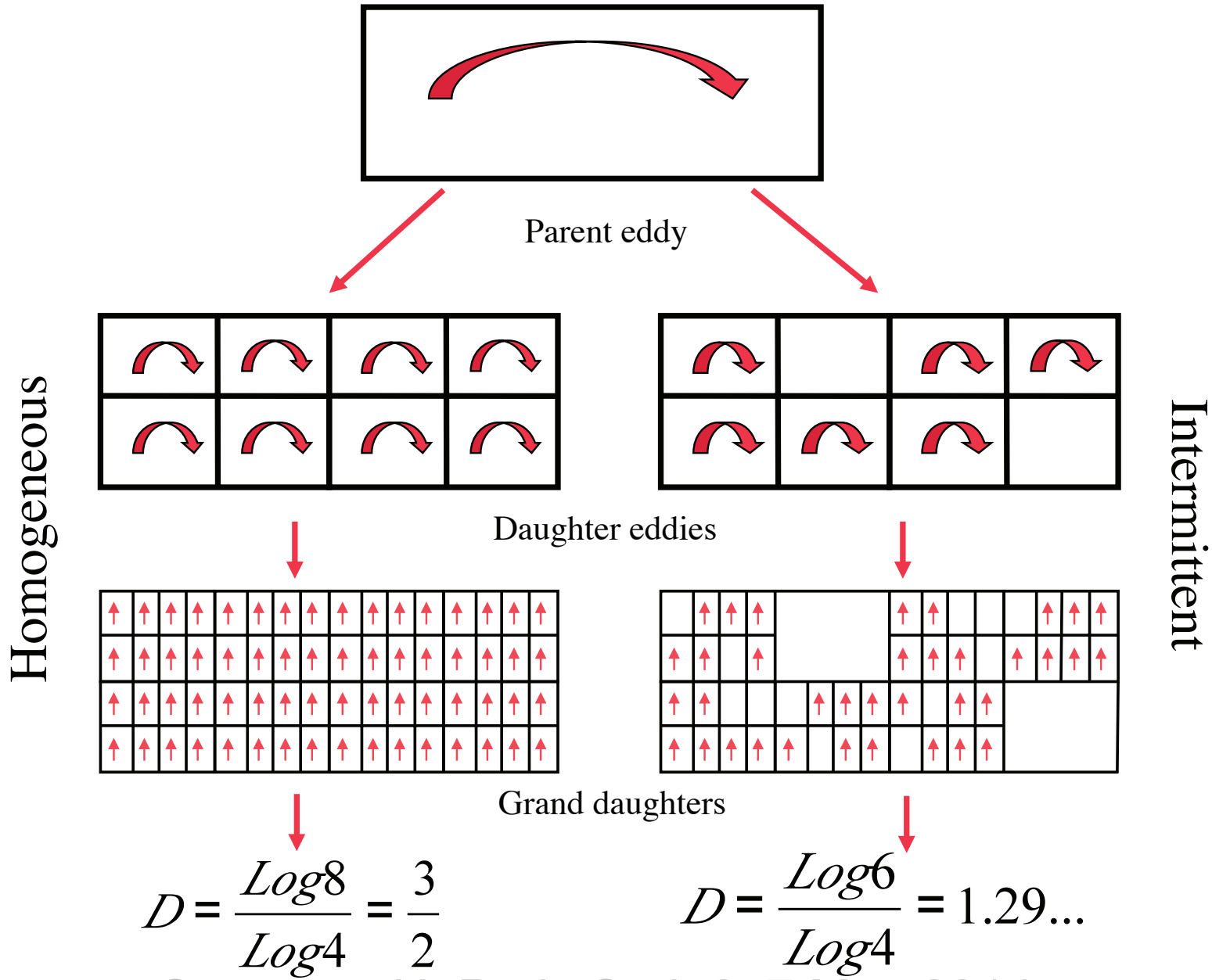

The unity of clouds and rocks

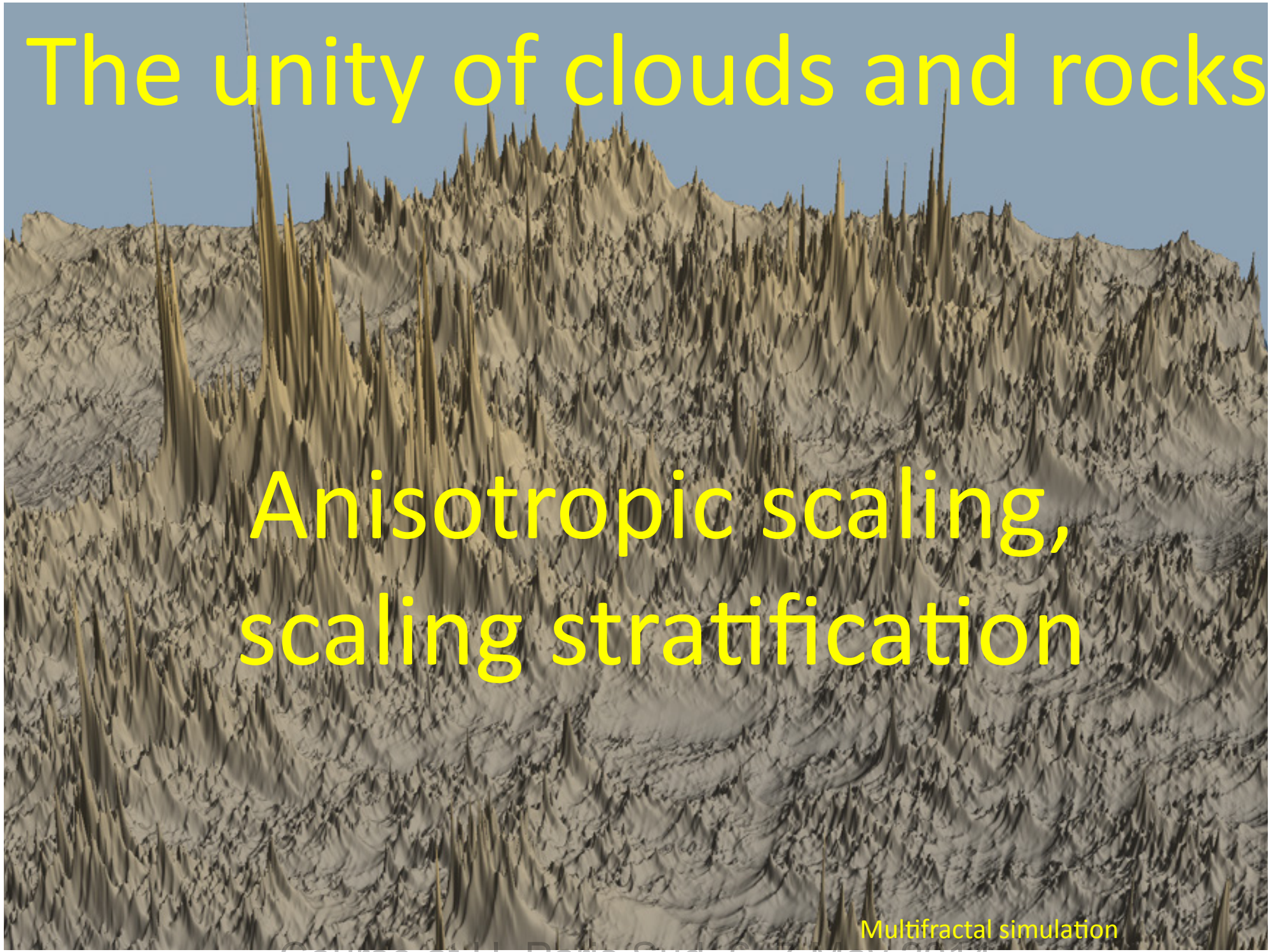

Anisotropic scaling, scaling stratification

Multifractal simulation

AERIAL Lidar Data

(courtesy of K. Strawbridge)

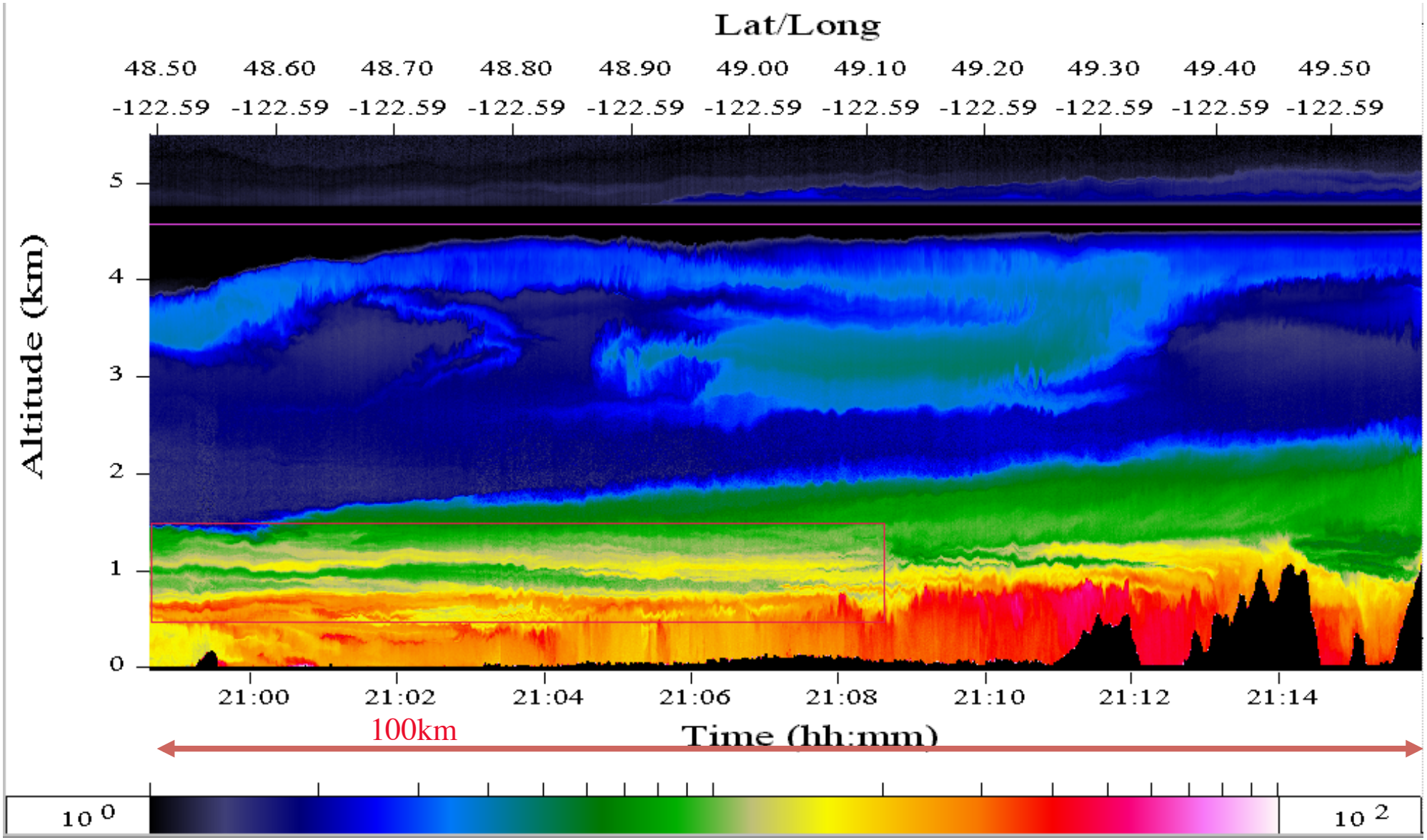

Zoomed

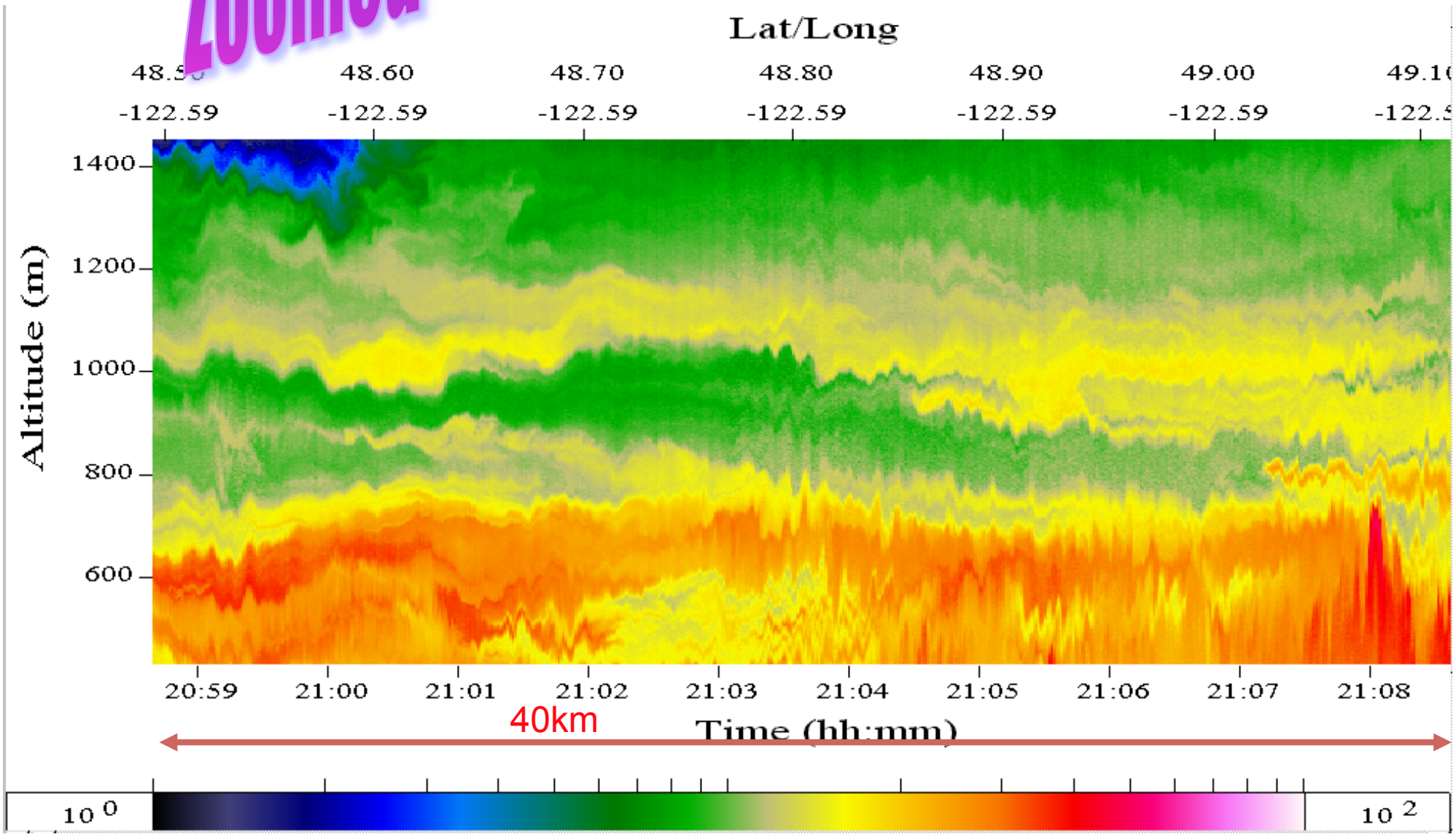
Lat/Long
48.60
48.70
48.80
48.90
49.00
-122.59
1400
1200
1000
800
600
Altitude (m)
20:59
21:00
21:01
21:02
21:03
21:04
21:05
21:06
21:07
21:08
40km
Time (hh:mm)
10 0
10 2

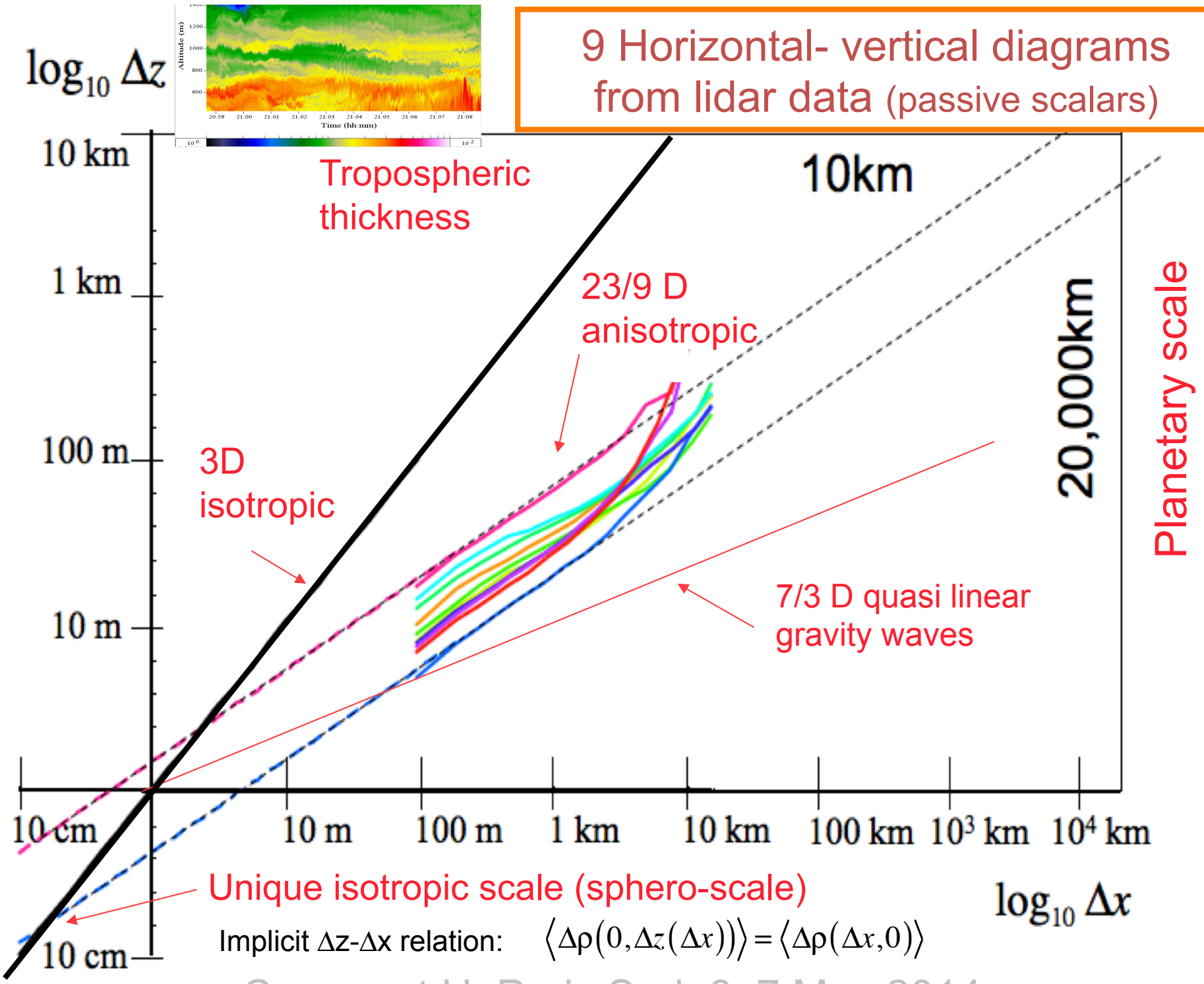
9 Horizontal- vertical diagrams from lidar data (passive scalars)
$\log_{10} \Delta z$
10 km
1 km
100 m
10 m
10 cm
Tropospheric thickness
10km
23/9 D anisotropic
3D isotropic
7/3 D quasi linear gravity waves
20,000km
Planetary scale
10 cm
10 m
100 m
1 km
10 km
100 km
10^3 km
10^4 km
$\log_{10} \Delta x$
Unique isotropic scale (sphero-scale)
Implicit Δz-Δx relation: $\langle \Delta\rho(0, \Delta z(\Delta x)) \rangle = \langle \Delta\rho(\Delta x, 0) \rangle$

The physical scale function and differential scaling

$$|\underline{\Delta r}| \rightarrow \|\underline{\Delta r}\|$$

Usual distance (=vector norm)

Scale function (scale notion)

Scale symmetry $\left\|\lambda^{-G}\underline{r}\right\| = \lambda^{-1}\|\underline{r}\|$

"canonical" scale function:

$$\|(\Delta x, \Delta z)\| = l_s \left(\left(\frac{\Delta x}{l_s} \right)^2 + \left(\frac{\Delta z}{l_s} \right)^{2/H_z} \right)^{1/2}$$

$$G = \begin{pmatrix} 1 & 0 \\ 0 & H_z \end{pmatrix}$$

Vertical sections

Isotropic function $H_z=1$

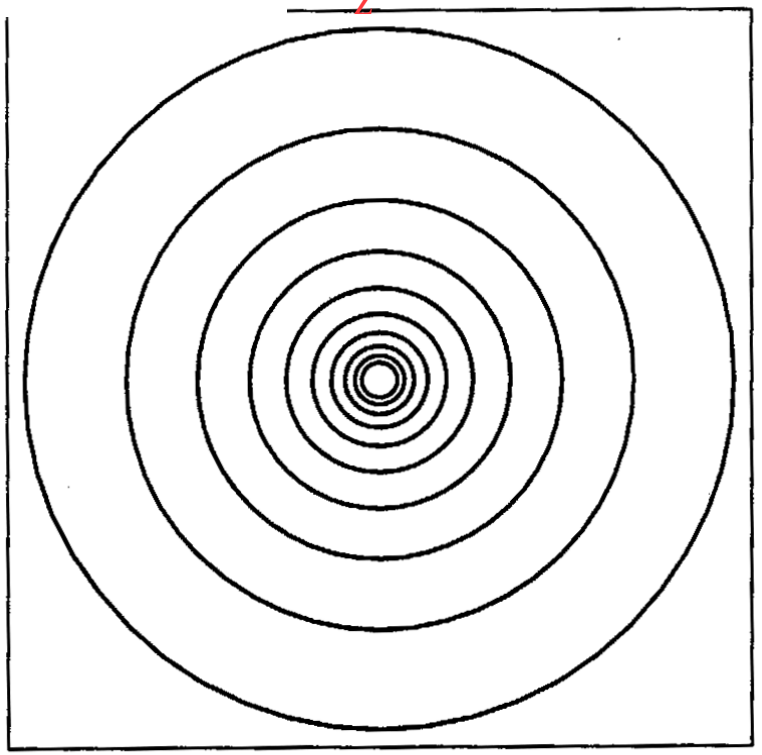

Anisotropic physical scale function $H_z=5/9$

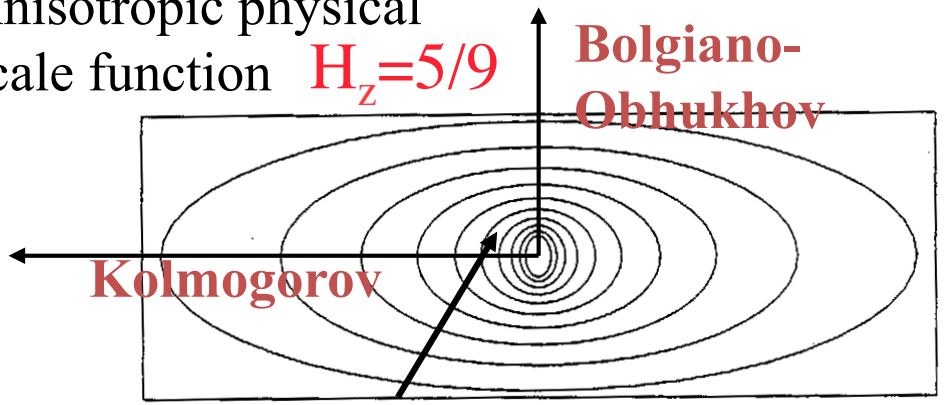

Sphero-scale

Anisotropic Scaling

D_{el}=2

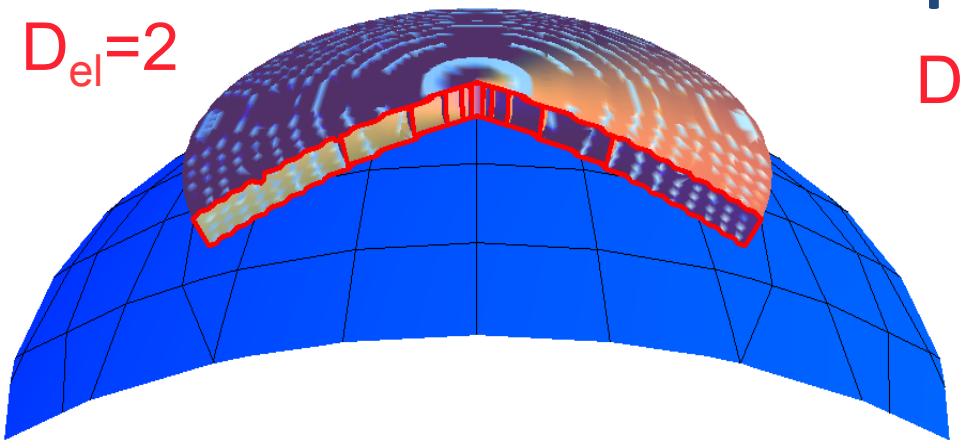

D_{el}=2.33

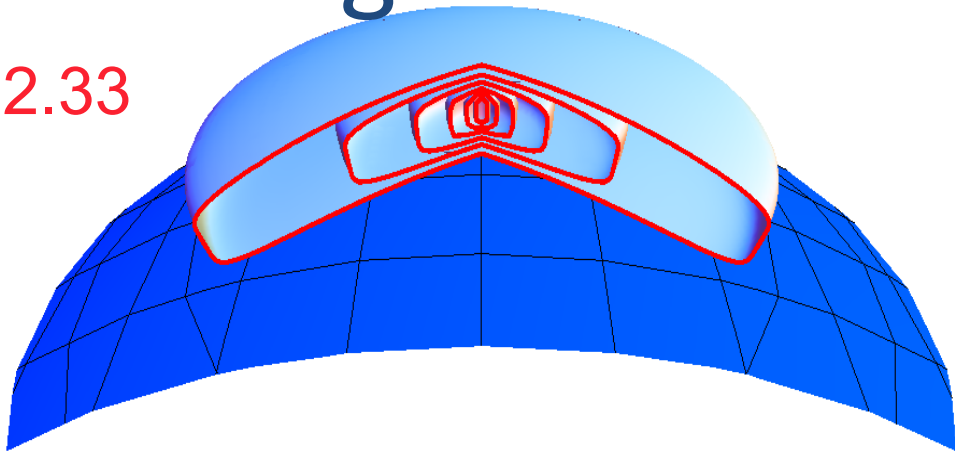

c.f. empirical: 2.57

D_{el}=23/9=2.55

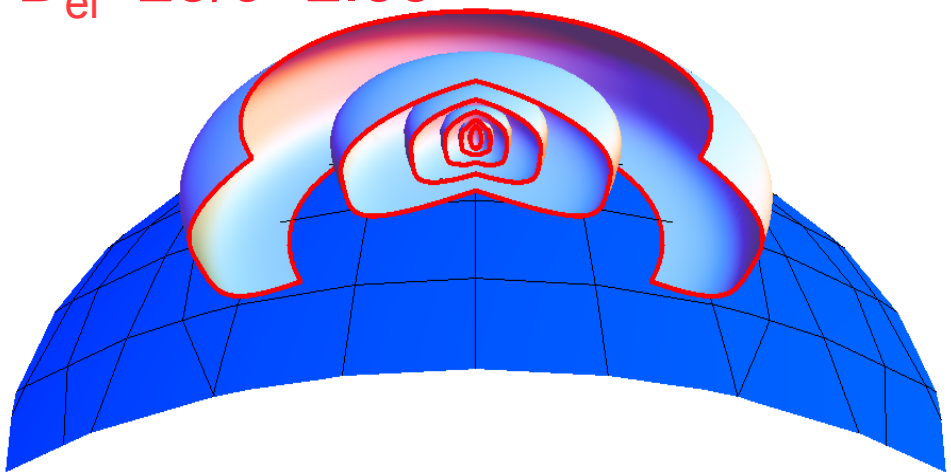

D_{el}=3

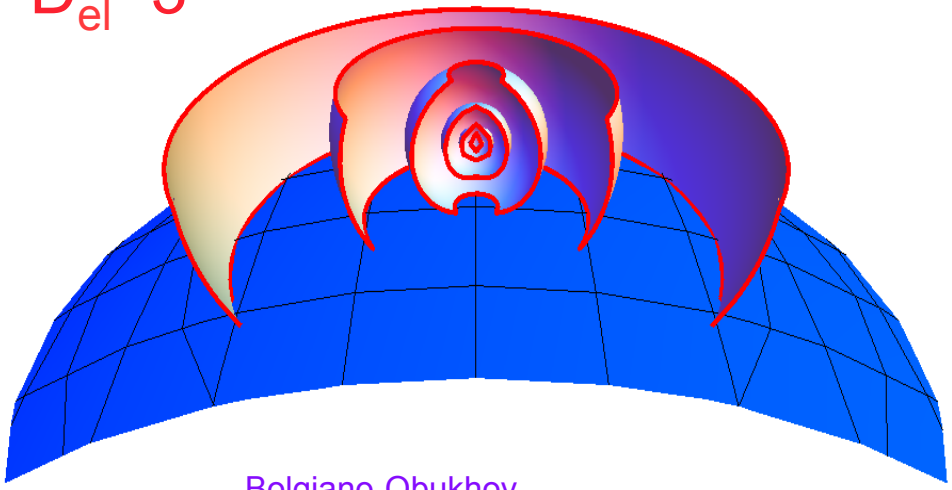

Bolgiano-Obukhov

The 23/9D model:

$$\underbrace{\Delta v(\Delta x) = \varepsilon^{1/3}\Delta x^{1/3}}_{\text{Kolmogorov}};\quad \overbrace{\Delta v(\Delta z) = \phi^{1/5}\Delta z^{3/5}}^{\text{Bolgiano-Obukhov}} \qquad H_z=(1/3)/(3/5)=5/9$$

Volume≈LxLxL^{Hz}≈L^{Del} $\qquad D_{el}=2+H_z=23/9$

Fly by of anisotropic (multifractal, cascade) cloud

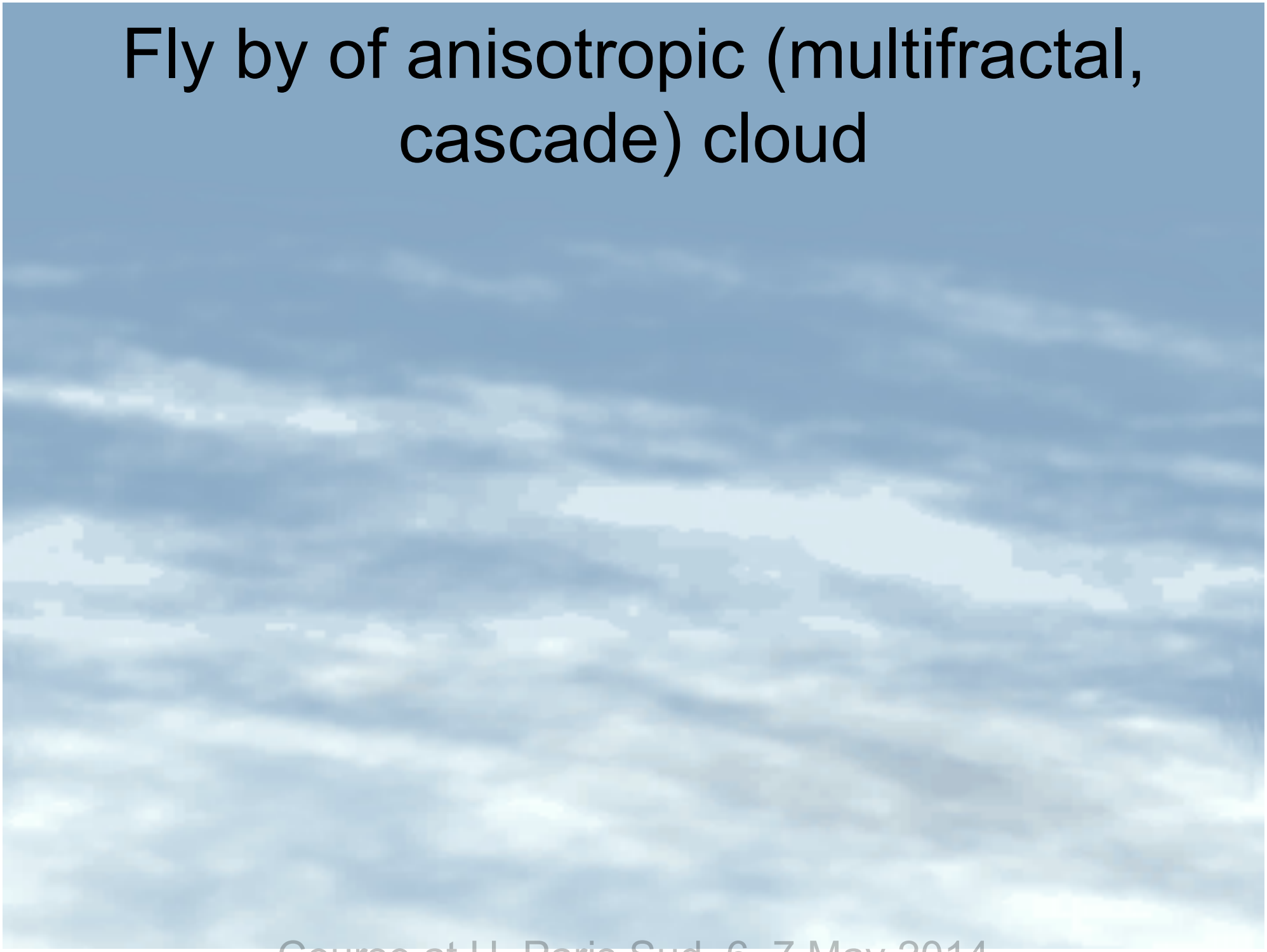

Flyby 1

This 4096X4096 simulation is flown over

α=1.8, C_1=0.12, H=0.7

$$G = \begin{pmatrix} 0.65 & -0.1 \\ 0.1 & 1.35 \end{pmatrix}$$

l_s=64 pixels

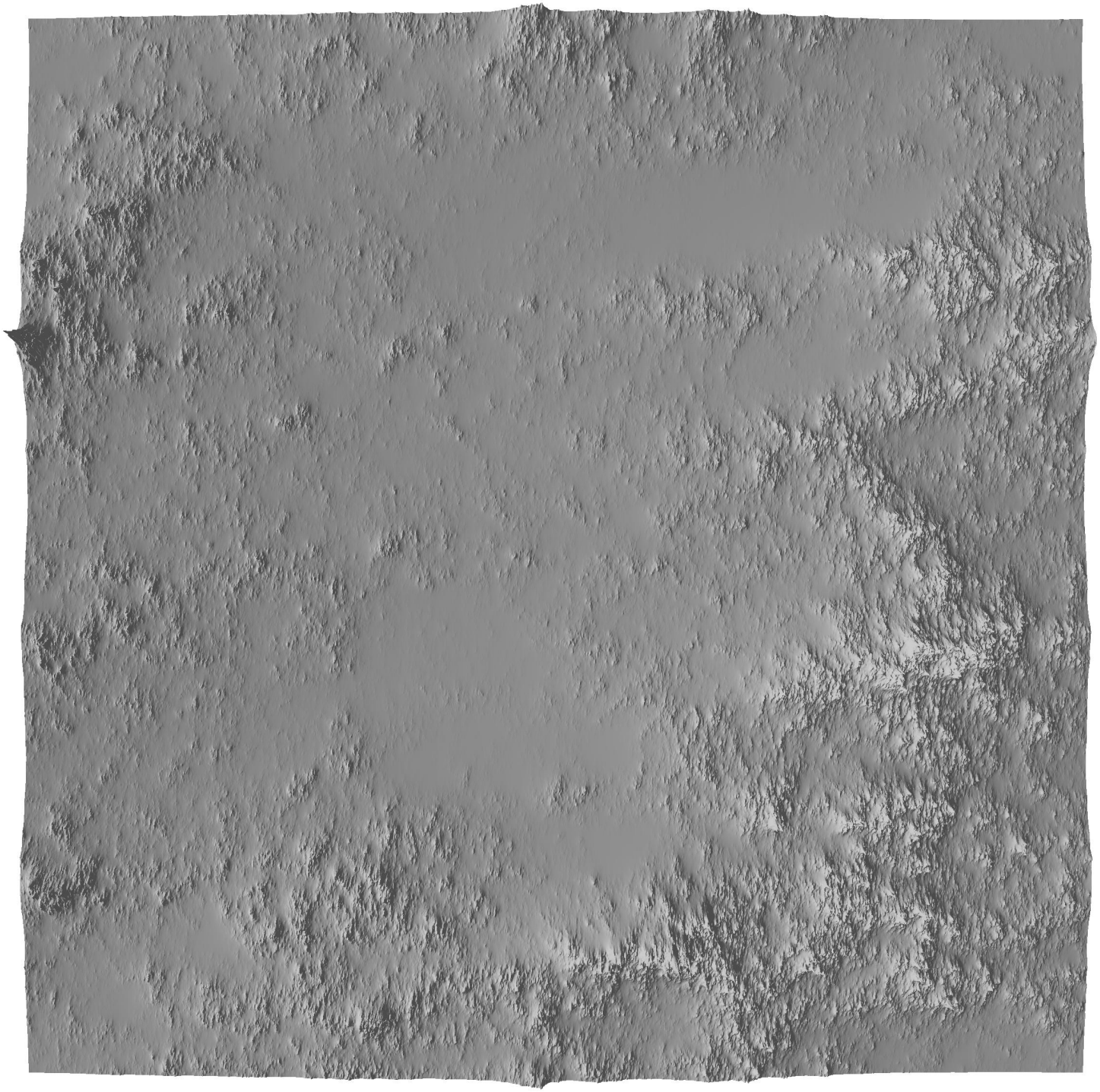

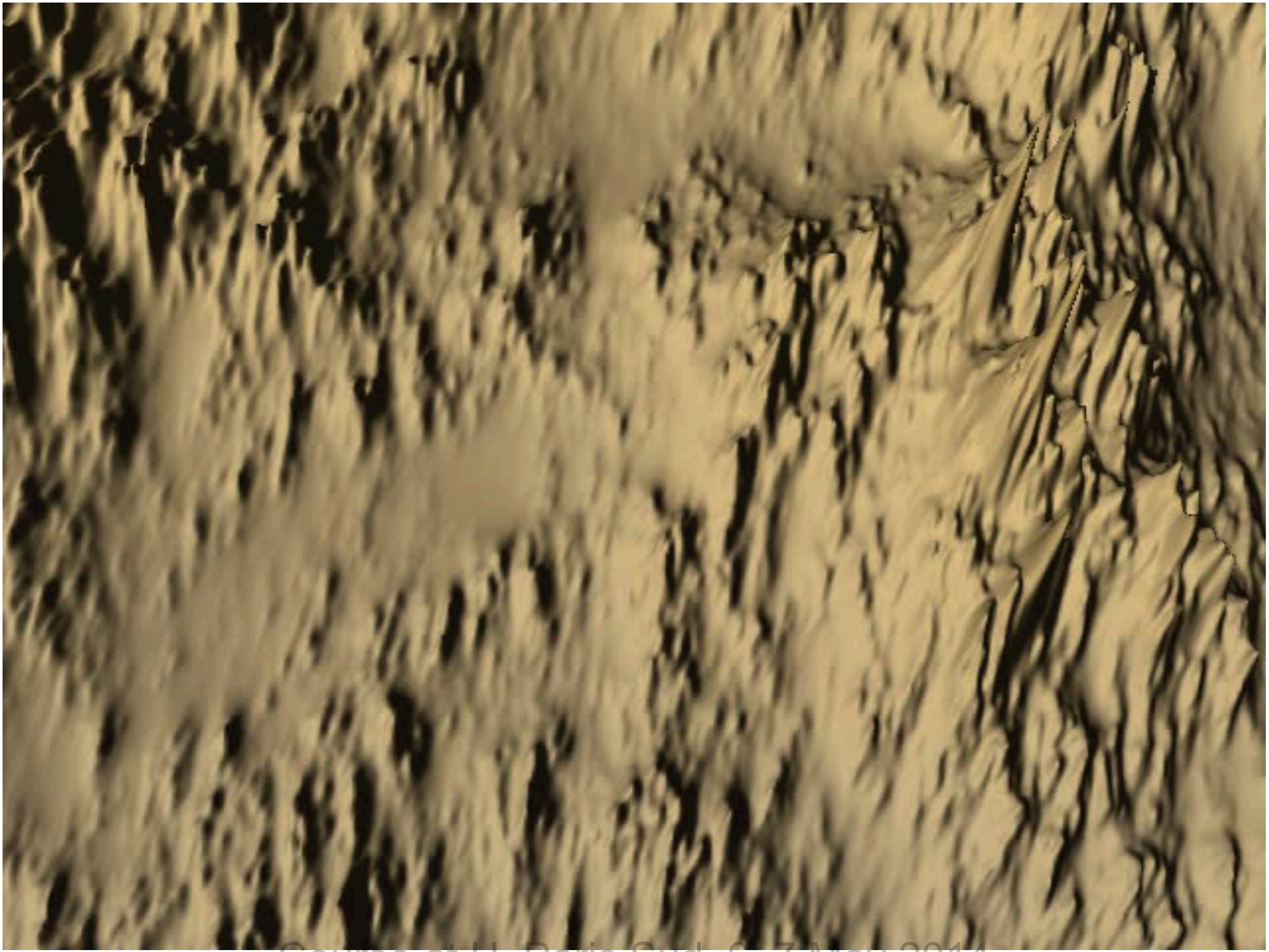

Horizontal versus vertical borehole rock densities

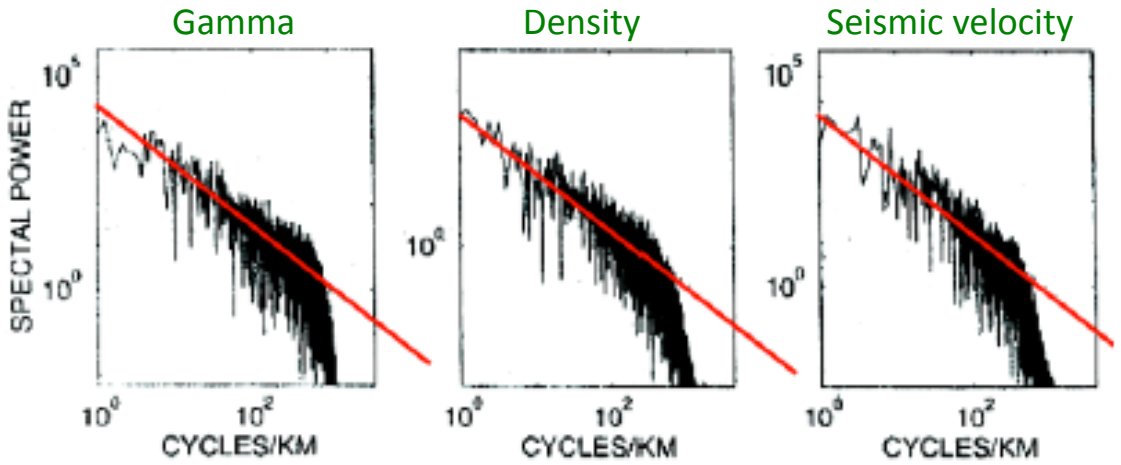

Horizontal boreholes (β_h =1.4)

$H_z = (\beta_h - 1)/(\beta_v - 1) = 2$

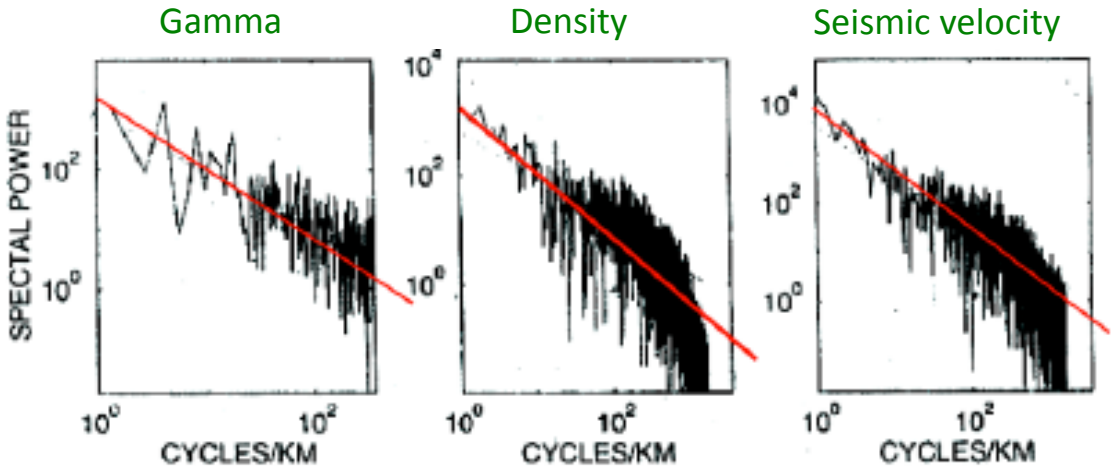

Vertical boreholes (β_v =1.2)

Lovejoy and Schertzer 2007 (adapted from Leary 1997)

Stratified Multifractal Crust, Mantle rock density simulation

Vertical cross-sections $D_{el}=3$

Lithospheric rock density

128km

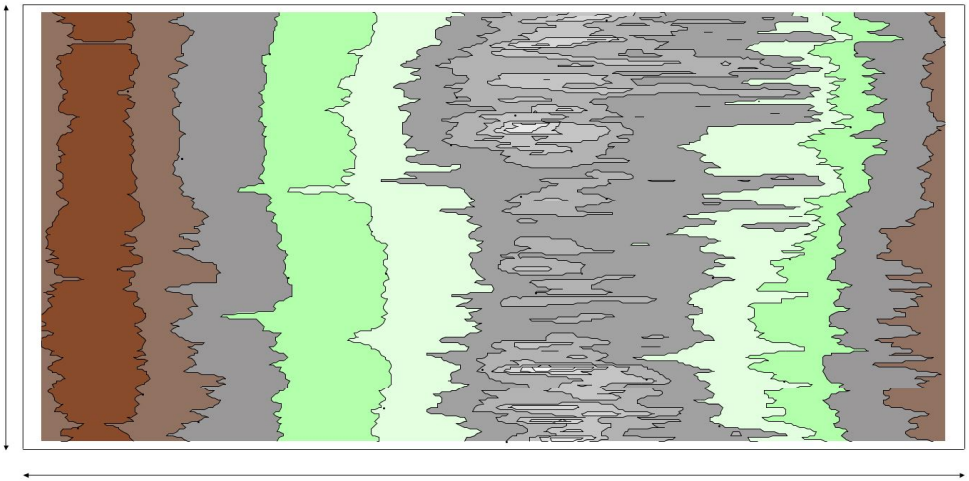

512km

Sphero-scale l_s=256km, with 1 pixel = 1km.

Mantle density

3000km

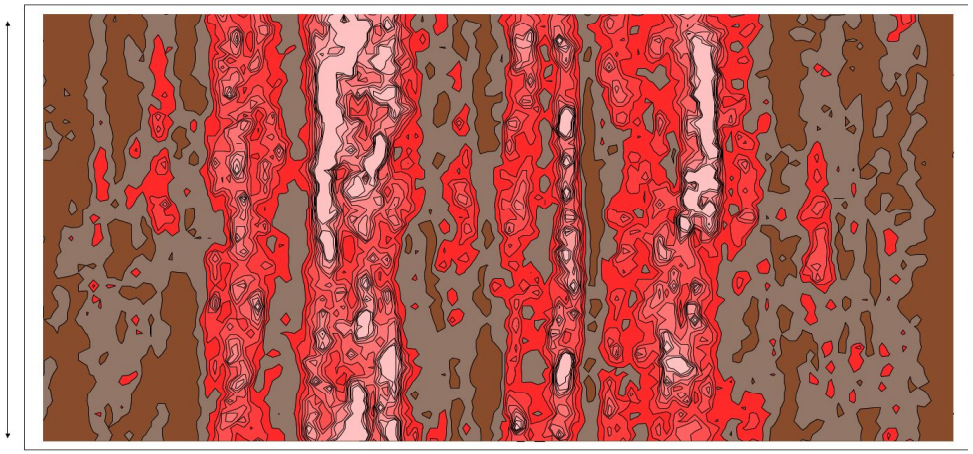

6000km

Sphero scale = 1 pixel. Each pixel is 50 km, sphero-scale = 25km. Hot (low density) plumes shown as white/red (this is a model for either density or temperature fluctuations (the two being proportional; we assume constant expansion coefficient). These are for fluctuations with respect to the mean vertical profile

Simulated magnetization field for horizontally isotropic crustal magnetization

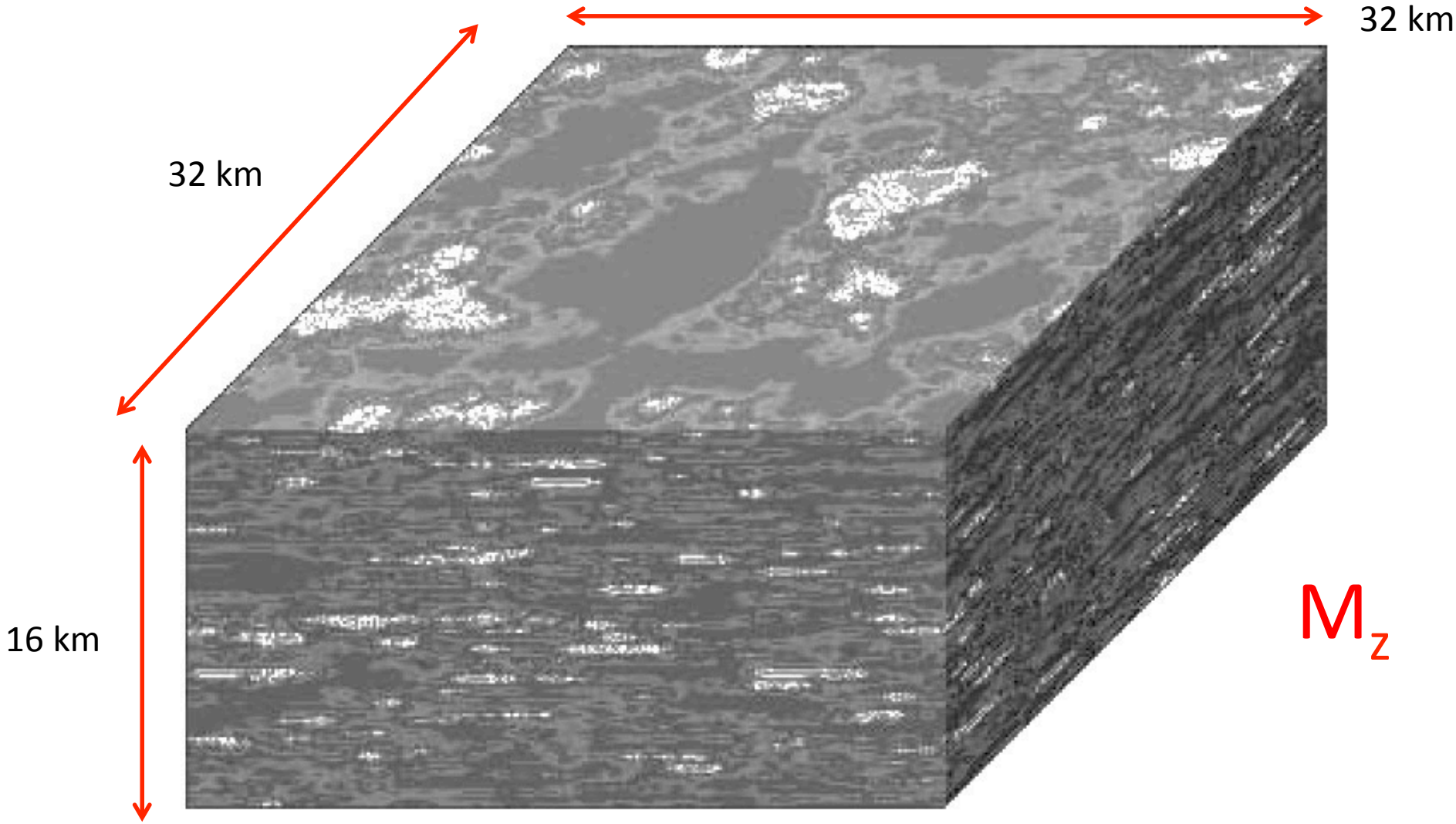

Parameters: are H_z =1.7, s = 4, H = 0.2, α =1.98, C_1 = 0.08, l_s = 2500 km,

The unity of geosciences: clouds and rocks

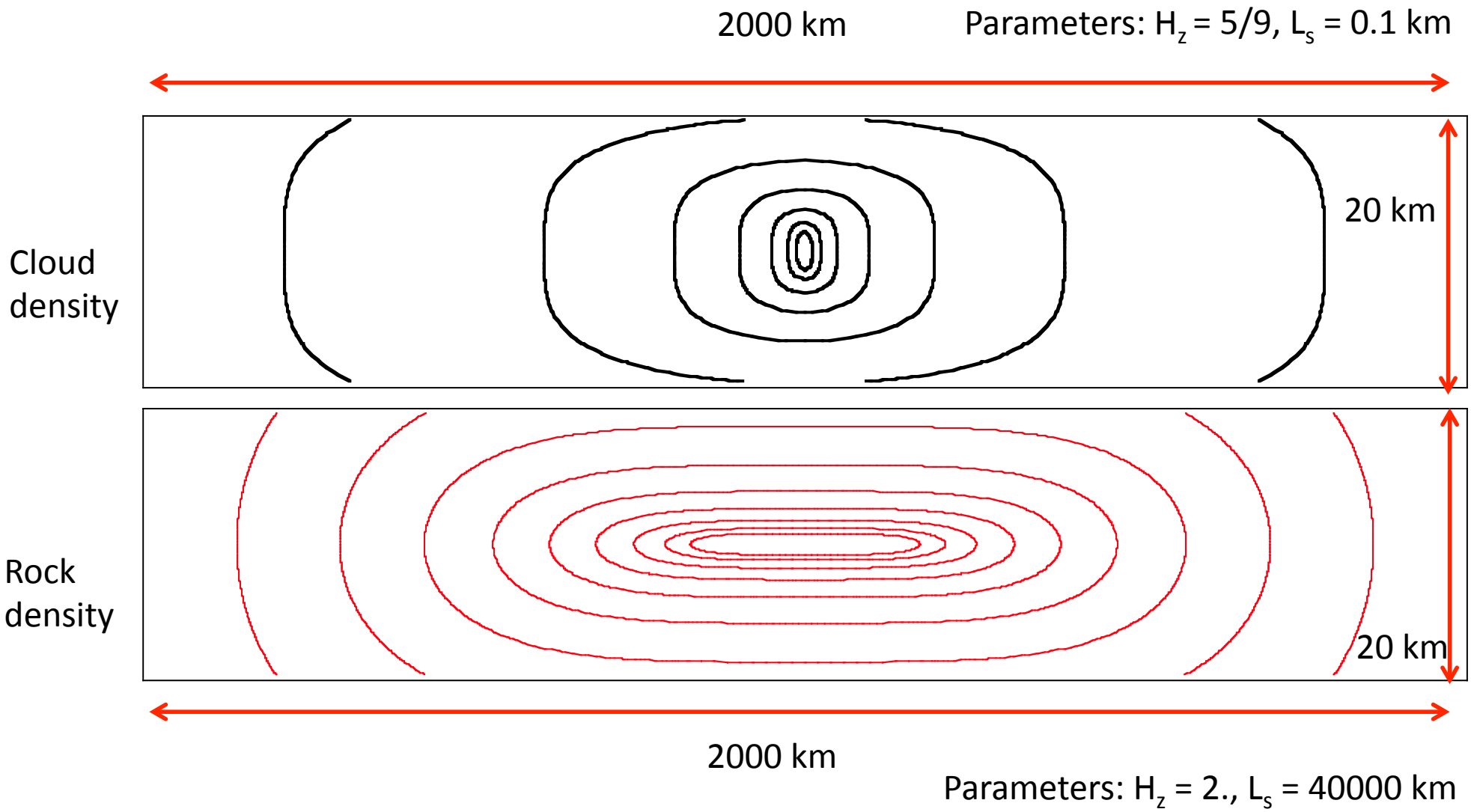

aspect ratios = 1/5

Generalized Scale Invariance

The scale changing operator T_λ which transforms the scale of vectors by scale ratio λ

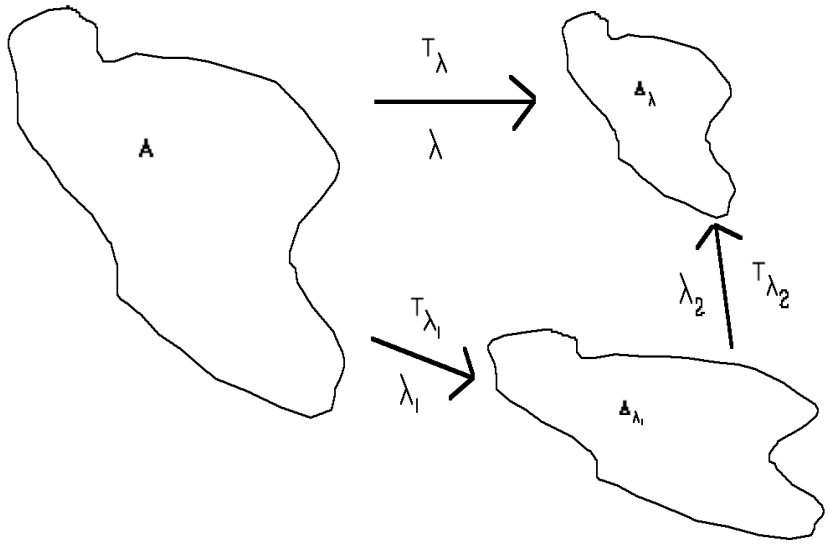

T_λ is the rule relating the statistical properties at one scale to another and involves only the scale ratio. This implies that T_λ has certain properties. In particular, if and only if $\lambda_1\lambda_2 = \lambda$, then:

$$B_\lambda = T_\lambda B_1 = T_{\lambda_1\lambda_2} B_1 = T_{\lambda_1} B_{\lambda_2} = T_{\lambda_2} B_{\lambda_1}$$

it is also commutative $\quad T_\lambda = T_{\lambda_2} T_{\lambda_1} = T_{\lambda_1} T_{\lambda_2}$

This implies that T_λ is a one parameter multiplicative group with parameter λ: $\boxed{T_\lambda = \lambda^{-G}}$

One parameter Lie group, G= generator

Example of anisotropic "Blow down"

$$T_\lambda = \lambda^{-G}$$

A generalized blow-down with increasing of the acronym "NVAG". If $G = I$, we would have obtained a standard reduction, with all the copies uniformly reduced converging to the centre of the reduction. Here the parameters are $G = \begin{pmatrix} 1.3 & -1.3 \\ 0.3 & 0.7 \end{pmatrix}$

and each successive reduction is by 28%.

Scale function equation

$$\left|\left|\lambda^{-G}\underline{r}\right|\right| = \lambda^{-1}\left|\left|\underline{r}\right|\right|$$

generator — Scale ratio — Scale function: size of vector $\underline{r}$

G=identity: $\left|\left|\underline{r}\right|\right| \longrightarrow \left|\underline{r}\right|$

$$\left|\lambda^{-1}\underline{r}\right| = \lambda^{-1}\left|\underline{r}\right|$$

Scale functions in linear GSI (position independent)

Isotropic (self similar)

$$T_\lambda = \lambda^{-G}$$

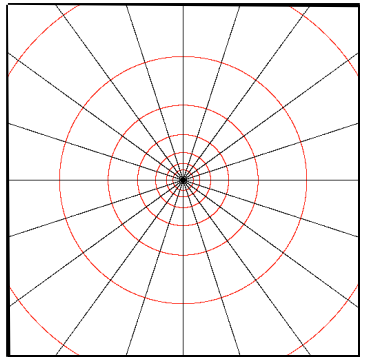

$$G = \begin{pmatrix} 1 & 0 \\ 0 & 1 \end{pmatrix}$$

Scale functions

$$\left|\left|\lambda^{-G}\underline{r}\right|\right| = \lambda^{-1}\left|\left|\underline{r}\right|\right|$$

Stratification dominant (real eigenvalues)

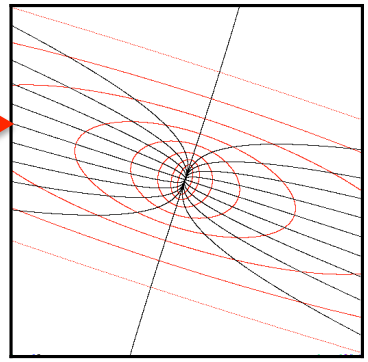

$$G = \begin{pmatrix} 1.35 & 0.25 \\ 0.25 & 0.65 \end{pmatrix}$$

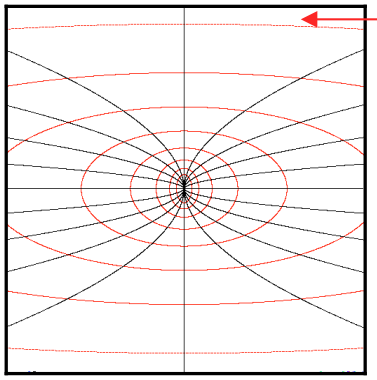

Scale isolines in red $\left|\left|\underline{r}\right|\right|$=contstant

Self-affine

$$G = \begin{pmatrix} 1.35 & 0 \\ 0 & 0.65 \end{pmatrix}$$

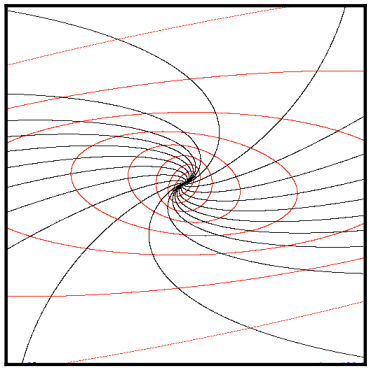

Rotation dominant (complex eigenvalues)

$$G = \begin{pmatrix} 1.35 & -0.45 \\ 0.85 & 0.65 \end{pmatrix}$$

Overall

Isotropy $\longrightarrow$ **anisotropy**

$$|\underline{x}| \rightarrow \|\underline{x}\|; \quad D \rightarrow D_{el}$$

Roundish unit ball

k =0: we vary *r* (denoted *i*) from -0.3, -0.15, …0.45 left to right and *e* (denoted *j*) from -0.5, -0.25, …0.75 top to bottom. On the right we show the contours of the corresponding scale functions.

$$G = \begin{pmatrix} 1 & r-e \\ r+e & 1 \end{pmatrix}$$

r

e

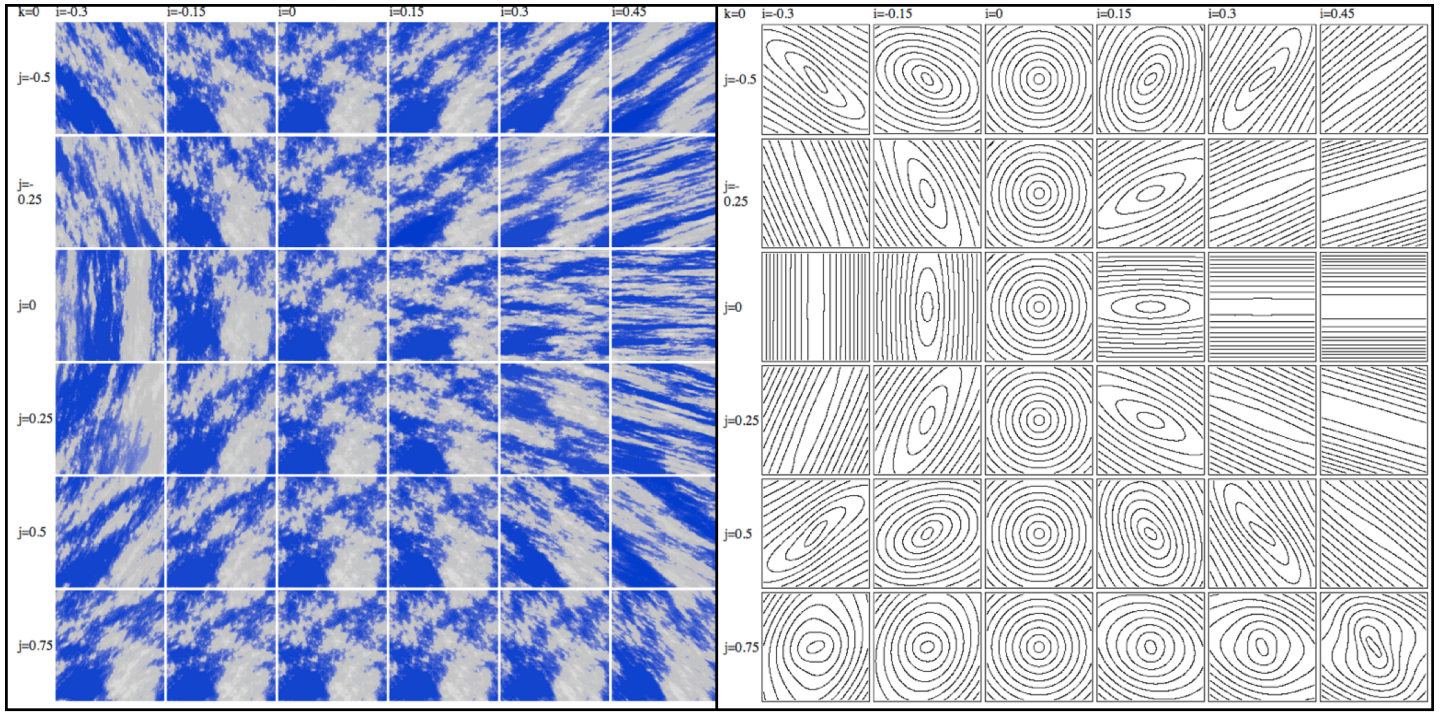

Highly anisotropic unit ball: *k* =10

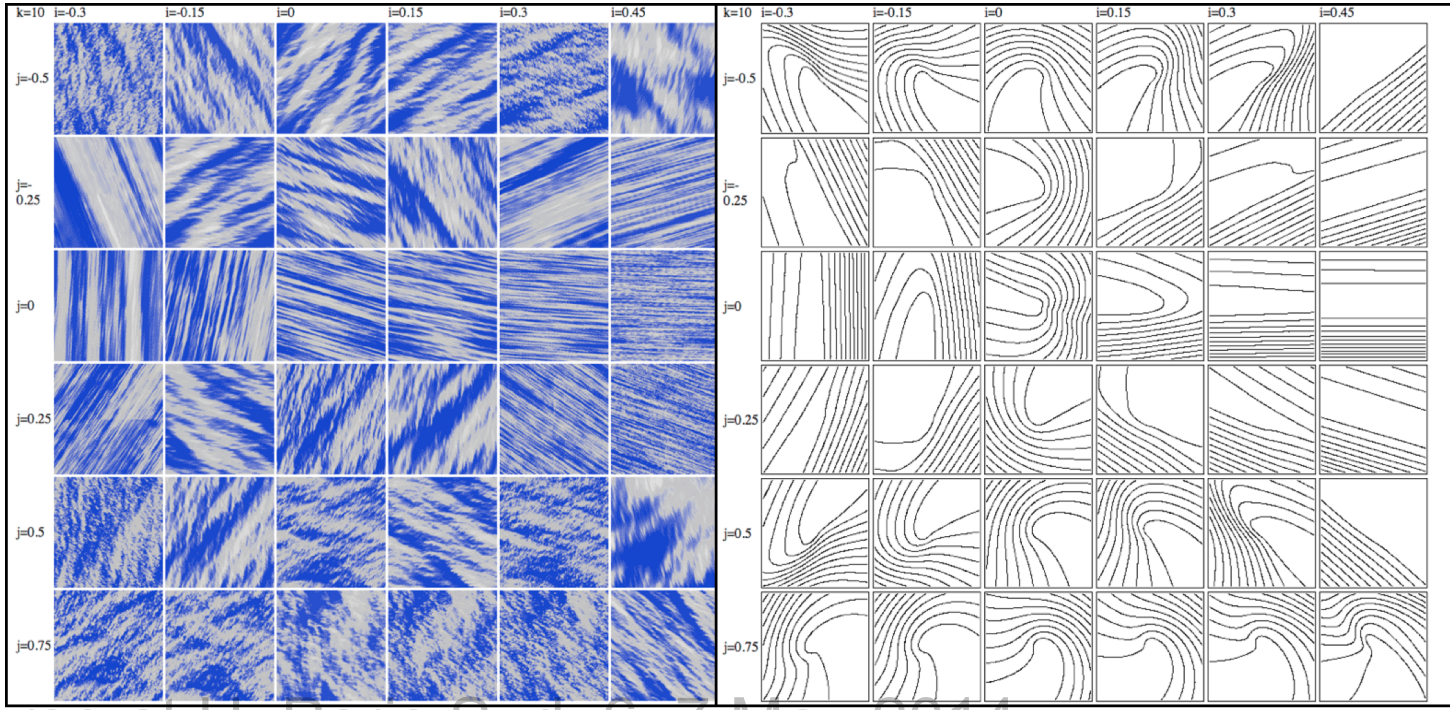

Polar coordinate scale function for unit ball

$$\|\underline{r}\| = r\Theta(\theta'') = 1 \quad \text{with}$$

$$\Theta(\theta'') = 1 + \frac{1-2^{-k}}{1+2^{-k}}\cos\theta''$$

Hence:

$$\max\left(\Theta(\theta'')\right) / \min\left(\Theta(\theta'')\right) = 2^k$$

$e = 0$

r is increased from -0.3, -0.15, …0.45 left to right, from top to bottom, *k* is increased from 0, 2, 4,..10.

r

k

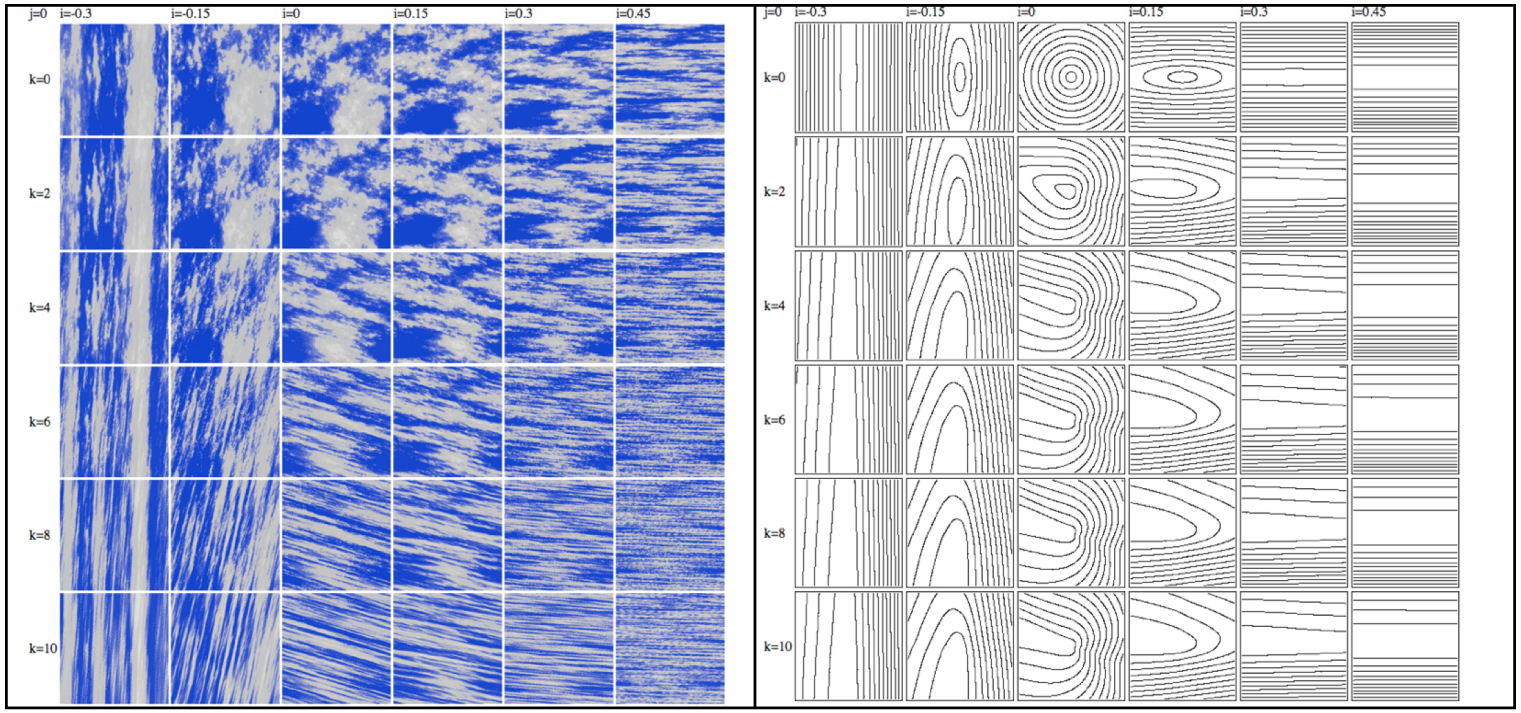

$e = 0.75$

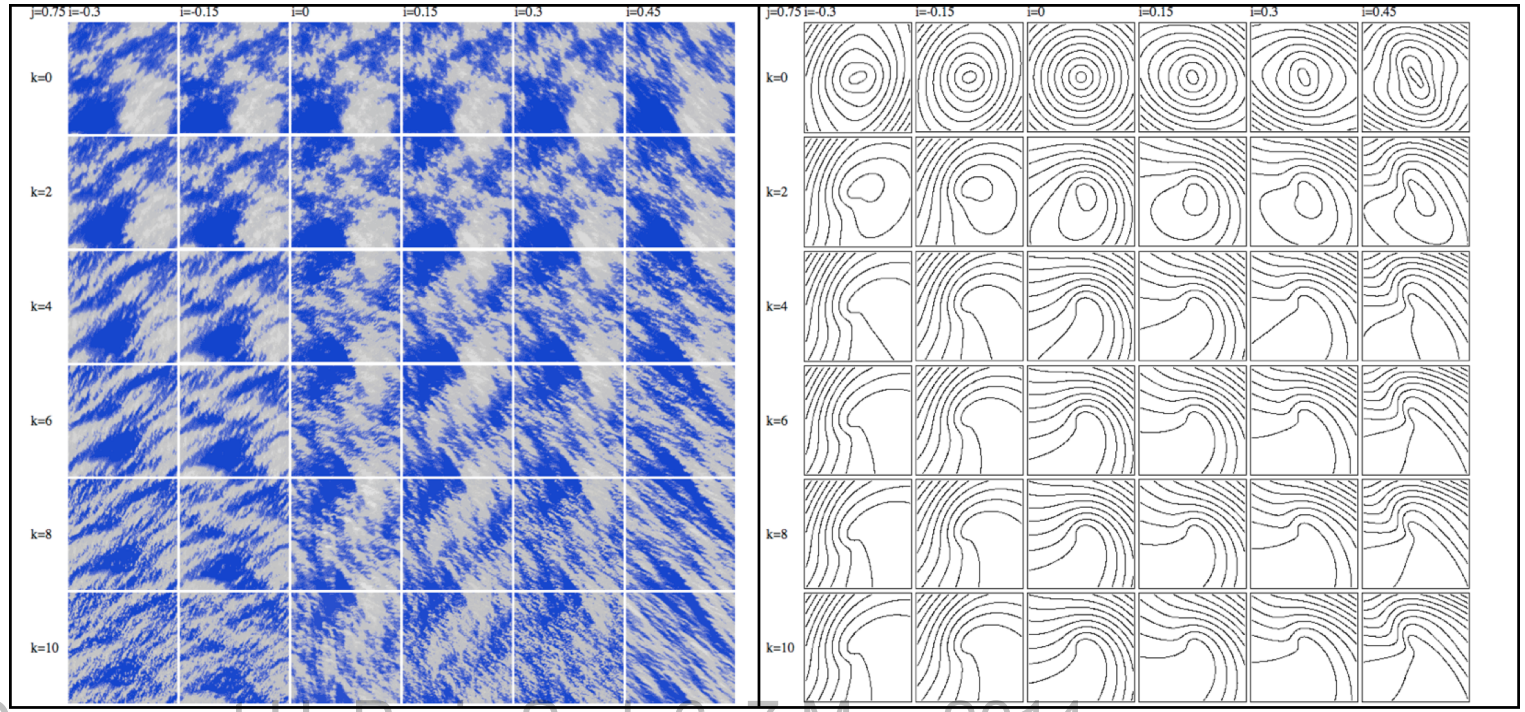

e

$r = 0$

e left to right is: -0.5, -0.25, …0.75.

k

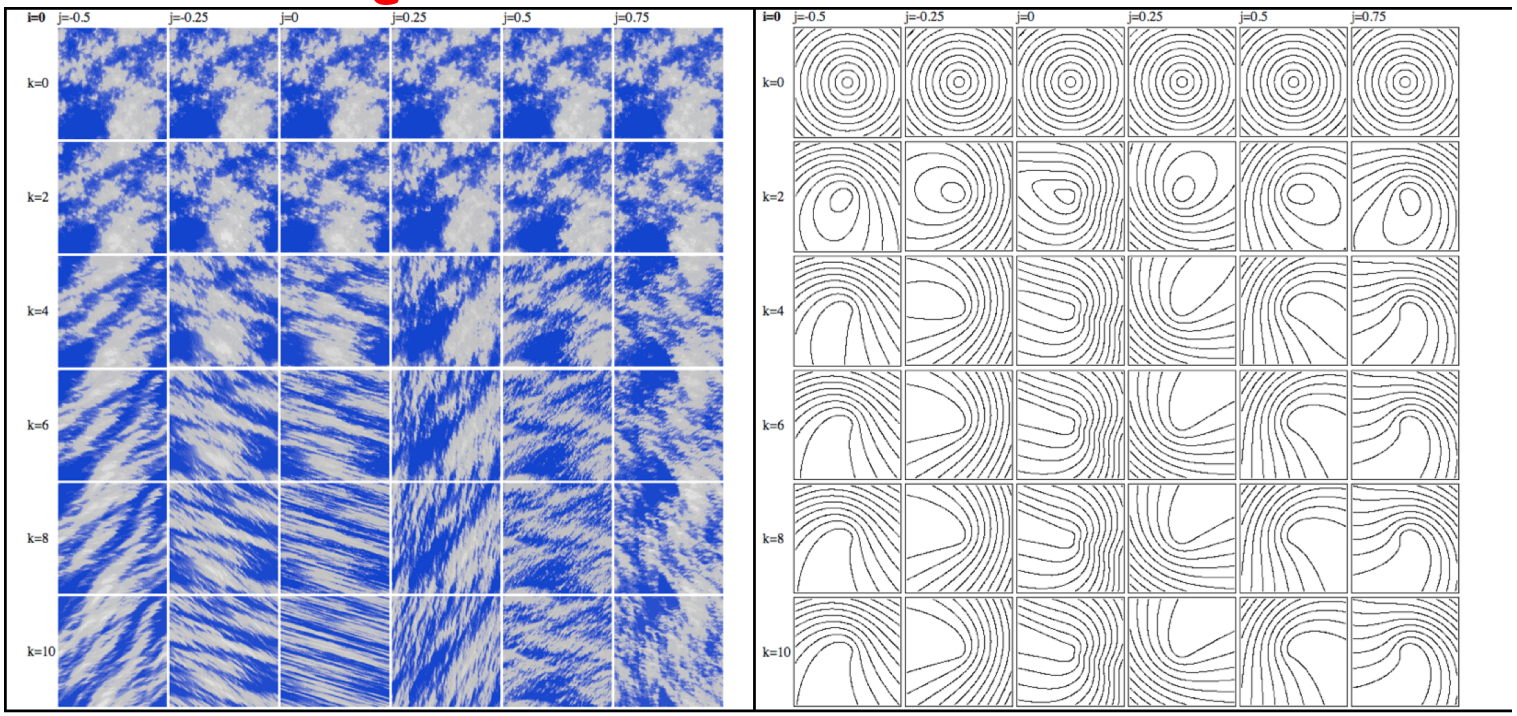

$r = 0.15$

In all rows, from top to bottom, *k* is increased (0, 2, 4,..10),

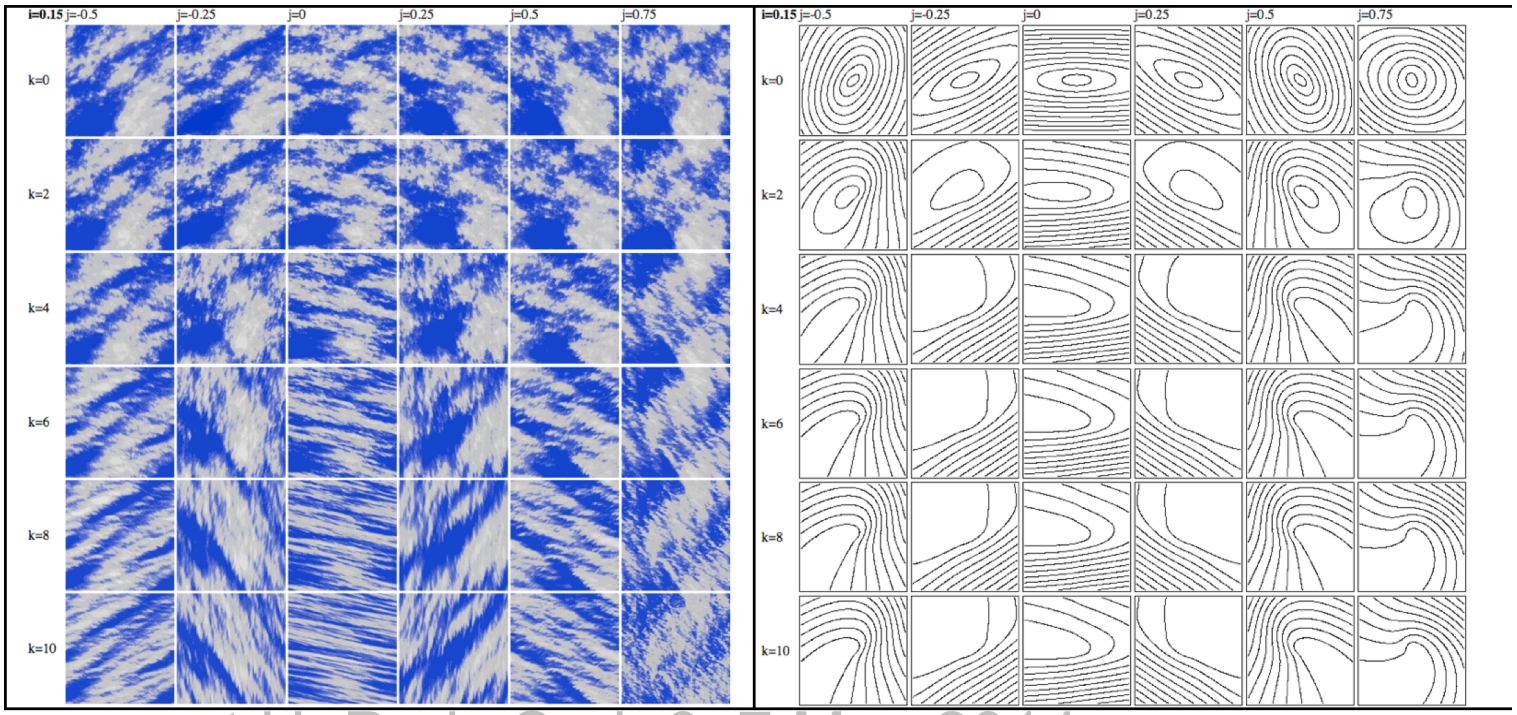

Changing G

http://www.physics.mcgill.ca/~gang/multifrac/index.htm

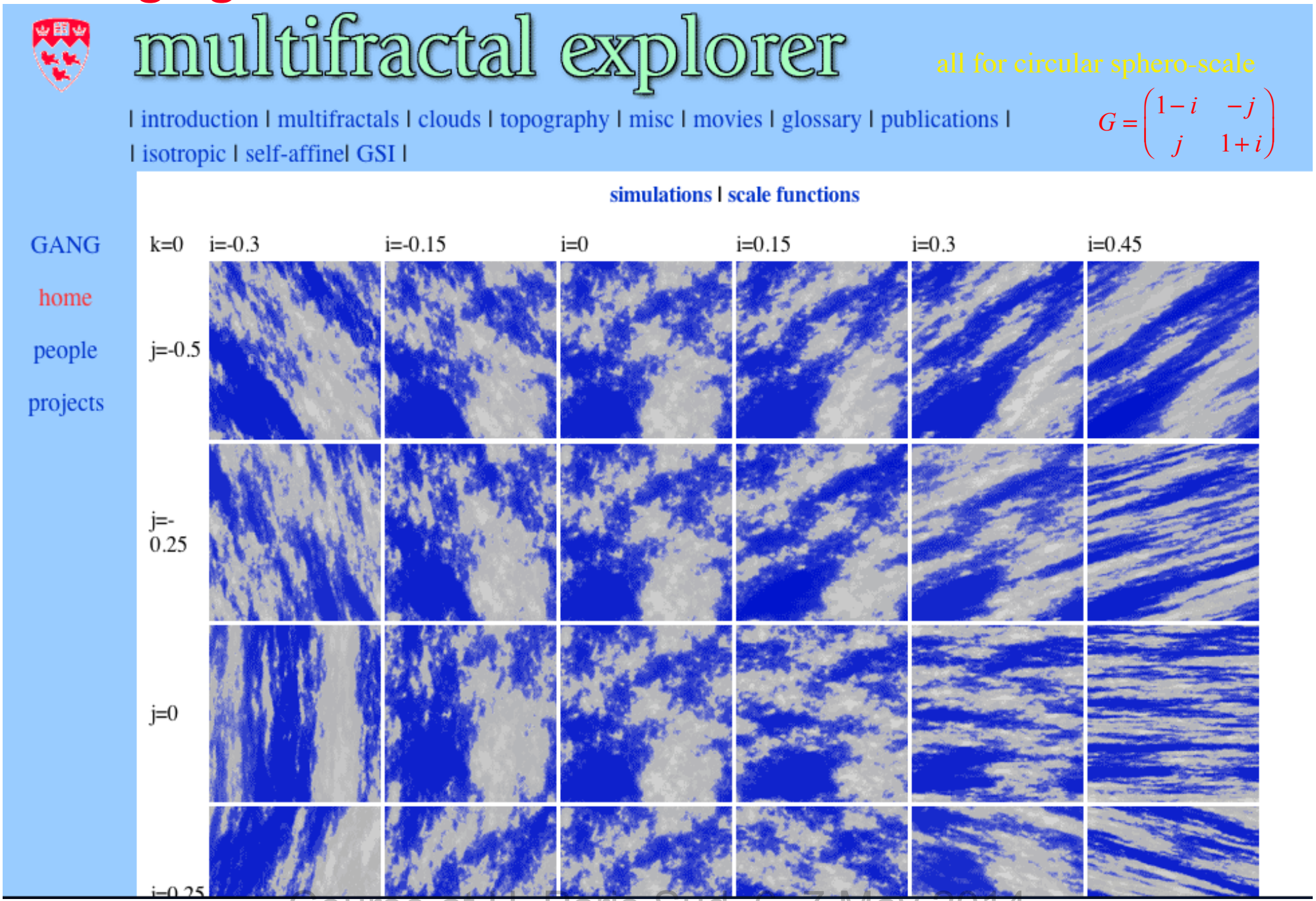

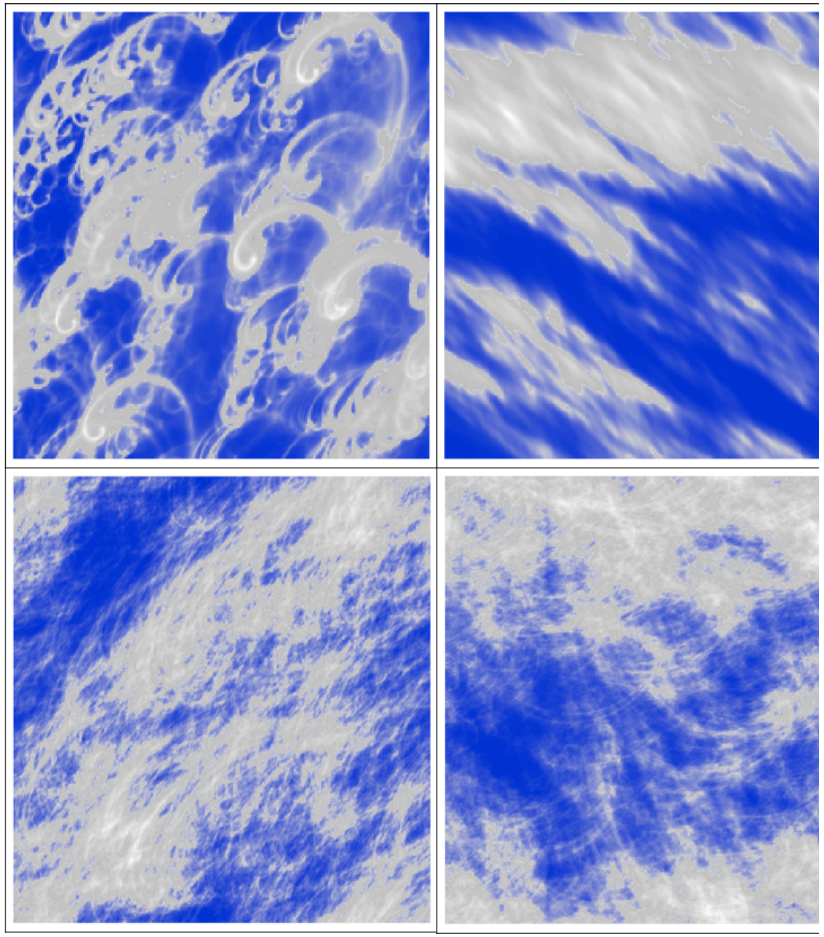

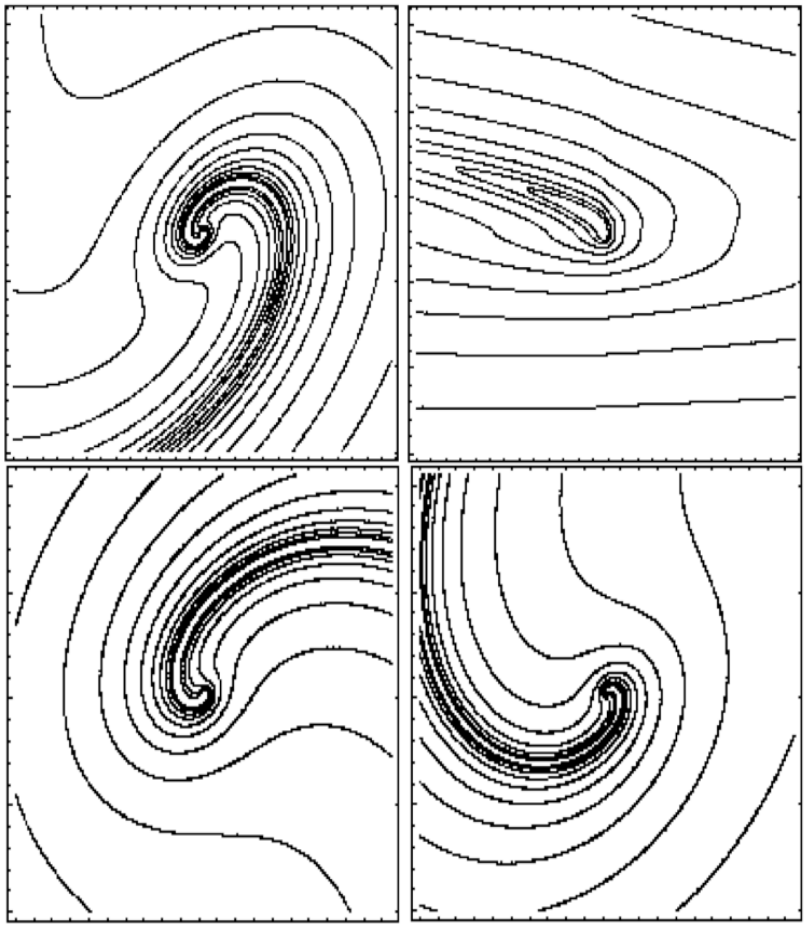

Examples of 2D simulations on 512x512 pixel grids with $\alpha = 1.8$, $C_1 = 0.1$, $H = 0.333$, $d = 1$, $f = 0$. Upper left: $c = 0.8$, $e = 2$, $l_s = 512$, x = 1.3 ($2^k = r_{max}/r_{min} \approx 54$), upper right: $c = -2/7$, $e = 0.1$, $l_s = 32$, $2^k \approx 5$, lower left: $c = 0.3$, $e = 1.2$, $l_s = 32$, $2^k \approx 800$, lower right: $c = 0.3$, $e = 1.2$, $l_s = 1$, $2^k \approx 800$.

Order emerging from chaos

Max X8 Max X16 Max X32 Max X64

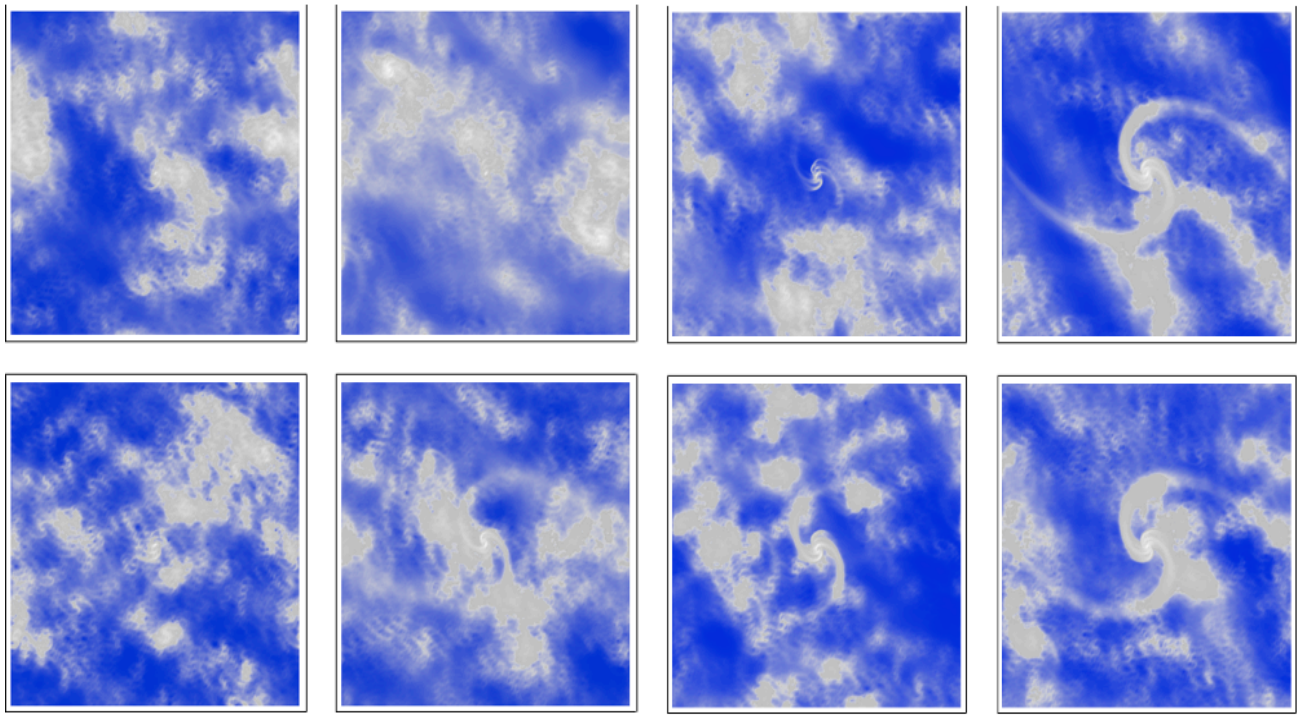

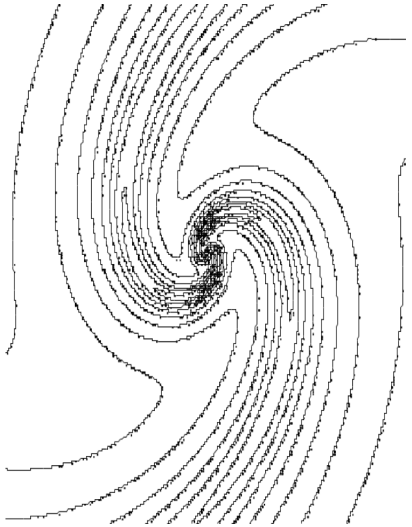

Each row shows a realization of a random multifractal process with a single value of of the subgenerator $\gamma(\underline{r})$ at the centre of a 512X512 grid replaced by the maximum of $\gamma(\underline{r})$ over the field boosted by factors of N increasing by 2 from left to right (from 8 to 64) in order to simulate very rare events (α = 1.8, C_1 = 0.1, H = 0.333). The scaling is anisotropic with complex eigenvalues of G, the scale function is shown at right.

Simulations in three dimensions, rendering with simulated radiative transfer

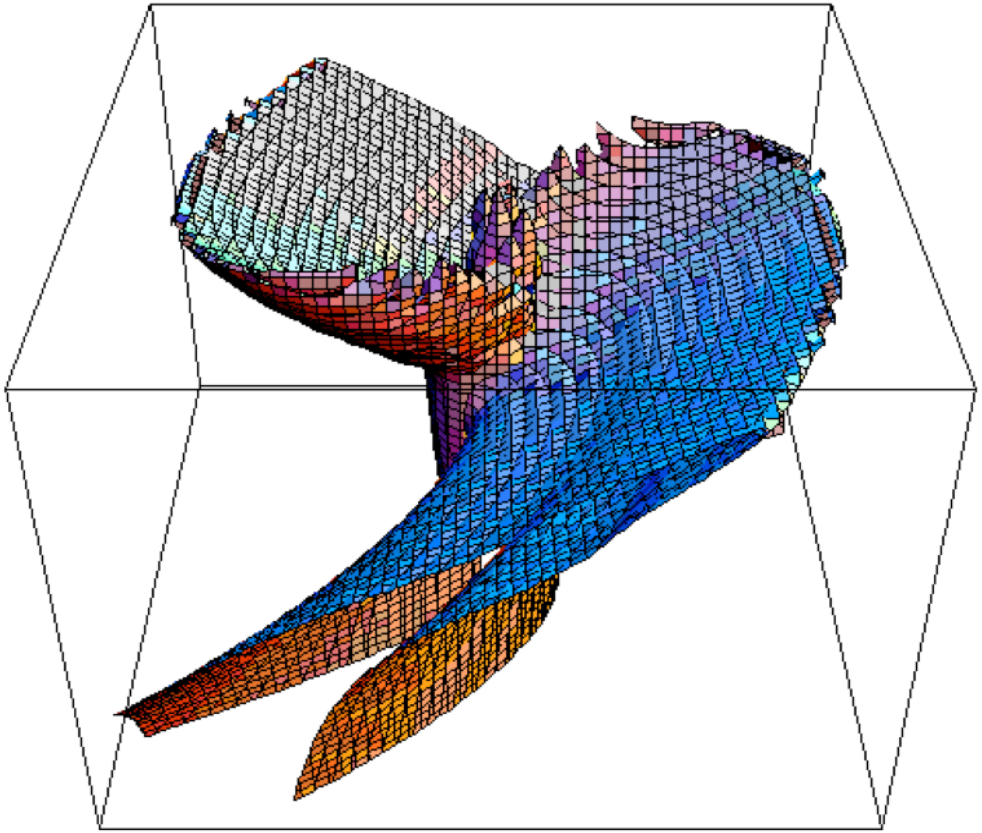

This is a contour of the scale function corresponding to a single scale; this is a strongly rotationally dominant case with $n = 2$, $x_q = x_f = 1.4$, $d = 1$, $c = 0.5$, $e = 1$, $f = 0$, $H_z = 0.8$, $l_s = 64$,

Top horizontal section (density)

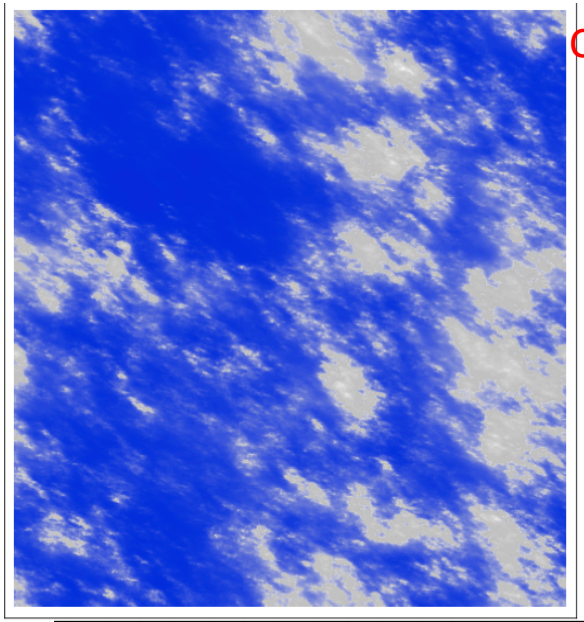

Corresponding scale function

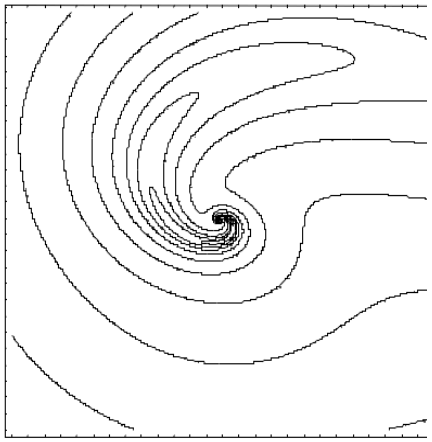

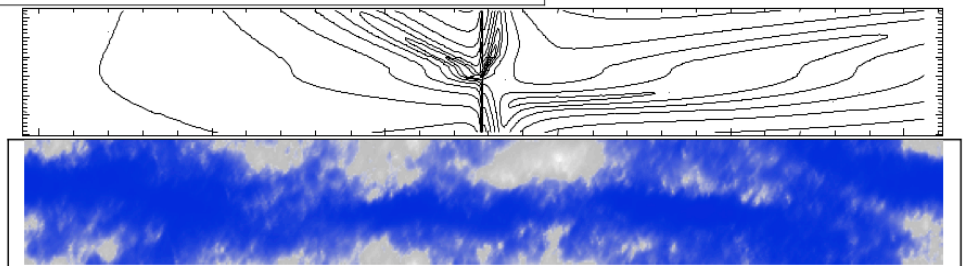

Side (density)

Corresponding top radiative transfer

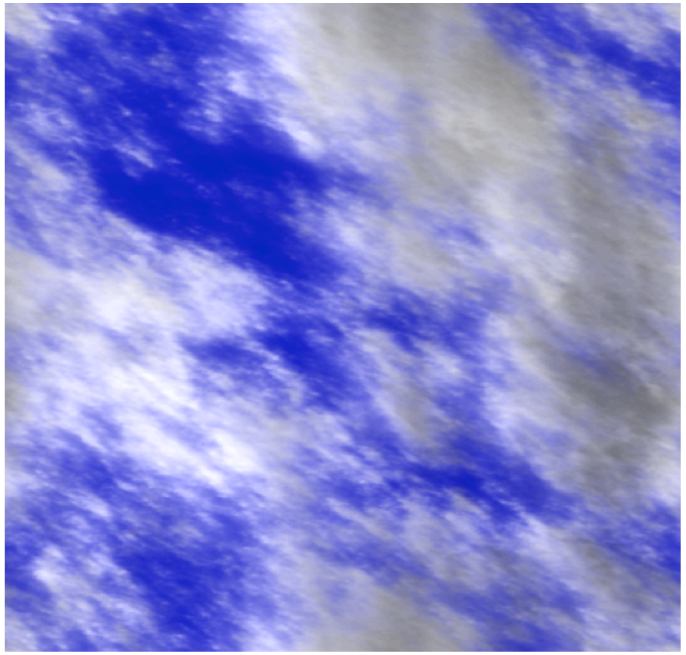

Corresponding side radiative transfer

An example with a = 1.8, C_1 = 0.1, H = 0.333, on a 512x512x64 grid (the latter is the thickness). The parameters are n_q =1, n_f = 2, x_q = 0.3, x_f = 0.8, c = 0.2, e = 0.5, f = 0.2 (rotation dominant), H_z = 0.555 with l_s = 128, l_{sz} = 32. The upper left is the liquid water density field, top horizontal section, to the right is the corresponding central hrizontal cross section of the scale function. The bottom row shows one of the sides (512x64 pixels) with corresponding central part of the vertical cross section.

Cloud tops (densities)

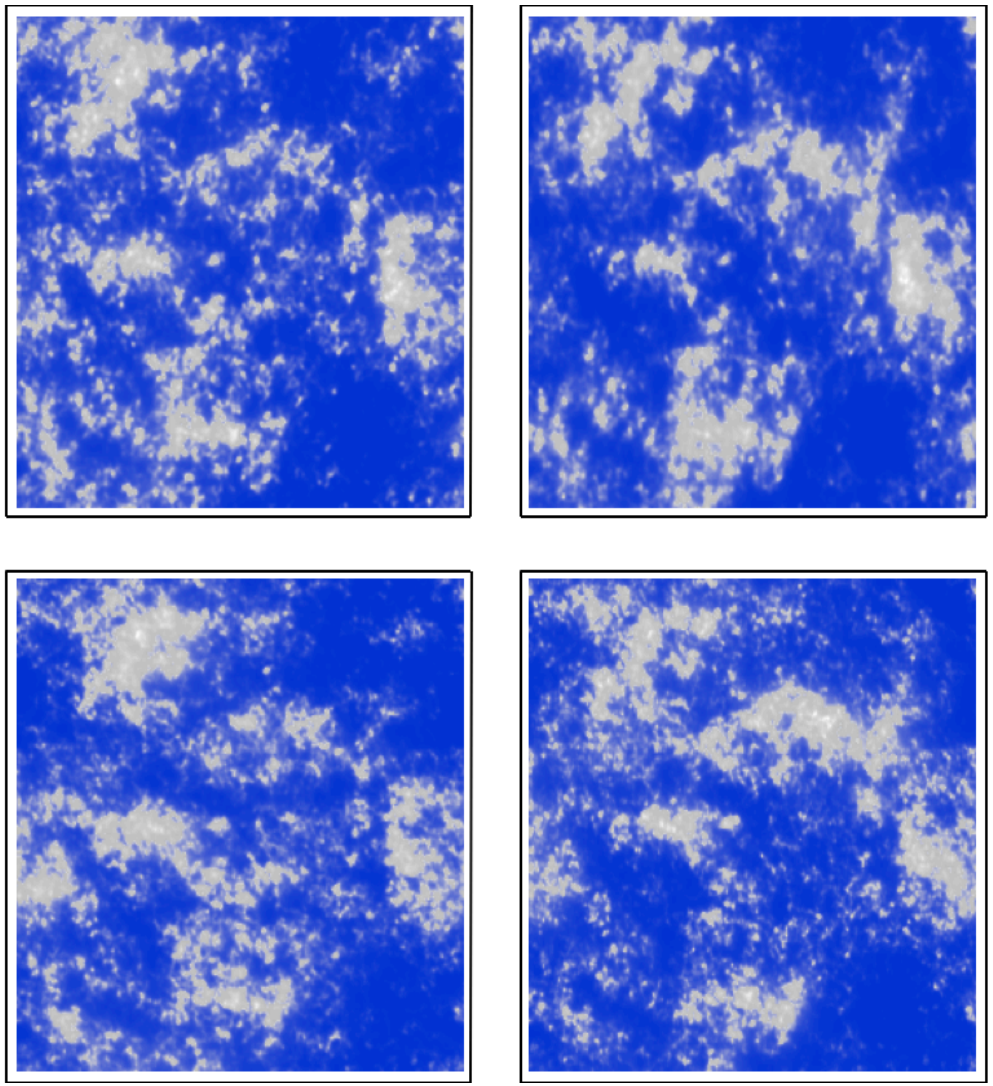

This shows the top layers of three dimensional cloud liquid water density simulations (false colours) all have d = 1, c = 0.05, e = 0.02, f = 0, H_z = 0.555, α = 1.8, C_1 = 0.1, H = 0.333 and are simulated on a 256x256x128 point grid (a^2>0; stratification dominant in the horizontal). The simulations in the top row have l_s = 8 pixels, (left column), 64 pixels (right column), k=0, k=32 (bottom row). Note that in these simulations, the l_s =8, 64 applies to both vertical and horizontal cross-sections (i.e. $l_s = l_{sz}$). Show an example with IR scattering?

Sides, same clouds (densities)

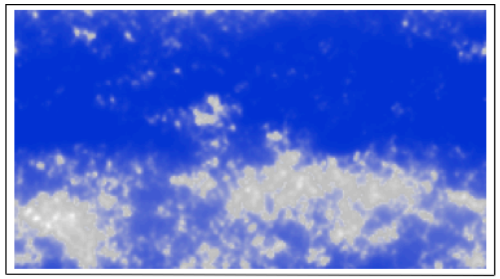

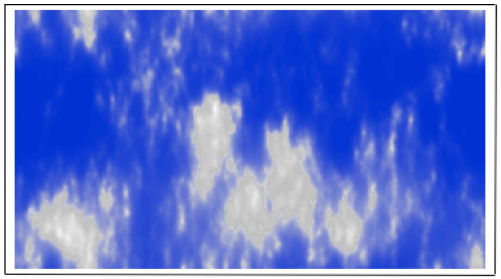

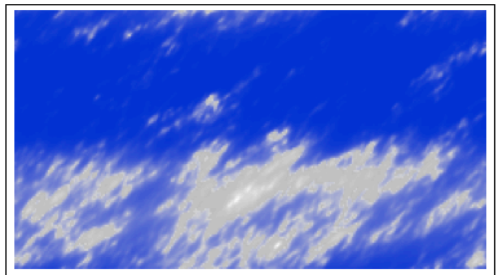

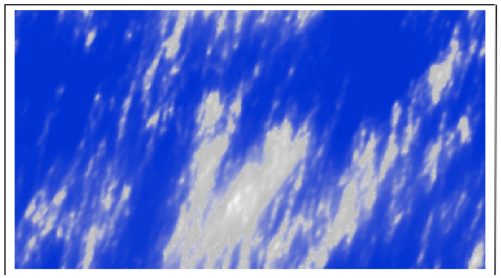

Same clouds radiative transfer, top view

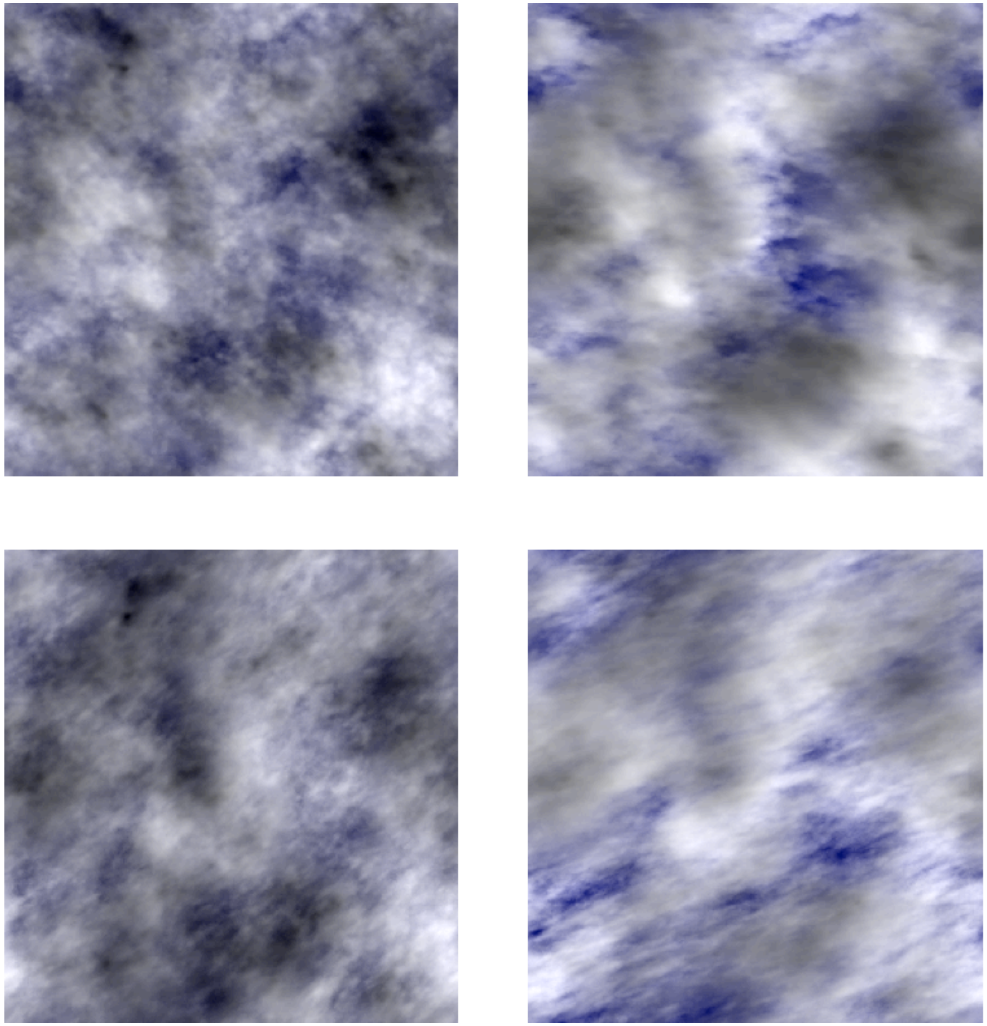

The top view with single scattering radiative transfer; incident solar radiation at 45^{o} from the right, mean vertical optical thickness = 50

Same clouds radiative transfer, bottom view

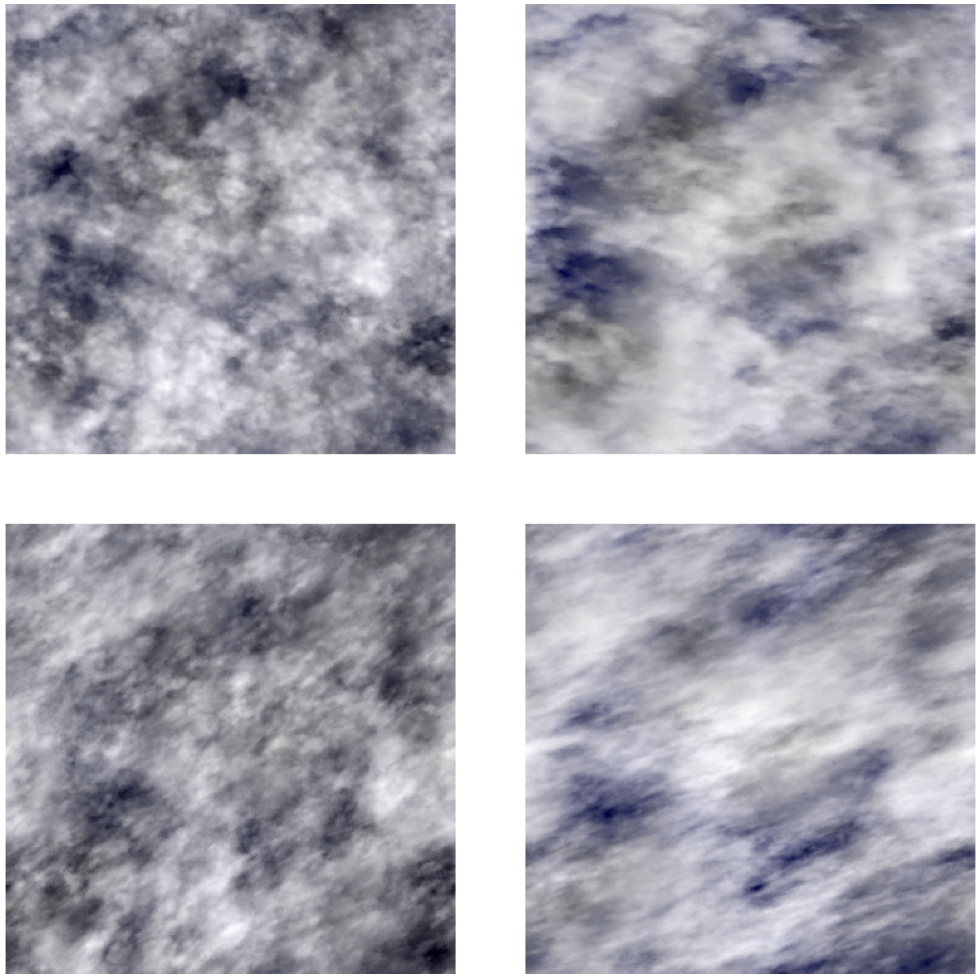

The same except viewed from the bottom.

Mono, multifractal Intercomparison,

stratification dominant

Contours of the s
functions

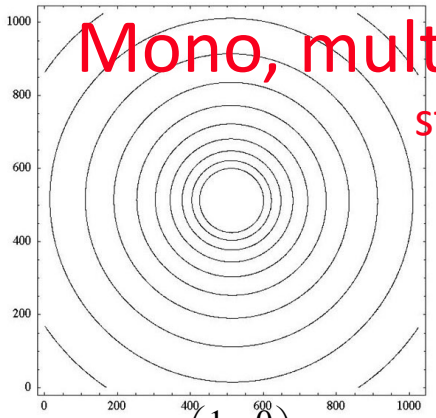

$$G=\begin{pmatrix}1 & 0\\ 0 & 1\end{pmatrix}$$

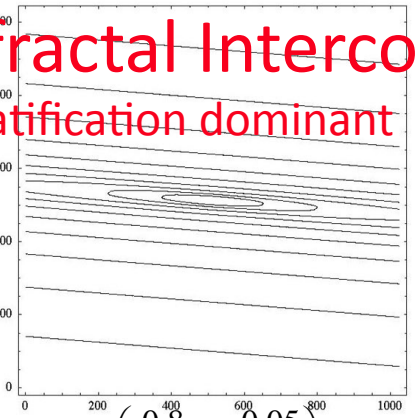

$$G=\begin{pmatrix}0.8 & -0.05\\ 0.05 & 1.2\end{pmatrix}$$

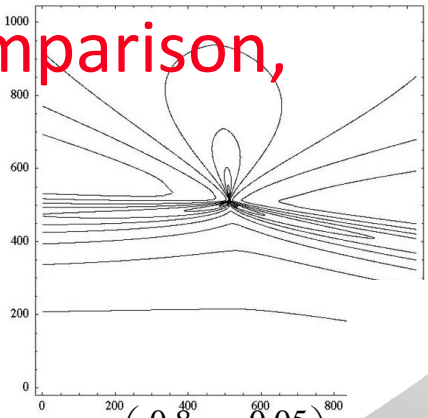

$$G=\begin{pmatrix}0.8 & -0.05\\ 0.05 & 1.2\end{pmatrix}$$

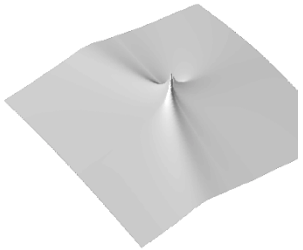

Fractional Brownian motion, H=0.7

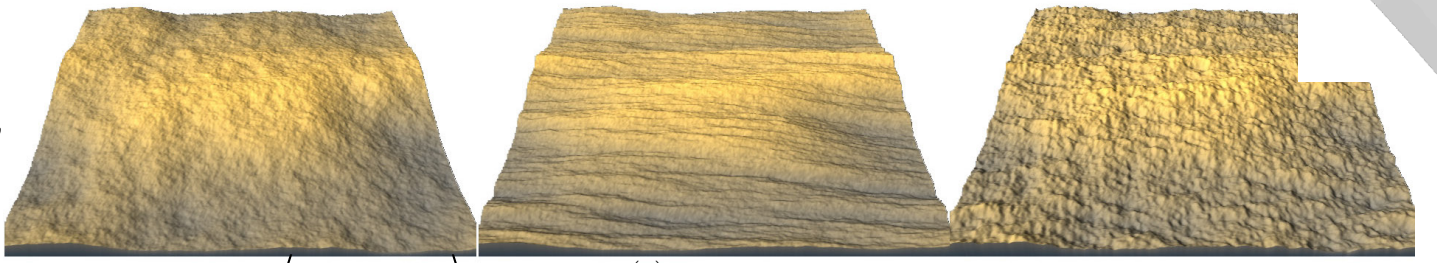

$$\left\langle \Delta h(\Delta r)^q \right\rangle \approx \Delta r^{qH-K(q)} \qquad K(q)=0$$

Fractional Levy motion, H=0.7, α =1.8

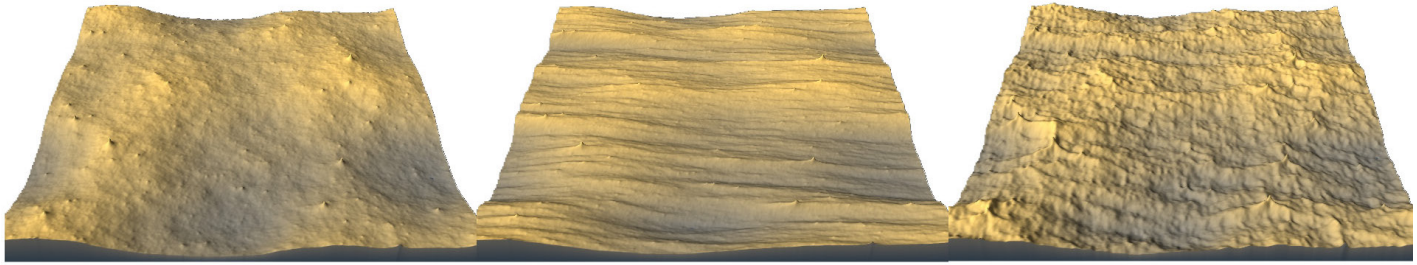

Multifractal FIF H=0.7, α =1.8, C_1=0.12

$$K(q)=\frac{C_1}{\alpha-1}\left(q^{\alpha}-q\right)$$

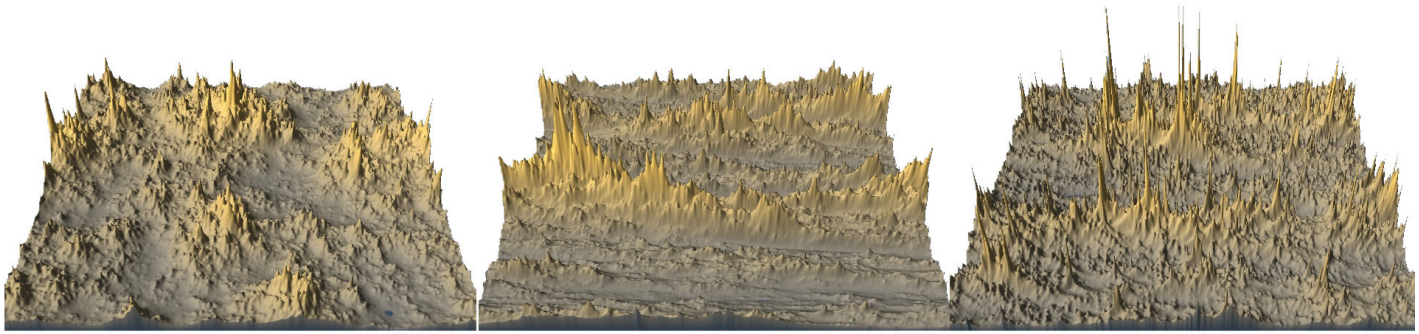

isotropic | Anisotropic no trivial anisotropy | Anisotropic with trivial anisotropy

Mono, multifractal Intercomparison

rotation dominant

Contours of the scale functions

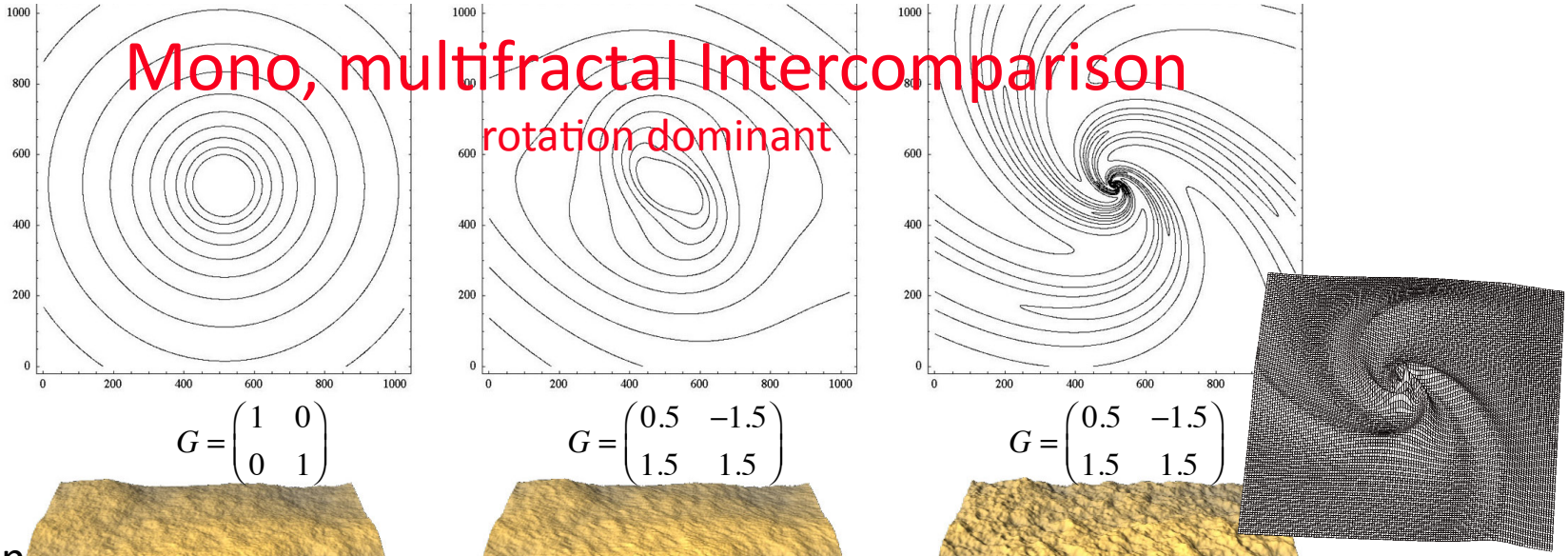

$G = \begin{pmatrix} 1 & 0 \\ 0 & 1 \end{pmatrix}$ $G = \begin{pmatrix} 0.5 & -1.5 \\ 1.5 & 1.5 \end{pmatrix}$ $G = \begin{pmatrix} 0.5 & -1.5 \\ 1.5 & 1.5 \end{pmatrix}$

Fractional Brownian motion, H=0.7

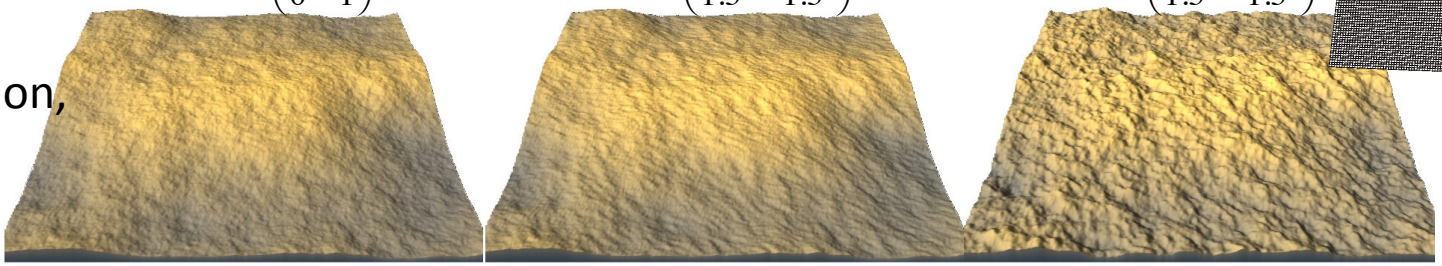

Fractional Levy motion, H=0.7, α=1.8

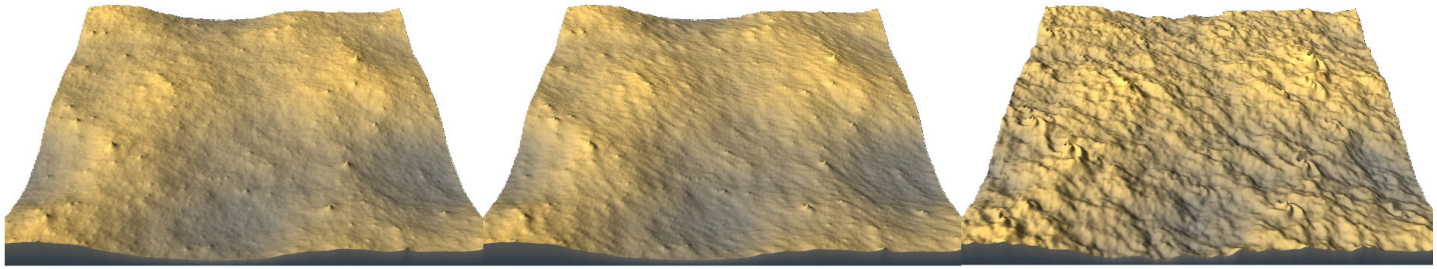

Multifractal, FIF H=0.7, α =1.8, C_1=0.12

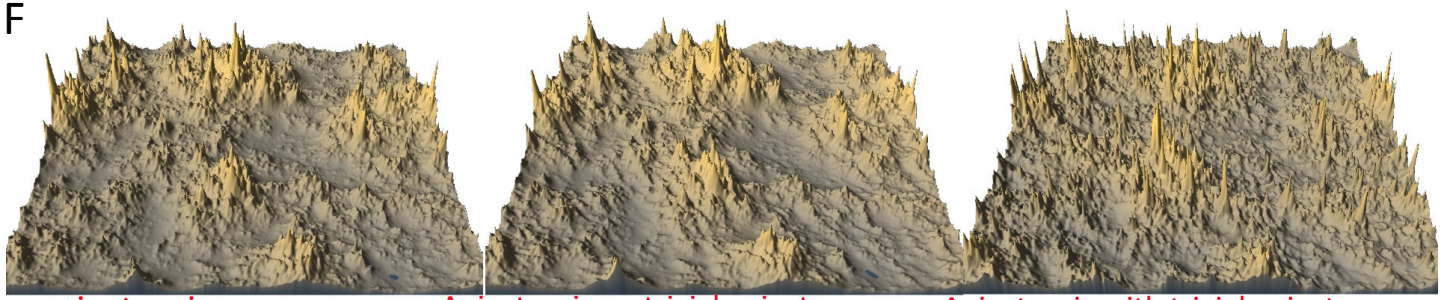

isotropic | Anisotropic no trivial anisotropy | Anisotropic with trivial anisotropy

Effect of varying C_1, H (self-affine, l_s=1)

C_1=0.05

All:

α=1.8

$$G = \begin{pmatrix} 0.8 & 0 \\ 0 & 1.2 \end{pmatrix}$$

H=0.2 H=0.5 H=0.8

C_1=0.15

C_1=0.25

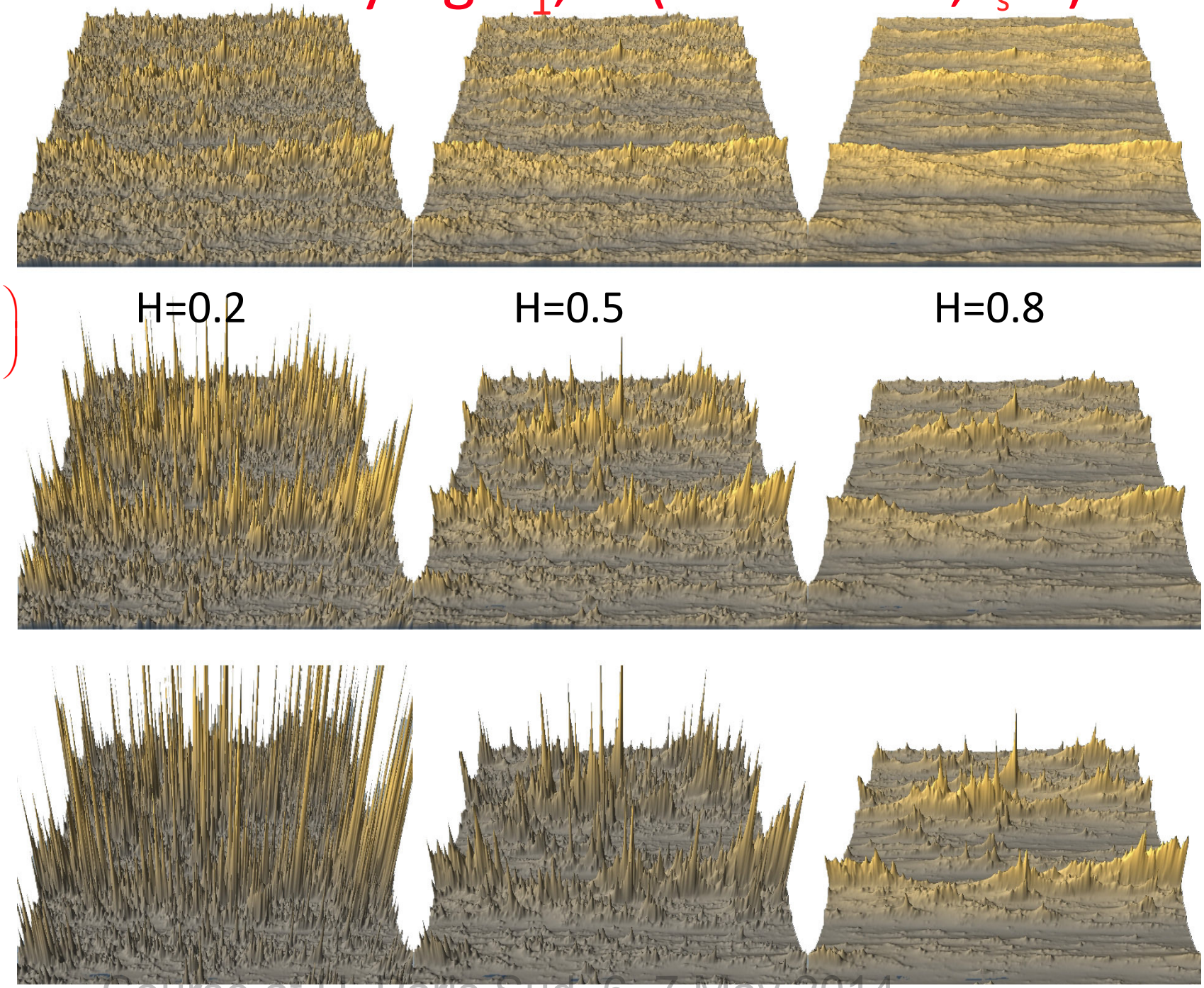

Effect of varying C_1, H (self-affine, l_s=64)

C_1=0.05

All:

α=1.8

$$G = \begin{pmatrix} 0.8 & 0 \\ 0 & 1.2 \end{pmatrix}$$

H=0.2 H=0.5 H=0.8

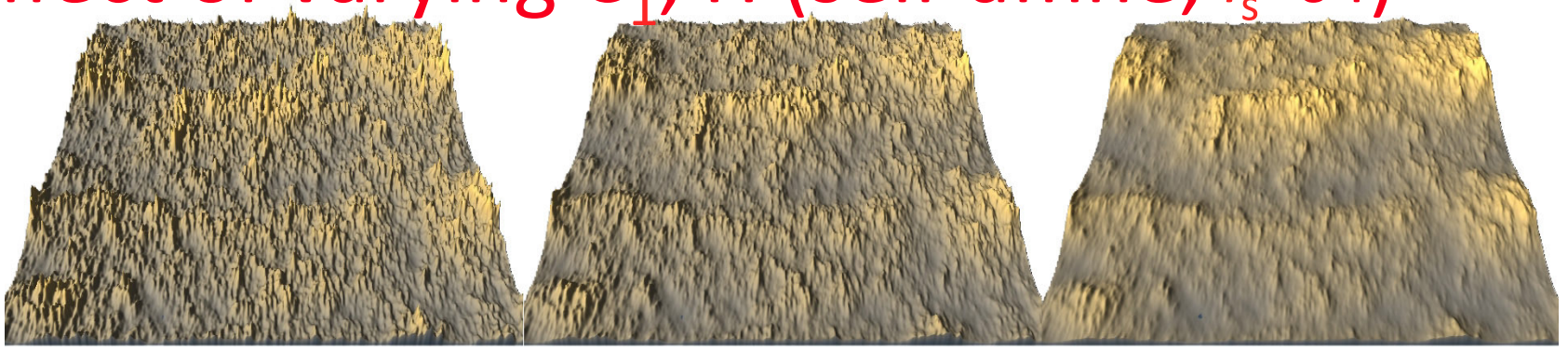

C_1=0.15

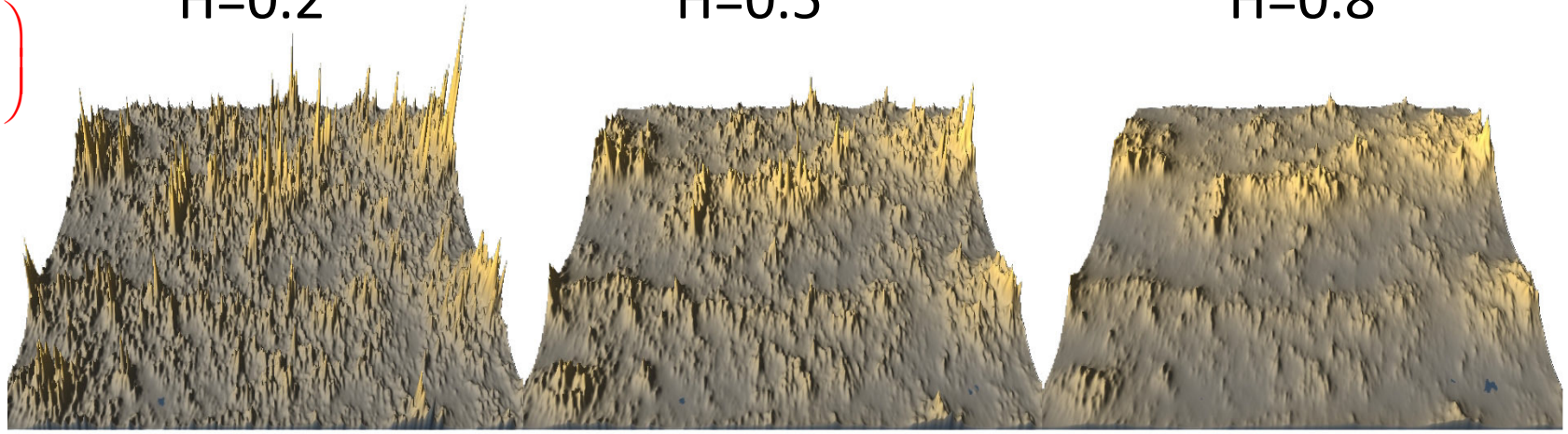

C_1=0.25

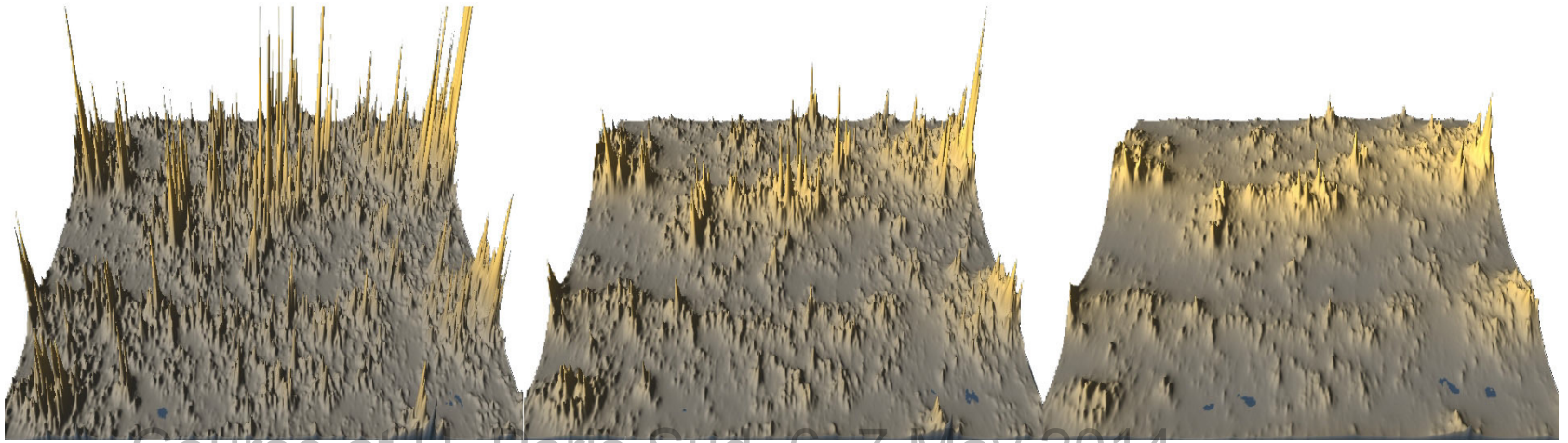

Extension from space to space-time (including waves)

Space-Time ("Stommel") diagramme

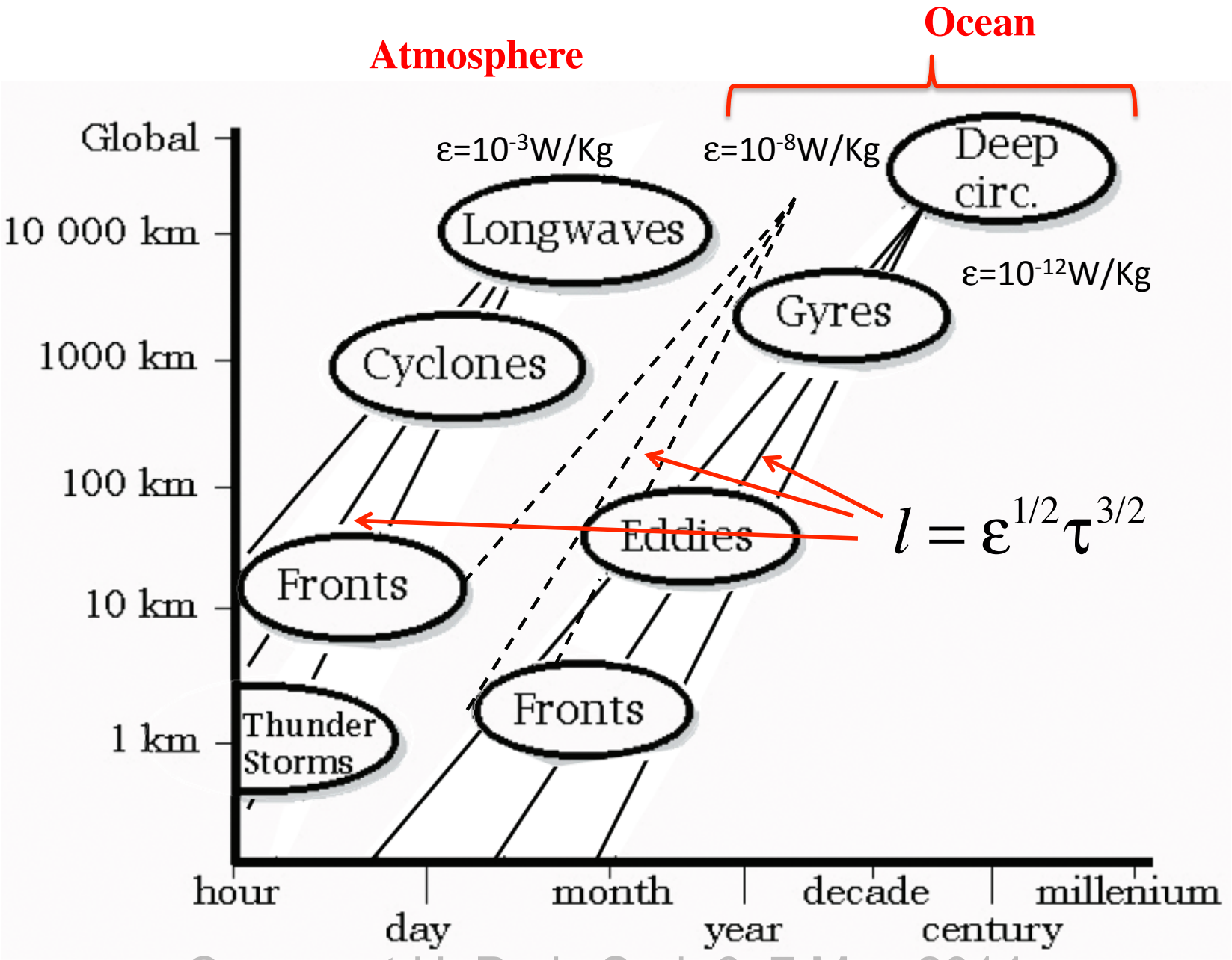

1400 MTSAT IR images

30°S - 40°N, Pacific (Spectrum, 1-D subspaces)

1 hour, 30 km resolution

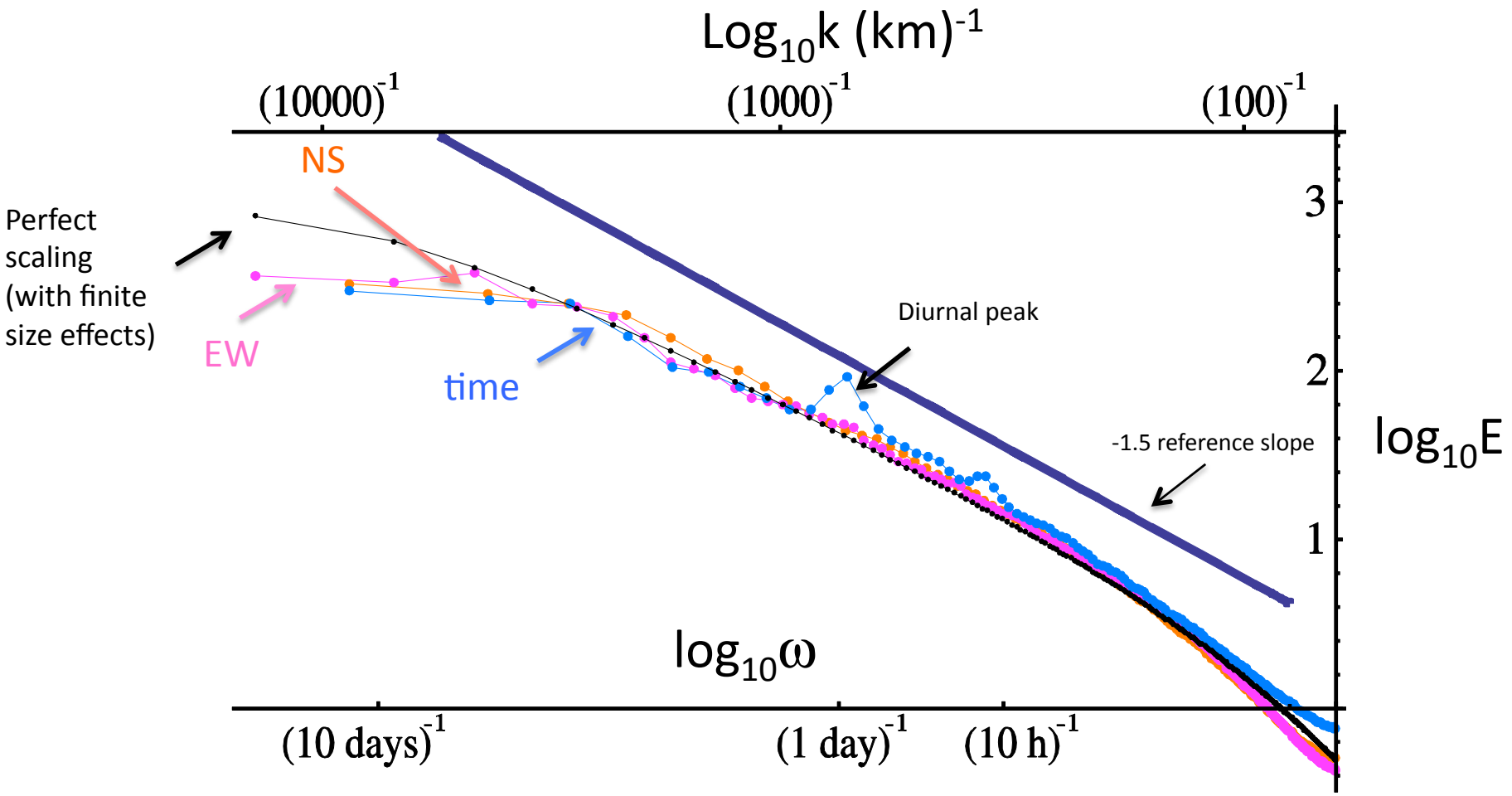

Space-time scaling is accurately respected:

$$\tilde{g}\left(\lambda^{-1}\left(\underline{k},\omega\right)\right)=\lambda^{H_{tur}}\tilde{g}\left(\left(\underline{k},\omega\right)\right)$$ implies $$E\left(k_x\right)\approx k_x^{-\beta};\quad E\left(k_y\right)\approx k_y^{-\beta};\quad E\left(\omega\right)\approx\omega^{-\beta}$$

Turbulence and (fractional) propagators

Example: The classical wave equation

$$\left(\nabla^2 - \frac{1}{V^2}\frac{\partial^2}{\partial t^2}\right) I(\underline{r},t) = f(\underline{r},t)$$

Solution by Fourier transforms

propagator

$$\tilde{I}(\underline{k},\omega) = \tilde{g}(\underline{k},\omega)\tilde{f}(\underline{k},\omega) \qquad \tilde{g}(\underline{k},\omega) = \left(\omega^2/V^2 - |\underline{k}|^2\right)^{-1}$$

$$\tilde{g}\left(\lambda^{-1}(\underline{k},\omega)\right) = \lambda^H \tilde{g}\left((\underline{k},\omega)\right); \quad H = 2$$

Isotropic scale change symmetry

Fractional wave equation

$$\left(\nabla^2 - \frac{1}{V^2}\frac{\partial^2}{\partial t^2}\right)^{H/2} I(\underline{r},t) = f(\underline{r},t) \;\; ; \;\; \tilde{g}(\underline{k},\omega) = \left(\omega^2/V^2 - |\underline{k}|^2\right)^{-H/2}$$

Note: the dispersion relation is independent of H (>0)

Spatial turbulence

Isotropic

FIF model

Turbulent law (space)

$$\Delta I\left(\underline{\Delta r}\right) = \varphi\left|\underline{\Delta r}\right|^{H}$$

Turbulent law (Fourier space)

$$\tilde{I}\left(\underline{k}\right) = \tilde{g}_{tur}\left(\underline{k}\right)\tilde{\varphi}\left(\underline{k}\right)$$

Kolmogorov values

$$\varphi = \varepsilon^{1/3}; \quad H = 1/3$$

$$\tilde{g}_{tur}\left(\underline{k}\right) = \left|\underline{k}\right|^{-H}$$

Anisotropic extension

$$\left|\underline{k}\right| \rightarrow \left\|\underline{k}\right\|$$

Fourier scale function

Scaling equation

$$\left\|\lambda^{G}\underline{k}\right\| = \lambda\left\|\underline{k}\right\|$$

$$G = \begin{pmatrix} 1 & . & . \\ . & 1 & . \\ . & . & H_z \end{pmatrix}$$

Generator of the anisotropy

Canonical scale function (vertical stratification)

$$\left\|\underline{k}\right\| = l_s^{-1}\left(\left(k_x l_s\right)^2 + \left(k_y l_s\right)^2 + \left(k_z l_s\right)^{2/H_z}\right)^{1/2}$$

Sphero-scale

Turbulence in Space-time (horizontal)

Theory (assuming largest eddies "sweep" smaller ones)

Observable

Turbulent flux forcing

$$g^{-1}(\underline{r},t) * I(\underline{r},t) = \varphi(\underline{r},t)$$

$$g(\underline{r},t) \overset{F.T.}{\leftrightarrow} \tilde{g}(\underline{k},\omega)$$

propagator

$$\omega' = (\omega + \underline{k}\cdot\underline{\mu})\sigma^{-1} \qquad \|\underline{k}\| = \left(k_x^2 + k_y^2/a^2\right)^{1/2}$$

$$\sigma = \left(1 - \left(\mu_x^2 + a^2\mu_y^2\right)\right)^{1/2}$$

$$\underline{\mu} = \left(\overline{v_x}, \overline{v_y}\right)/V_w \qquad V_w = \varepsilon_{L_e} L_e^{1/3}$$

EW/NS aspect ratio = a
mean horizontal wind= $\left(\overline{v_x}, \overline{v_y}\right)$
Mean planetary scale energy flux ε_{L_e}
Planet size: L_e = 20000 km

$$\tilde{I}(\underline{k},\omega) = \tilde{g}(\underline{k},\omega)\tilde{\varphi}(\underline{k},\omega)$$

$$\tilde{g}(\underline{k},\omega) = \left(-i\omega' + \|\underline{k}\|\right)^{-H_{tur}}$$

Turbulence and waves

Turbulence forcing

Turbulent flux

$$\tilde{I}(\underline{k},\omega) = \tilde{g}_I(\underline{k},\omega)\tilde{\varphi}(\underline{k},\omega)$$

Turbulence-waves

$$\tilde{g}_I(\underline{k},\omega) = \underbrace{\tilde{g}_{wav}(\underline{k},\omega)\tilde{g}_{tur}(\underline{k},\omega)}$$

Wheeler Kiladis 1999 factorization

Propagator symmetry constraints

Reality

$$\tilde{g}(\underline{k},\omega) = \tilde{g}^*(-\underline{k},-\omega)$$

Space-time scaling

$$\tilde{g}\left(\lambda^{-1}(\underline{k},\omega)\right) = \lambda^H \tilde{g}((\underline{k},\omega))$$

Causality

Poles of g in ω plane are below real axis:

$$\omega' = -i\|\underline{k}\| \quad \text{causal since} \quad \|\underline{k}\| \geq 0$$

General form

$$\tilde{g}(\underline{k},\omega) = \left[\left(-i\omega + |\underline{k}|\left(\Psi_+(\varphi) + i\Psi_-(\varphi)\right)\right)\Theta(\theta,\varphi)\right]^{-H}$$

(θ, φ) are angles in spherical polar coordinates of $(\underline{k}, \omega)$

Simple wave ansatz

Simple scaling wave propagator

Fractional (and anisotropic) wave equation propagator

$$\tilde{g}_{wav}(\underline{k},\omega)=\left(\omega'^2/v_{wav}^2-\left\|\underline{k}\right\|^2\right)^{-H_{wav}/2}$$

$$H=H_{tur}+H_{wav}$$

$$\omega'=\left(\omega+\underline{k}\cdot\underline{\mu}\right)\sigma^{-1}$$

$$\left\|\underline{k}\right\|=\left(k_x^2+k_y^2/a^2\right)^{1/2}$$

Dispersion relation

$$\omega=-\underline{k}\cdot\underline{\mu}\pm\sigma v_{wav}\left\|\underline{k}\right\| \quad\leftarrow\quad \omega'=\pm v_{wav}\left\|\underline{k}\right\|$$

Spectral density

Turbulent part Wave part

$$P_I(\underline{k},\omega)=P_\varphi(\underline{k},\omega)\left|\tilde{g}_I\right|^2$$

$$\left|\tilde{g}_I\right|^2=\left|\tilde{g}_{tub}\right|^2\left|\tilde{g}_{wav}\right|^2=\left(\omega'^2+\left\|\underline{k}\right\|^2\right)^{-H_{tur}}\left(\omega'^2/v_{wav}^2-\left\|\underline{k}\right\|^2\right)^{-H_{wav}/2}$$

$$P_\varphi(\underline{k},\omega)=P_0\left(\omega'^2+\left\|\underline{k}\right\|^2\right)^{-s_\varphi/2}$$

Spectrum of turbulence forcing

Multifractals with wave character

Localized in space, unlocalized in space-time (product of turbulent and wave-like scaling propagators).

$H_{wav} = 0$

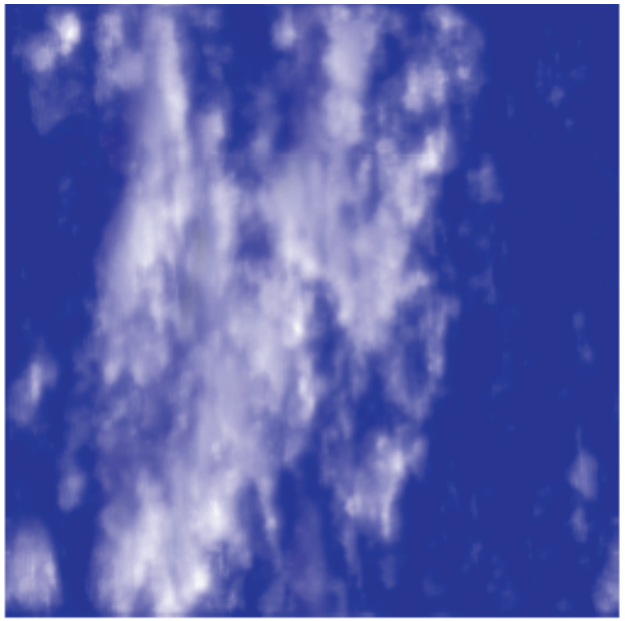

$H_{wav} = 0.33$

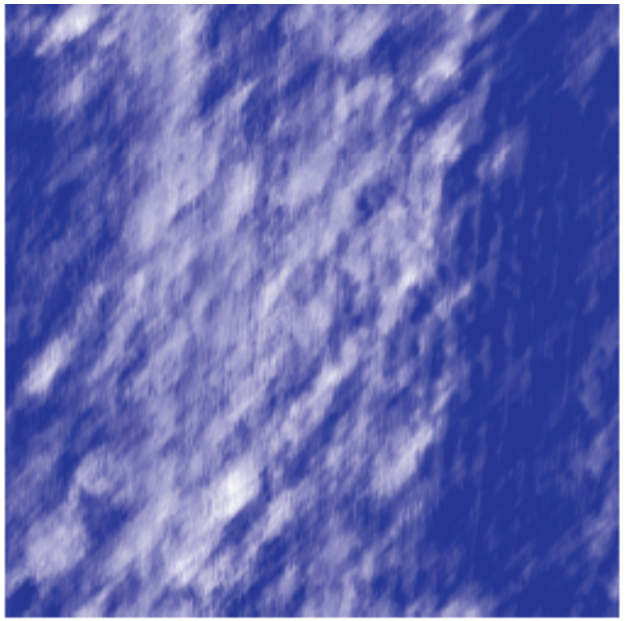

$H_{wav} + H_{tur} = H = 1/3$

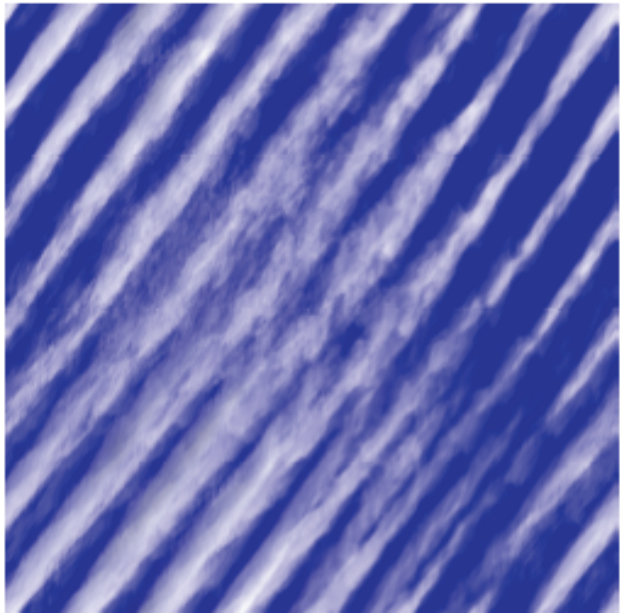

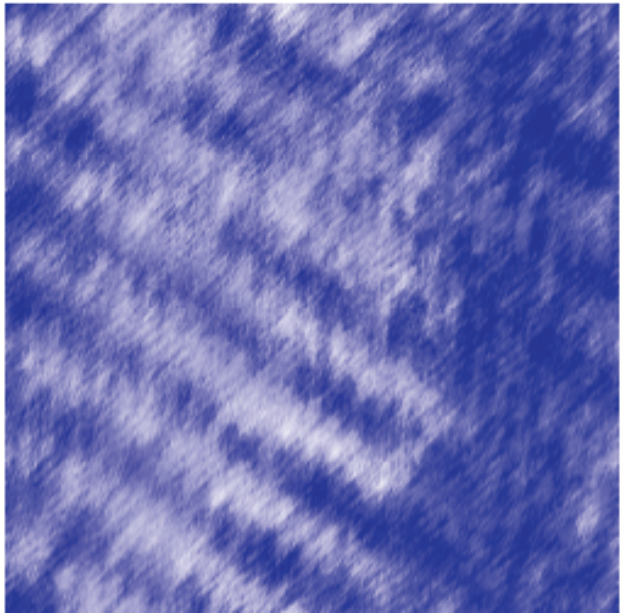

propagator

$$\tilde{I}(\underline{k},\omega) = \tilde{g}(\underline{k},\omega)\tilde{\varepsilon}(\underline{k},\omega)$$

$$\tilde{g}(\underline{k},\omega) = \left(-i\omega + \|\underline{k}\|\right)^{-H_{tur}} \left(\omega^2 V^{-2} - \|\underline{k}\|^2\right)^{-H_{wav}/2}$$

$H_{wav} = 0.52$

$H_{wav} = 0.38$

Predictability and stochastic forecasting

Course at U. Paris Sud, 6, 7 May 2014

Predictability limits algebraic:

Lyapunov exponent $\rightarrow \infty$

Prediction error: $E \approx \Delta t^{H}$

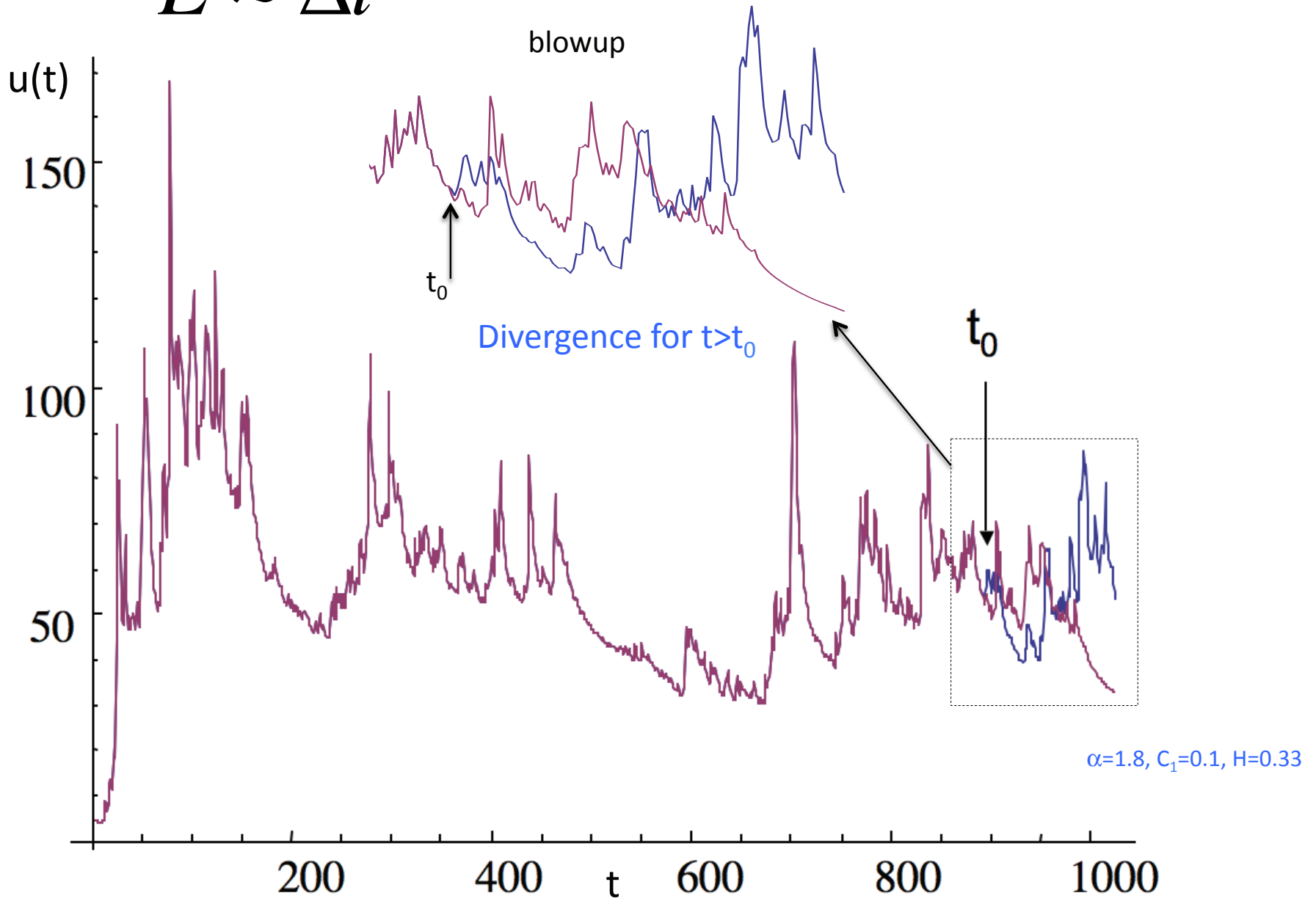

α=1.8, C_1=0.1, H=0.33

Two multifractal proceses with Identical subgenerators to t_0

Algebraic divergence of realizations

$$E = 2\left\langle \frac{I_2(t_0+\Delta t) - I_1(t_0+\Delta t)}{I_2(t_0+\Delta t) + I_1(t_0+\Delta t)} \right\rangle$$

Lyapunov exponent $\rightarrow \infty$

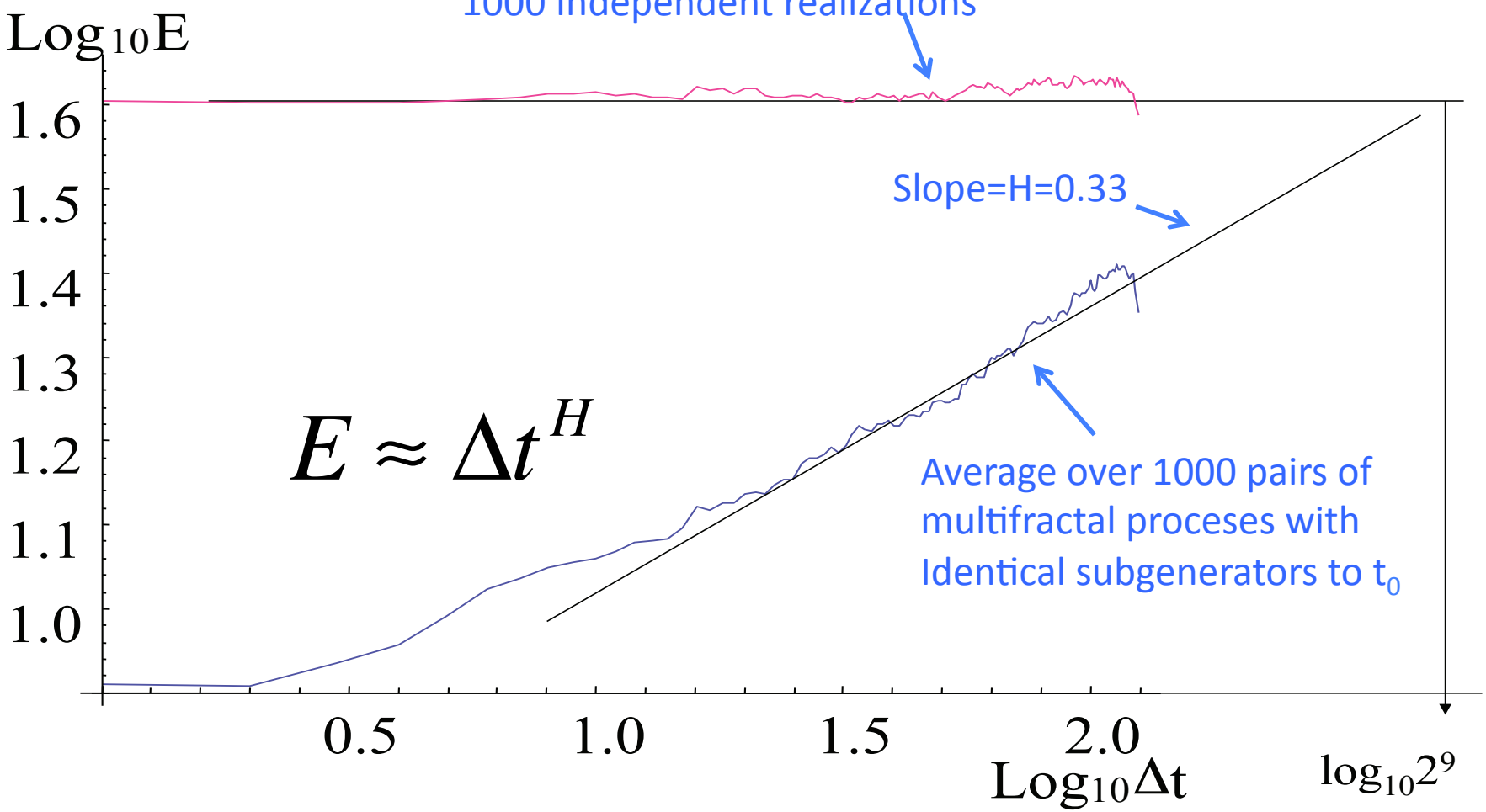

Space-time Cascades, stochastic nowcasting (rain)

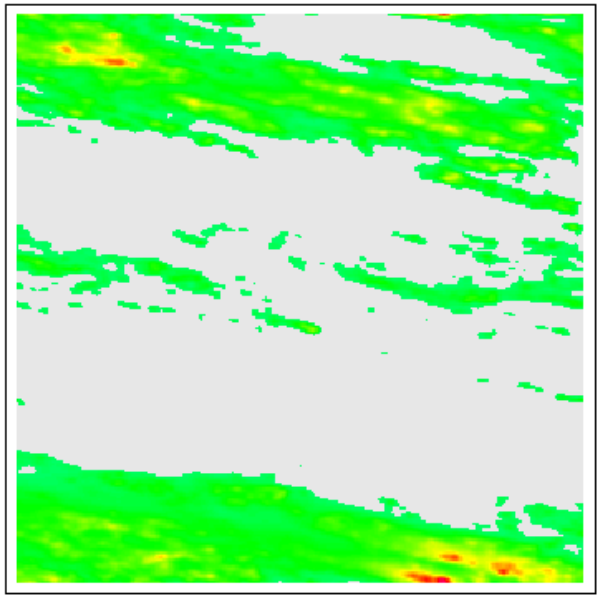

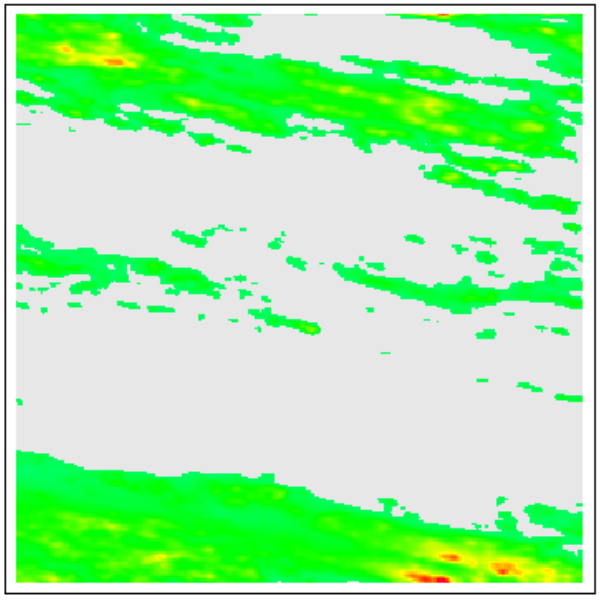

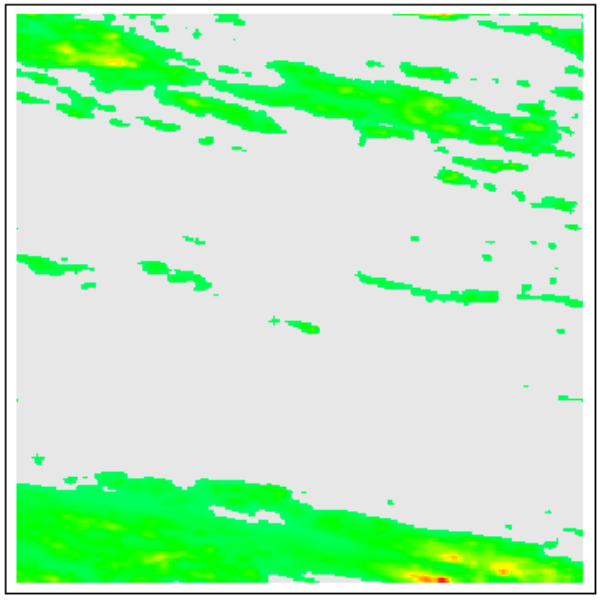

Realization A

Realization B

Forecast based on first 16 time steps

(all same initially)

Conclusions

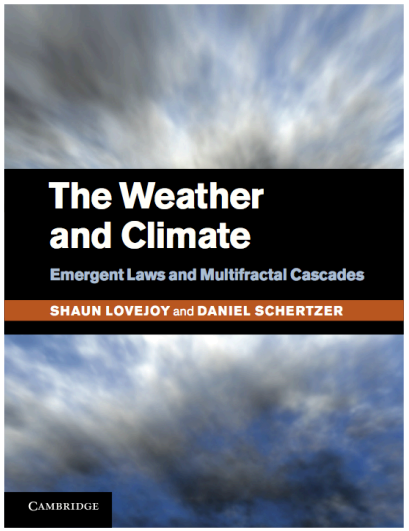

1. High level stochastic turbulence laws emerge from (deterministic) continuum mechanics at strong nonlinearity

2. Regimes: Weather, macroweather, climate

3. Analysis techniques: Haar fluctuations: accurate yet simple to interpret

4. Generalize classical laws: a) : Intermittency using cascades
b) wide range of scales using anisotropic scaling, stratification

5. Unity of the geosciences: anisotropic scaling, multifractality